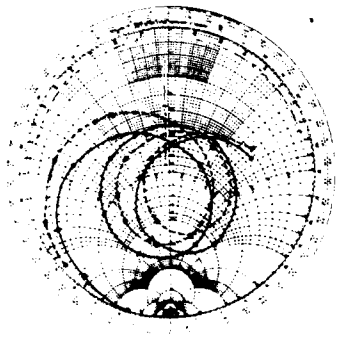

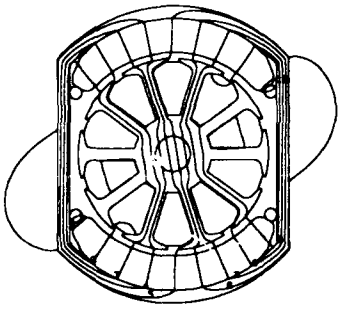

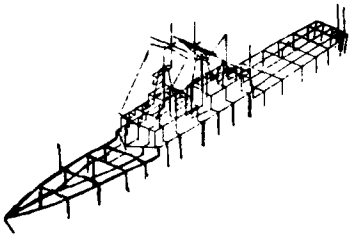

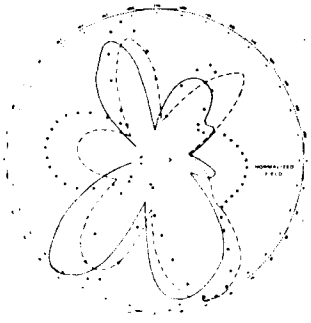

Applied Computational Electromagnetics Society Journal

Summer 1992
Vol. 7 No. 1

ISSN 1054-4887

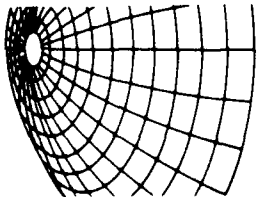

GENERAL PURPOSE AND SCOPE. The Applied Computational Electromagnetics Society Journal hereinafter known as the ACES Journal is devoted to the exchange of information in computational electromagnetics, to the advancement of the state-of-the-art, and to the promotion of related technical activities. A primary objective of the information exchange is the elimination of the need to "re-invent the wheel" to solve a previously-solved computational problem in electrical engineering, physics, or related fields of study. The technical activities promoted by this publication include code validation, performance analysis, and input/output standardization; code or technique optimization and error minimization; innovations in solution technique or in data input/output; identification of new applications for electromagnetics modeling codes and techniques; integration of computational electromagnetics techniques with new computer architectures; and correlation of computational parameters with physical mechanisms.

SUBMISSIONS CONTENT. The ACES Journal welcomes original, previously unpublished papers, relating to applied computational electromagnetics.

Typical papers will represent the computational electromagnetics aspects of research in electrical engineering, physics, or related disciplines. However, papers which represent research in applied computational electromagnetics itself are equally acceptable.

For additional details, see "Information for Authors", elsewhere in this issue.

SUBSCRIPTIONS. All members of the Applied Computational Electromagnetics Society (ACES) who have paid their subscription fees are entitled to receive the ACES Journal with a minimum of two issues per calendar year. Current annual subscription fees are:

AREAS: *U.S. and Canada*: AIRMAIL: $55 Individual, $105 Organizational, SURFACE MAIL N/A; *Mexico, Central & So. America*: AIRMAIL: $60 Individual, $115 Organizational, SURFACE MAIL: $58; *Europe, Former USSR, Turkey, Scandinavia*, AIRMAIL: $68 Individual, $115 Organizational, SURFACE MAIL: $58; *Asia, Africa, Middle East and Pacific Rim*: AIRMAIL: $75 Individual, $115 Organizational, SURFACE MAIL: $58. FULL-TIME STUDENTS: $25.00. REMIT BY: (1) BANK DRAFTS (MUST BE DRAWN ON U.S. BANK), (2) INTERNATIONAL MONEY ORDER, (3) TRAVELER'S CHECKS IN U.S. DOLLARS, (4) ELECTRONIC TRANSFER, (CONTACT ACES SECRETARY).

Back issues, when available, are $15.00 each. The Special Issue on Canonical Problems is $15.00. Subscriptions to ACES, orders for back issues of the ACES Journal and changes of addresses should be sent to:

Dr. Richard Adler
ACES Secretary
Naval Postgraduate School
Code EC/AB
Monterey, CA 93943 USA
Fax: (408) 649-0300

Allow four week's advance notice for change of address. Claims for missing issues will not be honored because of insufficient notice of address change or loss in mail unless the secretary is notified within 60 days for USA and Canadian subscribers or 90 days for subscribers in other countries, from the last day of the month of publication. For information regarding reprints of individual papers or other materials, see "Information for Authors".

LIABILITY. Neither ACES or the ACES Journal editors are responsible for any consequence of misinformation or claims, express or implied, in any published material in an ACES Journal issue. This also applies to advertising, for which only camera-ready copies are accepted. Authors are responsible for information contained in their papers. If any material submitted for publication includes material which has already been published elsewhere, it is the author's responsibility to obtain written permission to reproduce such material.

APPLIED COMPUTATIONAL ELECTROMAGNETICS SOCIETY

Journal

Summer 1992
Vol. 7 No. 1

ISSN 1054-4887

The ACES Journal is abstracted in INSPEC, in Engineering Index, and in DTIC.

The first, third, fourth, and fifth illustrations on the front cover have been obtained from Lawrence Livermore National Laboratory.

The second illustration on the front cover has been obtained from FLUX2D software --CEDRAT S.A. France -- MAGSOFT Corporation, New York.

THE APPLIED COMPUTATIONAL ELECTROMAGNETICS

SOCIETY JOURNAL

EDITORS

THE APPLIED COMPUTATIONAL ELECTROMAGNETICS

SOCIETY JOURNAL

Vol. 7 No. 1 Summer 1992

TABLE OF CONTENTS

ELECTROMAGNETIC SCATTERING FROM RADIALLY OR AXIALLY INHOMOGENEOUS OBJECTS

Ahmed A. Kishk
Department of Electrical Engineering
University of Mississippi
University MS 38677

Mohamed Abouzahra
Massachusetts Institute of Technology
Lincoln Laboratory
Lexington, MA 02173

ABSTRACT

A computer program based on the method of moments approach is developed to compute electromagnetic scattering from axisymmetric objects. The object may consist of N linear isotropic homogeneous regions. These regions may be arranged axially and/or radially with the axis of symmetry. Surface integral equations (SIE) formulation, E-PMCHW, is used to formulate the problem. Other formulations can easily be incorporated in the computer code. Bistatic and monostatic Radar Cross Sections (RCS) for several benchmark geometries are computed. The computed results are verified by comparison with measured and exact calculated results. In some cases the self-consistency method is used to perform the verification. The measured and calculated data presented in this paper are expected to serve as benchmarks for other researchers in the field.[1]

I INTRODUCTION

The study of electromagnetic scattering from composite materials has become of interest to many engineering societies. For example, in biomedicine modeling of human bodies and tissues requires very complex composite objects. With the relative increase in the complexity of the objects of interest, numerical solutions become necessary to study the electromagnetic characteristics of these objects. Various numerical methods can be used to solve such problems

1 This work was sponsored by the Department of the Air Force. The views expressed are those of the authors and do not reflect the official policy or position of the US Government.

[1-6], however, each method has limitations.

The method of moments has been proven to be efficient in solving Surface Integral Equations (SIE). The SIE formulation is most suitable for objects made of linearly isotropic homogeneous materials. For inhomogeneous objects, other formulations may be used, such as the Volume Integral Equations (VIE) or Partial Differential Equations (PDE) formulations. However, if the inhomogeneity of the material is simple, the use of SIE may be preferred, because the matrix size will be smaller using SIE than the matrices that can be obtained from other formulations.

In this paper, the SIE formulation is used to assess the problem of electromagnetic scattering from bodies of revolution made of multihomogeneous regions. The present formulation is similar to the one given in [1]. The method of moments is used to solve the SIE. The resulting matrix system is a buildup of the basic Z and Y matrix obtained for conducting or dielectric bodies of revolution [7-8]. The computer program that has been developed to compute the bistatic or monostatic Radar Cross Sections (RCS) is tested and verified, and several examples are selected to show the accuracy of this program in predicting RCS. Only one formulation is discussed; however, the program has been written to implement easily other surface formulations, such as those reported in [9]. Also, the program is written to efficiently fill the matrix. The properties of symmetry in reference to the impedance and admittance matrices that are used to build the final matrix are implemented. All the numerical results presented in this paper are obtained by the same program (MRBOR) to show its flexibility and generality.

II DEVELOPMENT OF THE SIE

a. Statement of the Problem:

In this section, the concept of the equivalence principle is used to derive the SIE formulation for composite scatterers with N homogeneous regions. The geometry and notations for such a scatterer are given in Fig. 1. The whole space is divided into N+1 homogeneous regions with permittivities ϵ_i and permeabilities μ_i, i = 0, 1, 2, ..., N. Lossy materials are considered by allowing ϵ_i, μ_i, i = 1, 2, ..., N to be complex. Some homogeneous regions are considered to be perfect conductors. The region V_i is surrounded by a closed surface S_i and recognized by the inward normal unit vector **n**. The surface interface between regions V_i and

V_j is S_{ij}, $i \neq j$. Thus, S_i is the set of all interface surfaces S_{ij}, where j represents all region numbers interfacing with region V_i. Note that S_{ij} is the same surface as S_{ji}; however, the normal unit vectors $\mathbf{n}_i$ and $\mathbf{n}_j$ are in opposite directions to each other on S_{ij}.

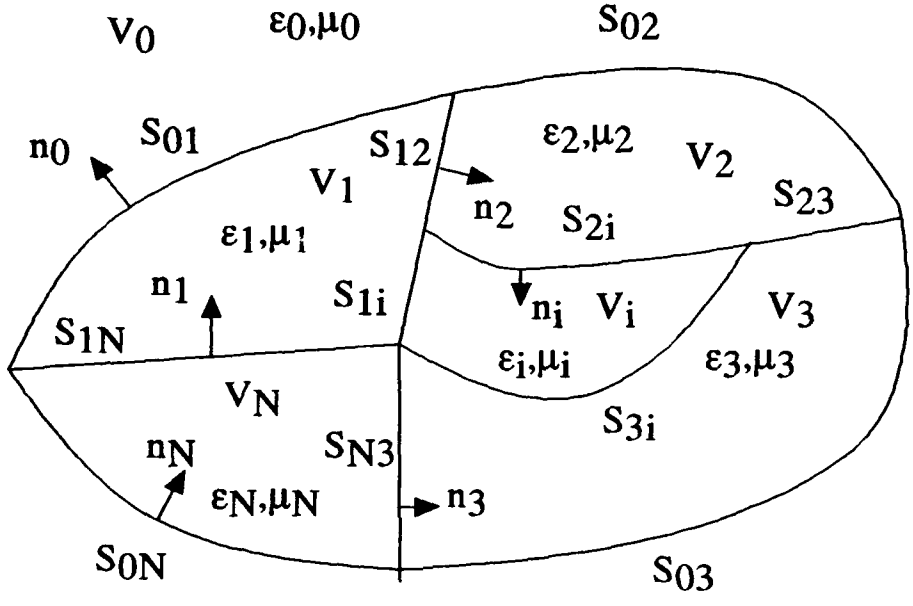

Fig. 1. General geometry of an object consisting of N regions.

b.SIE Formulation:

The total fields in each homogeneous region are denoted by $\mathbf{E}_i$ and $\mathbf{H}_i$, i = 0, 1, 2, ..., N for the electric and magnetic fields, respectively. If V_i is a perfectly conducting region, the fields are equal to zero. In the free-space region V_0, the total fields ($\mathbf{E}_0$, $\mathbf{H}_0$) are the summation of the incident and scattered fields ($\mathbf{E}^{inc} + \mathbf{E}^{sc}$, $\mathbf{H}^{inc} + \mathbf{H}^{sc}$). From Maxwell's equations and the equivalence principle, one can express the field in each region in terms of unknown electric- and magnetic-equivalent surface currents. In this paper, the sources of excitation are considered to be due to a plane wave in the free space region; therefore, the fields at any observation point $\mathbf{r}$ in the free space can be expressed as [1] (these expressions are given here for convenience)

$$\theta(\mathbf{r})\,\mathbf{E}_0(\mathbf{r}) = \mathbf{E}^{inc} - L^0_{S_0}\mathbf{J}_0(\mathbf{r}') + \kappa^0_{S_0}\mathbf{M}_0(\mathbf{r}') \tag{1}$$

$$\theta(\mathbf{r})\,\mathbf{H}_0(\mathbf{r}) = \mathbf{H}^{inc} - \kappa^0_{S_0}\,\mathbf{J}_0(\mathbf{r}') - (1/\eta_0^2)\,L^0_{S_0}\,\mathbf{M}_0(\mathbf{r}') \tag{2}$$

and

$$\theta(\mathbf{r})\ \mathbf{E}_i(\mathbf{r}) = -L^i_{S_i}\ \mathbf{J}_i(\mathbf{r}') + \kappa^i_{S_i}\ \mathbf{M}_i(\mathbf{r}') \tag{3}$$

$$\theta(\mathbf{r})\ \mathbf{H}_i(\mathbf{r}) = -\kappa^i_{S_i}\ \mathbf{J}_i(\mathbf{r}') - (1/\eta_i^2)\, L^i_{S_i}\ \mathbf{M}_i(\mathbf{r}') \tag{4}$$

in the region V_i, where i = 1, 2, ... N. Time variation of $e^{j\omega t}$ is implied and suppressed throughout. The electric- and magnetic-surface currents along the boundaries are

$$\begin{aligned} \mathbf{J}_i &= \mathbf{n}_i \times \mathbf{H}_i \\ \mathbf{M}_i &= -\mathbf{n}_i \times \mathbf{E}_i \end{aligned} \qquad \text{on } S_i \tag{5}$$

In these equations, $\eta_i = \eta_0 \sqrt{\mu_{ir}/\epsilon_{ir}}$, $\epsilon_i = \epsilon_0\ \epsilon_{ir}$, $\mu_i = \mu_0\mu_{ir}$, ϵ_{ir} and μ_{ir} are the relative permittivity and permeability in the region V_i, and η_0 is the intrinsic impedance of the free space. The operators L^i_S and κ^i_S are defined as

$$L^i_{S_i}\mathbf{C}_i(\mathbf{r}') = j\omega\mu_i \int_{S_i} [\mathbf{C}_i(\mathbf{r}') + (1/\omega^2\epsilon_i\mu_i)\ \nabla\nabla'.\mathbf{C}_i(\mathbf{r}')]\Phi_i\, dS' \tag{6}$$

$$\kappa^i_{S_i}\ \mathbf{C}_i\ (\mathbf{r}') = \int_{S_i} \mathbf{C}_i\ (\mathbf{r}') \times \nabla\ \Phi_i\ dS' \tag{7}$$

where $\mathbf{C}_i(\mathbf{r}')$ represents the currents $\mathbf{J}_i$ or $\mathbf{M}_i$. For $\mathbf{r} = \mathbf{r}'$, the operators are interpreted as Cauchy principal-value integrals. Φ_i is the Green's function of unbounded region, which can be represented as

$$\Phi_i\ (\mathbf{r} - \mathbf{r}') = e^{-jk_i|\mathbf{r} - \mathbf{r}'|}/|\mathbf{r} - \mathbf{r}'| \tag{8}$$

where k_i is the wave number of the region i, which is equal to $\omega\sqrt{\epsilon_i\mu_i}$. In Equations (1) to (4) the value of $\theta(\mathbf{r})$ is constant, depending on the position of $\mathbf{r}$ as

$$\theta(\mathbf{r}) = \begin{Bmatrix} 1 \text{ for } \mathbf{r} \in V_i \\ 1/2 \text{ for } \mathbf{r} \in S_i \\ 0 \text{ elsewhere} \end{Bmatrix} \tag{9}$$

Applying the boundary conditions on each S_{ij} yields a set of coupled integral equations for the unknown electric and magnetic currents on these surfaces. On the dielectric interfaces, the tangential fields are continuous. Thus,

$$\mathbf{E}_i|_{tan} = \mathbf{E}_j|_{tan} \quad \text{on } S_{ij} \tag{10}$$

$$\mathbf{n}_i \times \mathbf{H}_i = \mathbf{n}_i \times \mathbf{H}_j \quad \text{on } S_{ij} \tag{11}$$

On the conductor interfaces, the tangential electric fields vanish, yielding

$$\mathbf{E}_i|_{tan} = \mathbf{0} \quad \text{on } S_{ij} \text{ (conductor surfaces)} \tag{12}$$

Substituting Equations (1) to (4) into (10) to (12), one obtains

$$[L^i_{S_i}\mathbf{J}_i - \kappa^i_{S_i}\mathbf{M}_i - L^j_{S_j}\mathbf{J}_j + \kappa^j_{S_j}\mathbf{M}_j]_{tan} = \begin{Bmatrix} \mathbf{0} \text{ i nor j} = 0 \\ \mathbf{E}^{inc}_{tan} \text{ i or j} = 0 \end{Bmatrix} \quad \text{on } S_{ij} \tag{13}$$

$$\mathbf{n}_i \times [\kappa^i_{S_i}\mathbf{J}_i + (1/\eta_i^2)\, L^i_{S_i}\mathbf{M}_i] - \mathbf{n}_i \times [\kappa^j_{S_j}\mathbf{J}_j + 1/\eta_j^2\, L^j_{S_j}\mathbf{M}_j] = \begin{Bmatrix} \mathbf{0} \text{ i nor j} = 0 \\ \mathbf{n}_i \times \mathbf{H}^{inc} \text{ i or j} = 0 \end{Bmatrix} \quad \text{on } S_{ij} \tag{14}$$

$$[L^i_{S_i}\mathbf{J}_i - \kappa^i_{S_i}\mathbf{M}_i]_{tan} = \begin{Bmatrix} \mathbf{0} \text{ i nor j} = 0 \\ \mathbf{E}^{inc}_{tan} \text{ i or j} = 0 \end{Bmatrix} \quad \text{on } S_{ij} \tag{15}$$

To enable the reader to have better understanding of Equations (13) to (15) (which yield a coupled system of integral equations), a specific example will be considered. Consider a scatterer consisting of two dielectric regions attached to a perfectly conducting body, all in free space, as shown in Fig. 2. The boundary conditions in integral forms are

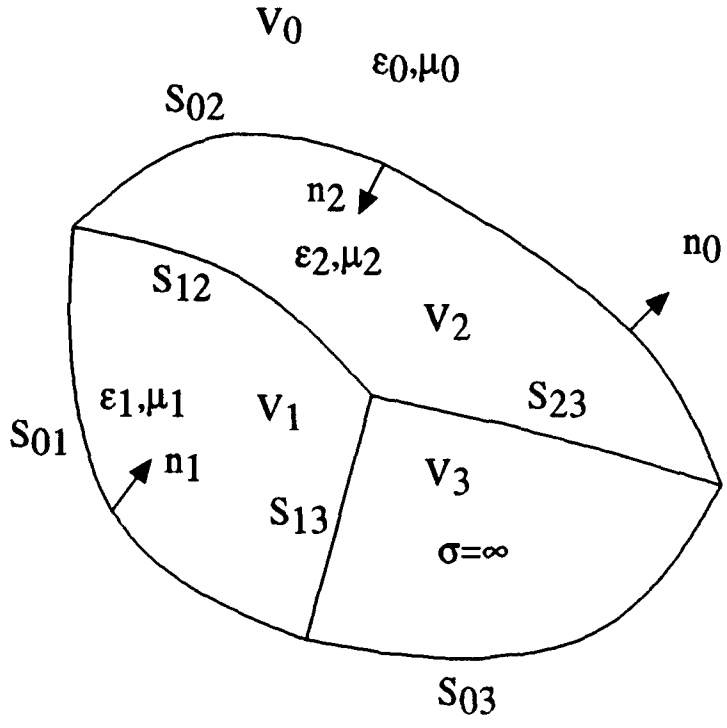

Fig. 2. Example of a three regions object.

$$[L^0_{S_0} J_0 - \kappa^0_{S_0} M_0 - L^1_{S_1} J_1 + \kappa^1_{S_1} M_1]_{tan} = E^{inc}_{tan} \quad \text{on } S_{01} \tag{16}$$

$$\begin{aligned} n_0 \times [\kappa^0_{S_0} J_0 + (1/\eta_0^2) L^0_{S_0} M_0] - n_0 \times [\kappa^1_{S_1} J_1 + (1/\eta_1^2) L^1_{S_1} M_1] \\ = n_0 \times H^{inc} \quad \text{on } S_{01} \end{aligned} \tag{17}$$

where

$$\begin{aligned} J_0 &= (J_{01}, J_{02}, J_{03}) \\ J_1 &= (-J_{01}, J_{12}, J_{13}) \\ M_0 &= (M_{01}, M_{02}) \\ M_1 &= (-M_{01}, M_{12}) \end{aligned} \tag{18}$$

$$[L^0_{S_0} J_0 - \kappa^0_{S_0} M_0 - L^2_{S_2} J_2 + \kappa^2_{S_2} M_2]_{tan} = E^{inc}_{tan} \quad \text{on } S_{02} \tag{19}$$

$$\begin{aligned} n_0 \times [\kappa^0_{S_0} J_0 + (1/\eta_0^2) L^0_{S_0} M_0] - n_0 \times [\kappa^2_{S_2} J_2 + (1/\eta_2^2) L^2_{S_2} M_2] \\ = n_0 \times H^{inc} \quad \text{on } S_{02} \end{aligned} \tag{20}$$

where

$$\begin{aligned} J_2 &= (-J_{02}, J_{12}, J_{23}) \\ M_2 &= (-M_{02}, -M_{12}) \end{aligned} \tag{21}$$

$$[L^0_{S_0} J_0 - \kappa^0_{S_0} M_0]_{tan} = E^{inc}_{tan} \quad \text{on } S_{03} \tag{22}$$

$$[L^1_{S_1} J_1 - \kappa^1_{S_1} M_1 - L^2_{S_2} J_2 + \kappa^2_{S_2} M_2]_{tan} = E^{inc}_{tan} \quad \text{on } S_{12} \tag{23}$$

$$\begin{aligned} n_1 \times [\kappa^1_{S_1} J_1 + (1/\eta_1^2) L^1_{S_1} M_1] - \hat{n}1 \times [\kappa^2_{S_2} J_2 + (1/\eta_2^2) L^2_{S_2} M_2] \\ = n_1 \times H^{inc} \quad \text{on } S_{12} \end{aligned} \tag{24}$$

$$[L^1_{S_1} J_1 - \kappa^1_{S_1} M_1]_{tan} = E^{inc}_{tan} \quad \text{on } S_{13} \tag{25}$$

$$[L^2_{S_2} J_2 - \kappa^2_{S_2} M_2]_{tan} = E^{inc}_{tan} \quad \text{on } S_{23} \tag{26}$$

These are nine vectorial equations in nine vectorial unknowns. The unknowns are the electric- and magnetic-surface currents J_{01}, J_{02}, J_{03}, J_{12}, J_{13}, J_{23}, M_{01}, M_{02}, and M_{12}. The integral equations are reduced to matrix equations using the method of moments by using triangle testing and triangle expansion functions [8].

The above surface integral equations are applied to rotationally-symmetric bodies. The reduction of the integral equations to matrix equations involving unknown surface currents follows a well-known procedure [9]. After the necessary manipulations of the method of moments, the general matrix takes the form

$$[\ T\ ]_n\ [I]_n\ =\ [V]_n \tag{27}$$

where T is a square matrix, representing a combination of impedance and admittance submatrices that are given in [9]; I_n is a column matrix for the unknown expansion coefficients of the unknown current components J and M; and V_n is the excitation column matrix. Once the matrix is solved, the induced currents on all surface interfaces can be determined. Scattered far fields can be determined from the induced currents on the outer surfaces.

III RESULTS AND DISCUSSION

a. Bistatic RCS:

In this section the bistatic RCS is computed numerically. The numerical results are verified by comparison with analytical and supplemental numerical results.

Dielectric sphere: First, to verify the numerical results of objects made of more than one homogeneous region, the example of a sphere geometry is considered. The series solution for a dielectric sphere [10] having ϵ_r= 4-j0.5, μ_r= 2-j0.25, and ka=3 is obtained and compared with the numerical solution of the same object when it is divided into three homogeneous regions of the same material type. The results obtained from both solutions must be identical, because physically both cases represent the same object. The agreement between the two solutions is excellent, as shown in Fig. 3. Several spherical objects have been considered, such as the coated sphere and the multilayered sphere; however, their results have been omitted for brevity.

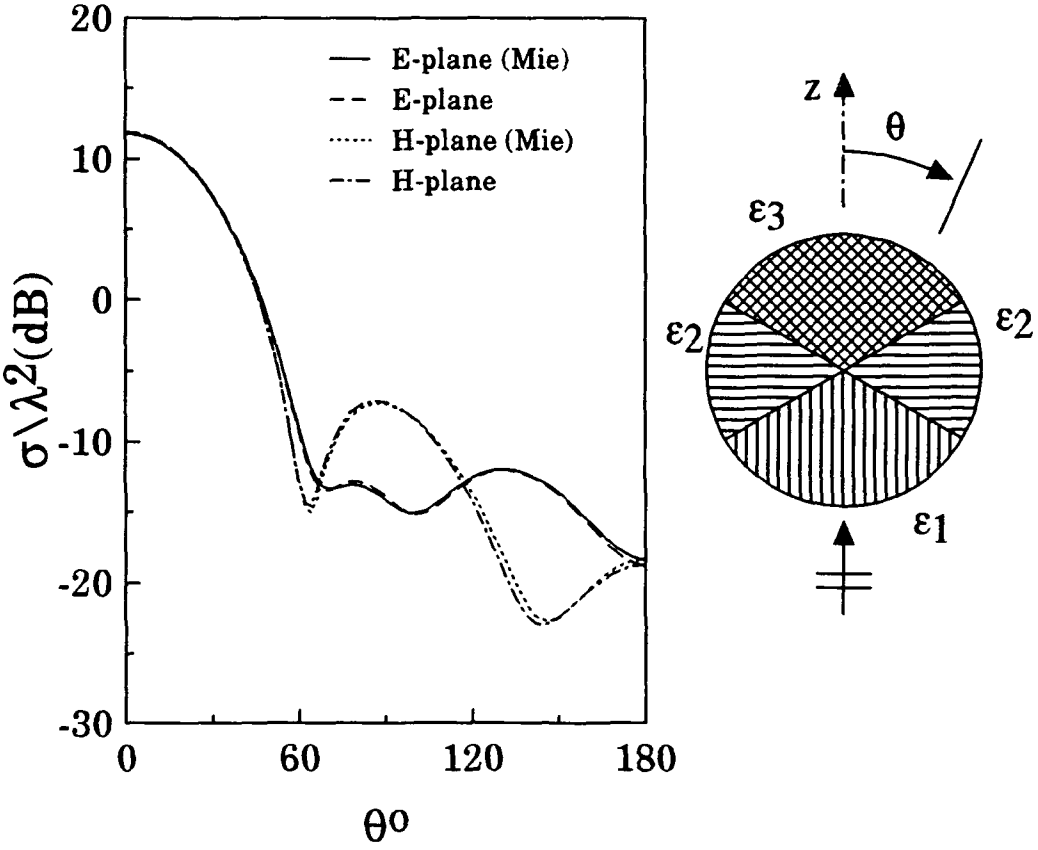

Fig. 3. Bistatic RCS of dielectric sphere divided into three regions of the same materials, ϵ_r=4-j0.5, μ_r=2-j0.25, and ks=3.

Dielectric toroid: Another geometry, of a dielectric toroid, is considered, as shown in Fig.4a. The numerical solution is obtained, once, when the circular cross section is divided into six regions, all of which have the same type of material. This numerical solution is compared with the numerical solution of the same object when it is treated as one region. The agreement between both solutions is excellent, as shown in Fig.4b. When each region is filled with different homogeneous materials, the computed bistatic RCS is shown in Fig. 5. Notice that the scattering level has increased in the whole bistatic range.

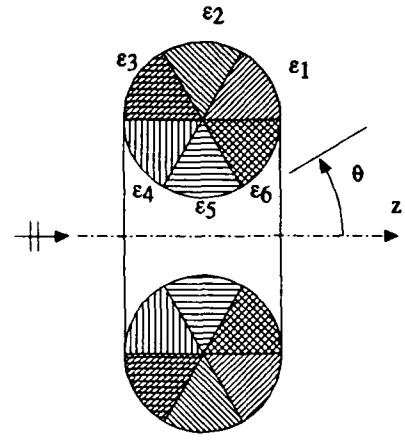

Fig. 4a. Toroid cross section divided into six homogeneous regions.

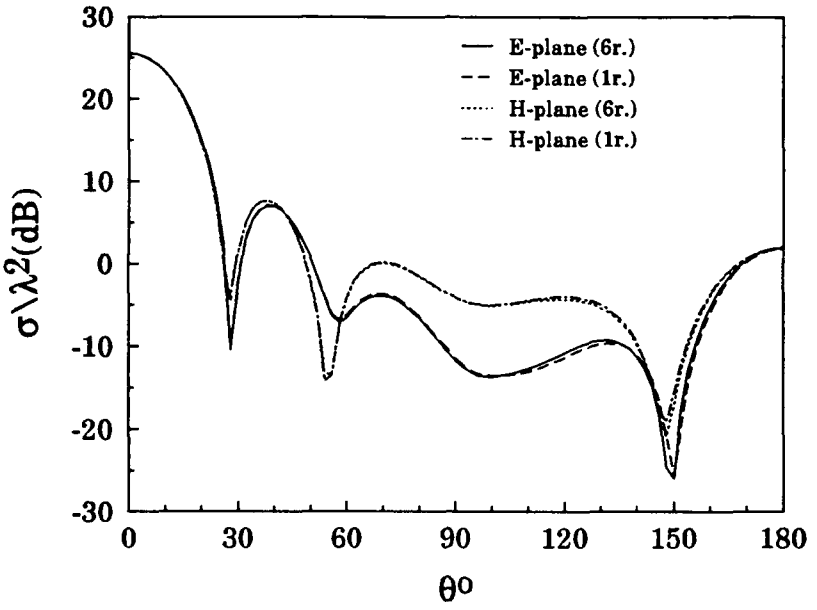

Fig. 4b. Bistatic RCS of the toroid when all regions have the same materials, ϵ_r=4-j0.5, μ_r=2-j0.25, ka=3, kb=4.4.

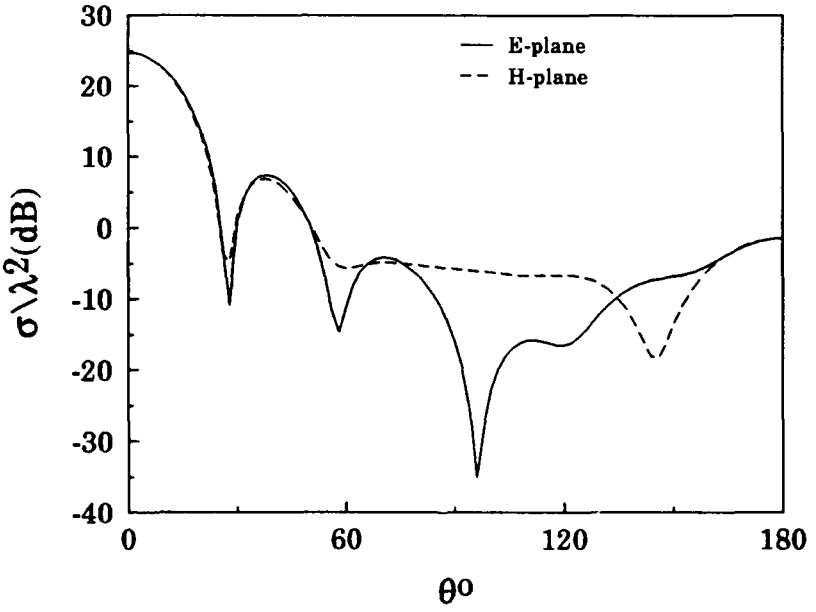

Fig. 5. Bistatic RCS of the toroid with, ϵ_{r1}=3-j3, ϵ_{r2}=2-j2, ϵ_{r3}=4-j0.5, ϵ_{r4}=6-j6, ϵ_{r5}=5-j5, ϵ_{r6}=4-j4, and μ_r=2-j0.25 in all regions.

Loaded conducting bicone: To examine the numerical solution performance of objects made of dielectric and conductors, the case of a biconical conducting object is selected. The numerical solution of this object and the conducting bicone is compared with the numerical solution of a conducting bicone surrounded by an artificial dielectric material of free-space permittivity and permeability, as shown in Fig. 6. In this example, the bicone is illuminated by a plane wave of normal incidence (θ=90°). Therefore, the number of the azimuthal modes that is used to obtain the bistatic RCS is eleven, n=0,..., $\pm$5; for the axial incident cases the required modes are $\pm$1. Figure 6 shows the excellent agreement between the two solutions. Also shown is the symmetry around θ=90°. In this example, the H-plane shows a zero-back and forward-scattering, and the E-plane shows its maximum values at these directions. When the free-space part of this object is filled with homogeneous materials of ϵ_r = 4, the RCS is computed as shown in Fig. 7. The sidelobes of the scattered H-plane patteren disappear, and the forward scattering for the E-plane pattern becomes higher than the back-scattering.

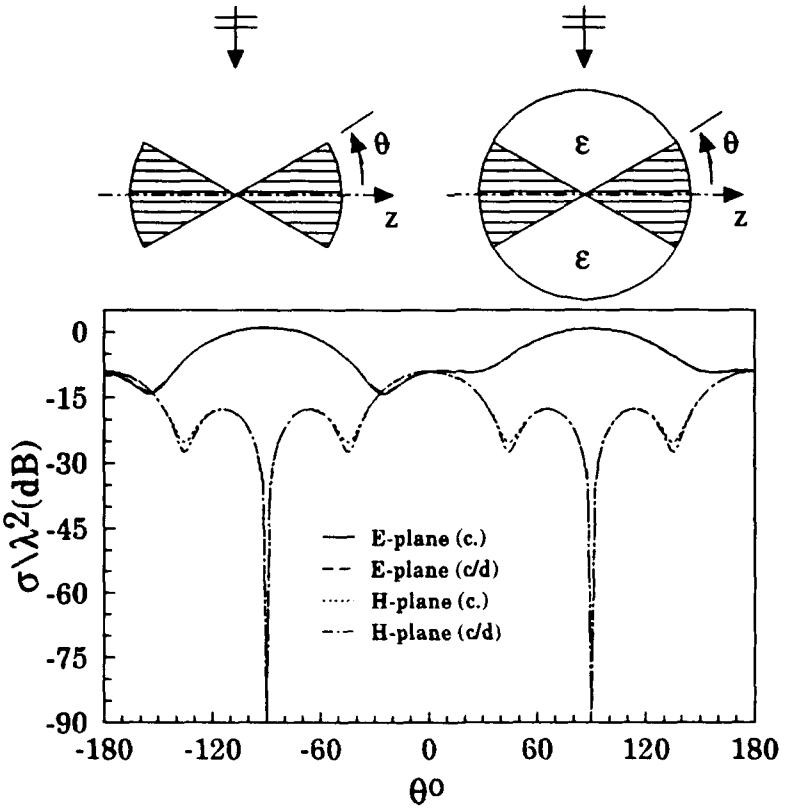

Fig. 6. Bistatic RCS of a conducting bicone, ka=3, ϵ_r=1., μ_r=1.

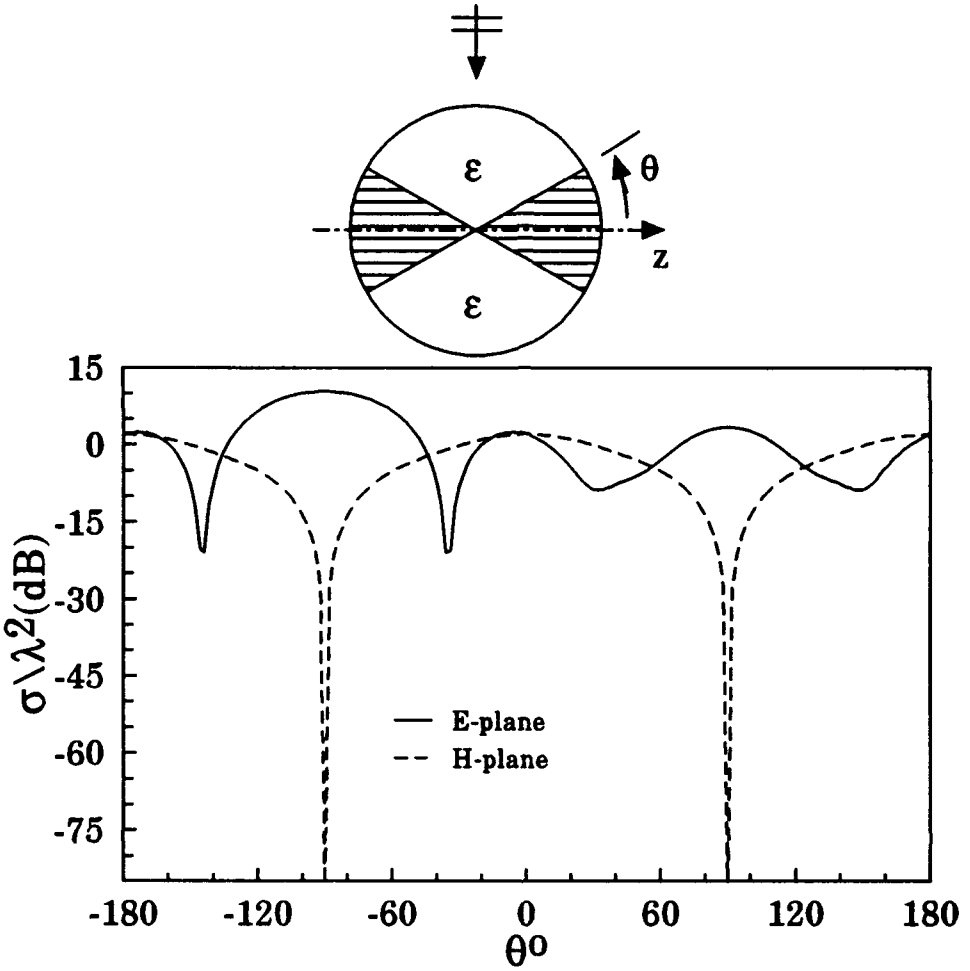

Fig. 7. Bistatic RCS of the bicone when ϵ_r=4., μ_r=1.

b. Monostatic RCS:

In the above examples, the bistatic RCS were considered. Next monostatic RCS are also verified numerically and experimentally.

Half-conducting sphere: The first example is the perfectly-conducting dielectric hemisphere. For numerical verification, the dielectric is considered as a free space. The monostatic RCS is compared with the numerical solution of a conducting hemisphere, as shown in Fig. 8. This figure indicates excellent agreement between both solutions in the whole θ range. When the free-space part is replaced by materials of ϵ_r=2-j0.5, and μ_r=3-j0.5, the monostatic RCS is computed as shown in Fig. 9. The effect of the presence of dielectric materials

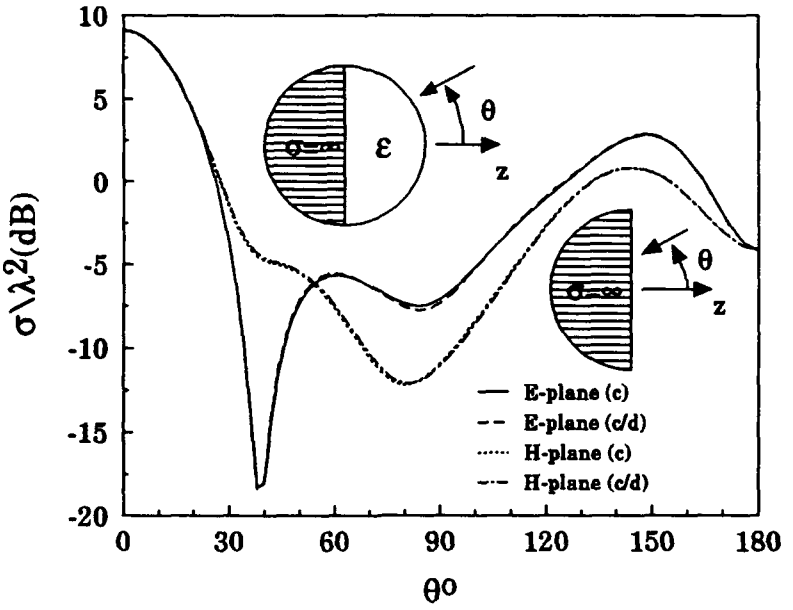

Fig. 8. Monostatic RCS of a conducting hemisphere compared with the scattering from a conducting hemisphere-air hemisphere object, ka=3.

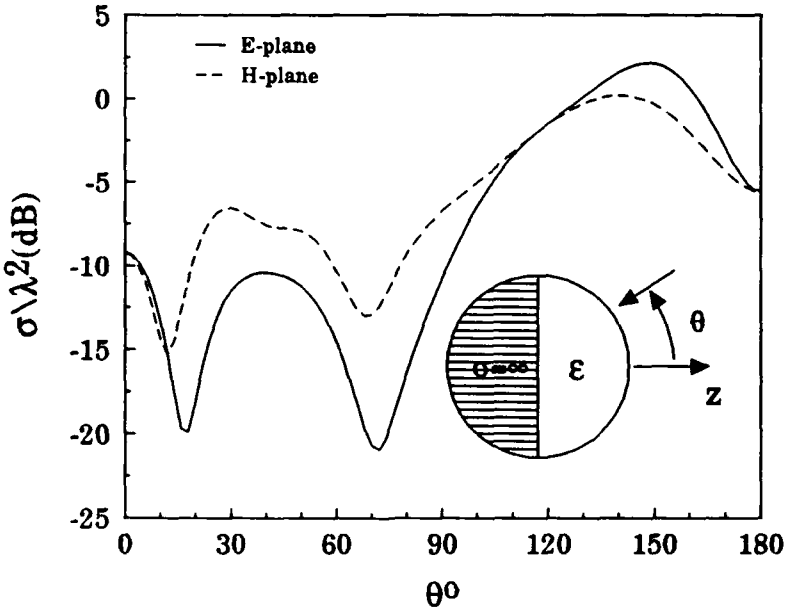

Fig. 9. Monostatic RCS of a conducting hemisphere-dielectric hemisphere object, ka=3, ϵ_r=2-j0.5, μ_r=3-j0.5.

is different from the free space. This difference is clear in the backscattering data for ranges of $\theta<90$, which is the dielectric side. Significant reduction of the backscattering level is observed. When $\epsilon_r=1$, the effect of the flat surface and the sharp edges obviously contributed to the high backscattering levels.

Round-tip cone: In this section, new numerical results are presented and verified with measurements, which have been collected at the RCS Range of Group 95 at Lincoln Laboratory. The first geometry that is considered is the partially coated, perfectly conducting round-tip cone, shown in Fig. 10. The first case that has been considered is the one that corresponds to a homogeneous coating; in other words, the materials in both coating regions are the same. The monostatic RCS are shown in Fig. 11 for both $\theta\theta$ polarization (left) and $\phi\phi$ polarization (right), respectively. When the coating on the second region is removed, the second region is then equivalent to free-space permittivity. The monostatic RCS is computed and compared with the measurements as shown in Fig. 12 for $\theta\theta$ polarization and $\phi\phi$ polarization, respectively. Figure 13 show the monostatic RCS of both polarizations when second region is filled with materials of $\epsilon_r=2.60$. In the above three cases, excellent agreement is obtained between the measured data and the computed data.

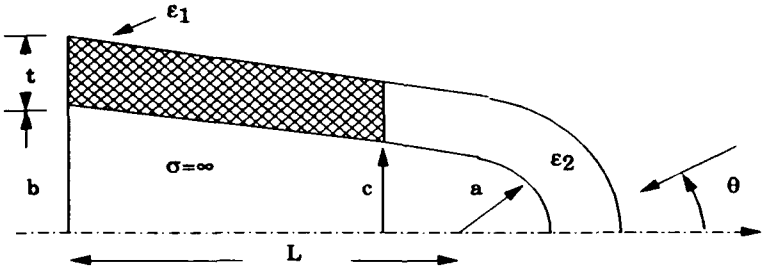

All dimensions in λ_0 (free space wavelength)

L = 1.978, b = 0.2328, a = 0.0424, t = 0.0847 c = 0.86

case	ϵ_{r1}	ϵ_{r2}
1	2.05	2.05
2	2.05	1.00
3	2.05	2.60

Fig. 10. Geometry of a partially coated, perfectly conducting round-tip cone.

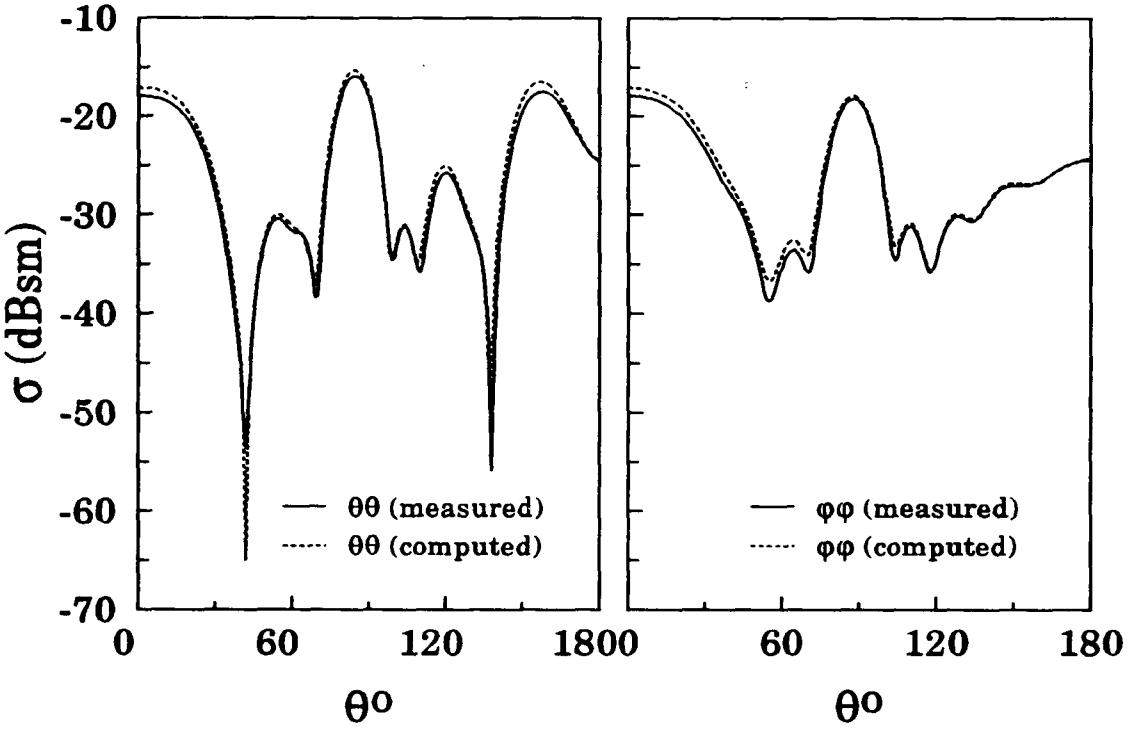

Fig. 11. Computed and measured monostatic RCS of case1 in Fig. 10.

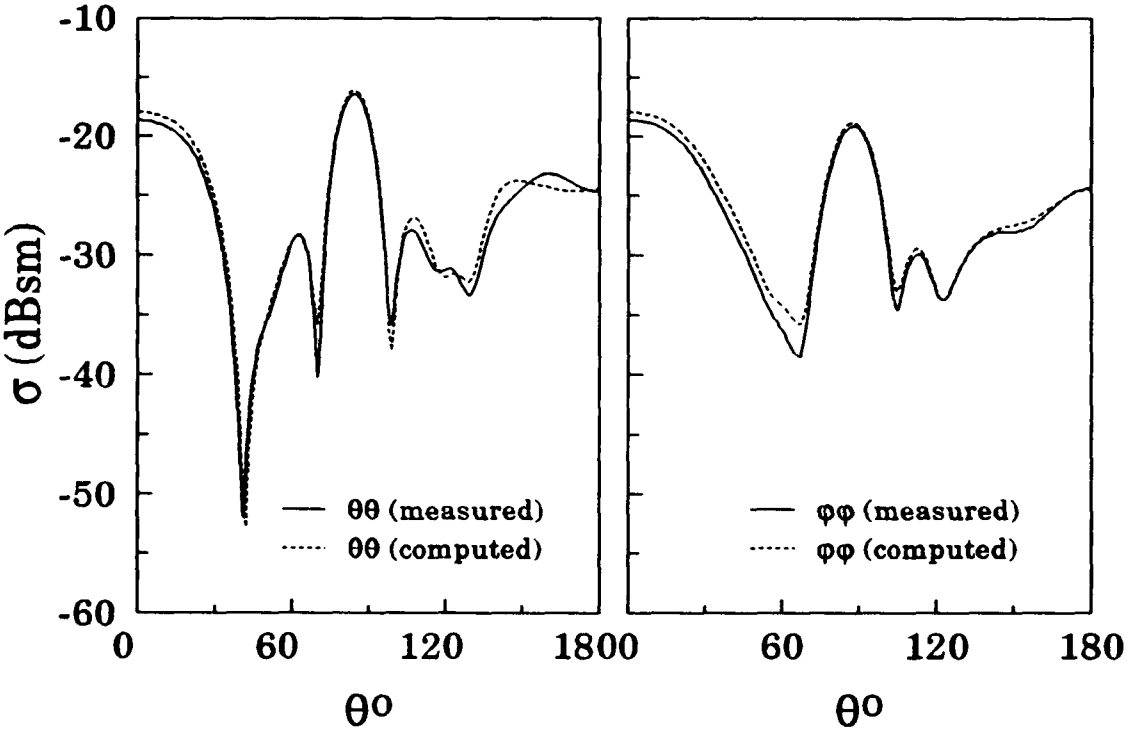

Fig. 12. Computed and measured monostatic RCS of case2 in Fig. 10.

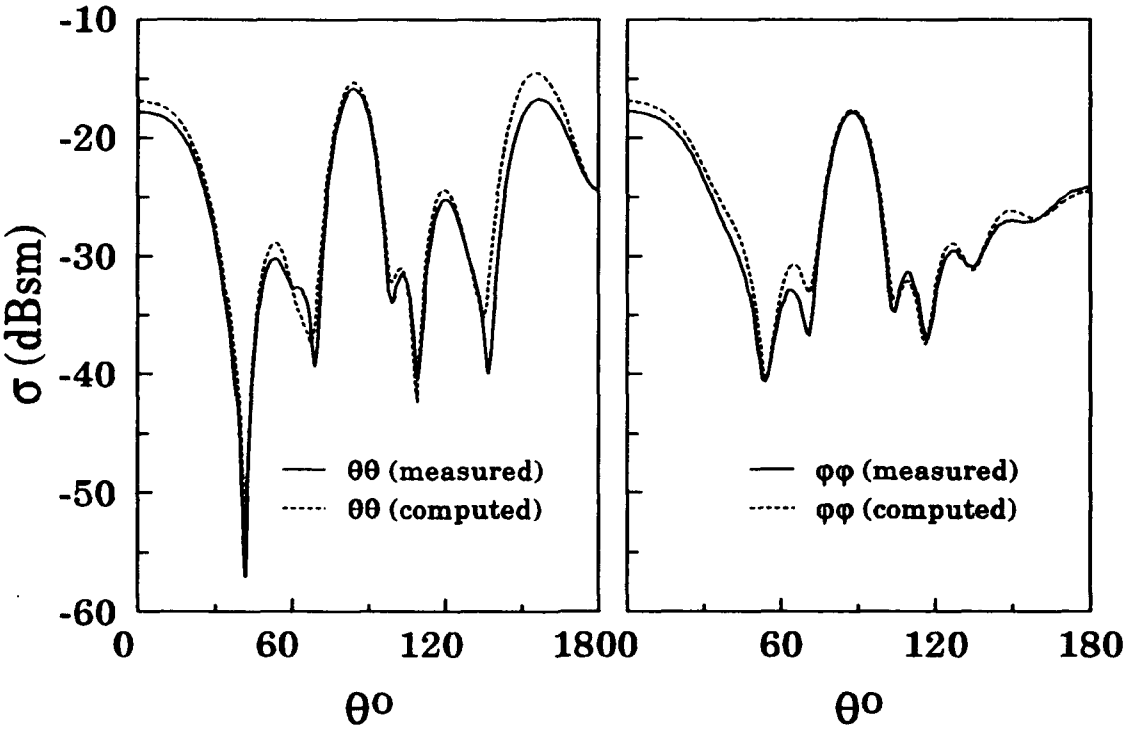

Fig. 13. Computed and measured monostatic RCS of case3 in Fig. 10.

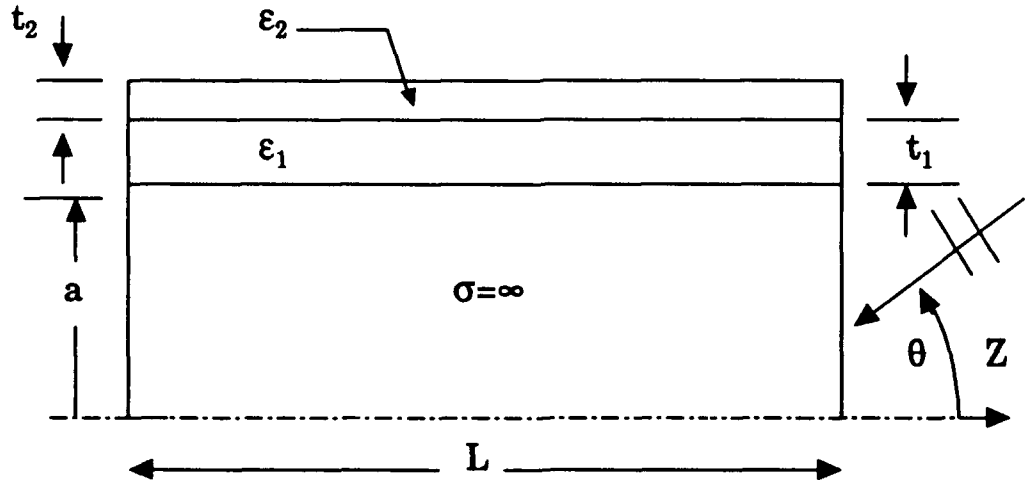

Fig. 14. Geometry of a perfectly-conducting cylinder partially coated with two dielectric layers

Finite cylinders: Another geometry, double layered coating of a finite conducting cylinder, is considered. Figure 14 shows the geometry of the cylinder. The values of the parameters of Fig. 14 are given in Table I for three cases. All the measurements in this section have been performed at 4GHz. Figure 15 (left) shows the comparison between the computed and measured data of the monostatic RCS for $\theta\theta$ polarization of case1 in Table I. In this case only one layer is considered.

Table I. Parameters of Figure 14

case	a(cm)	L(cm)	t_1(cm)	ϵ_{r1}	t_2(cm)	ϵ_{r2}
1	3.0	27.94	0.1528	35.2- j28.68	-	-
2	3.0	27.94	0.1528	35.2-j28.68	0.68	1.757-j1.569
3	2.814	21.59	0.988	2.05	0.1528	35.2-j28.68

The measured data of $\phi\phi$ polarization are not available, however, the computed data are shown in Fig. 15 (right). The monostatic RCS of the second case in Table I of the two layered coating is shown in Fig. 16. Again, only the measurements of the $\theta\theta$ polarization are available. In the last case, the first layer is a high loss material of large permittivity and the second one is high loss of small permittivity. In the third example of Table I, the first layer is made of a lossless material of small permittivity; the second layer is made of high-loss high-permittivity materials. The monostatic RCS is shown in Fig. 17 for the $\theta\theta$ and $\phi\phi$ polarization, respectively. The last three cases represent large objects. The agreement between the measured and computed data is satisfactory. In general, the above results show accuracy of the measurements within a wide dynamic range of sensitivity.

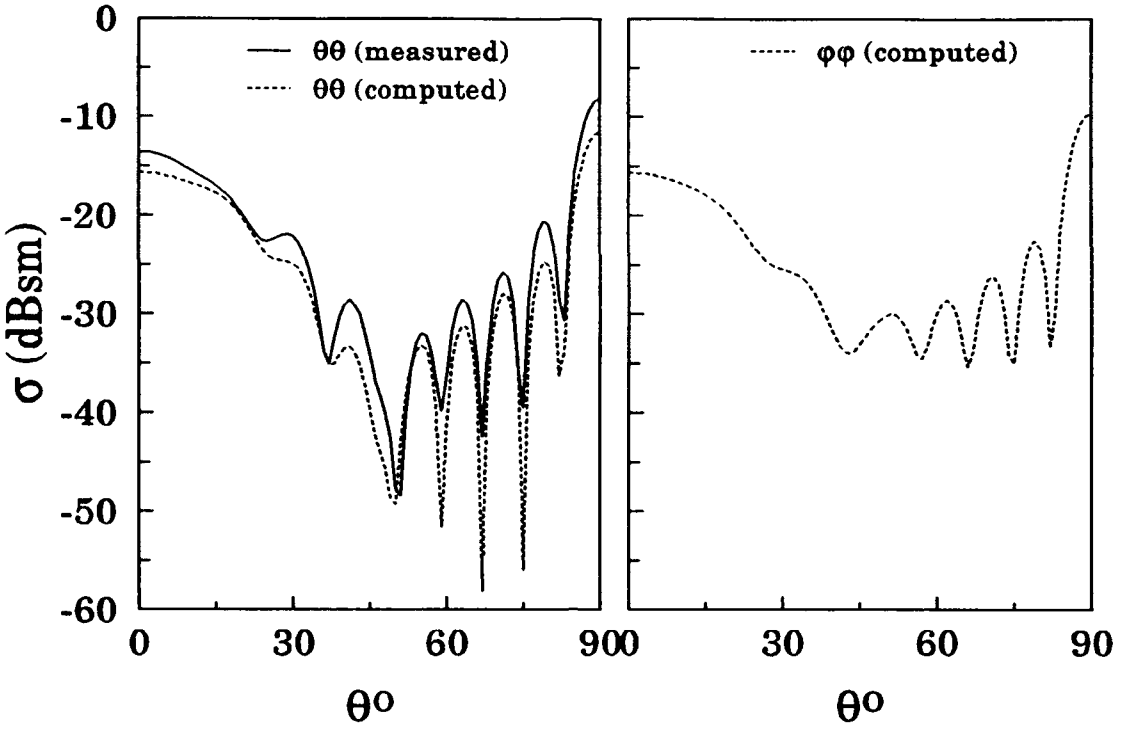

Fig. 15. Computed and measured monostatic RCS of case1 in Table I.

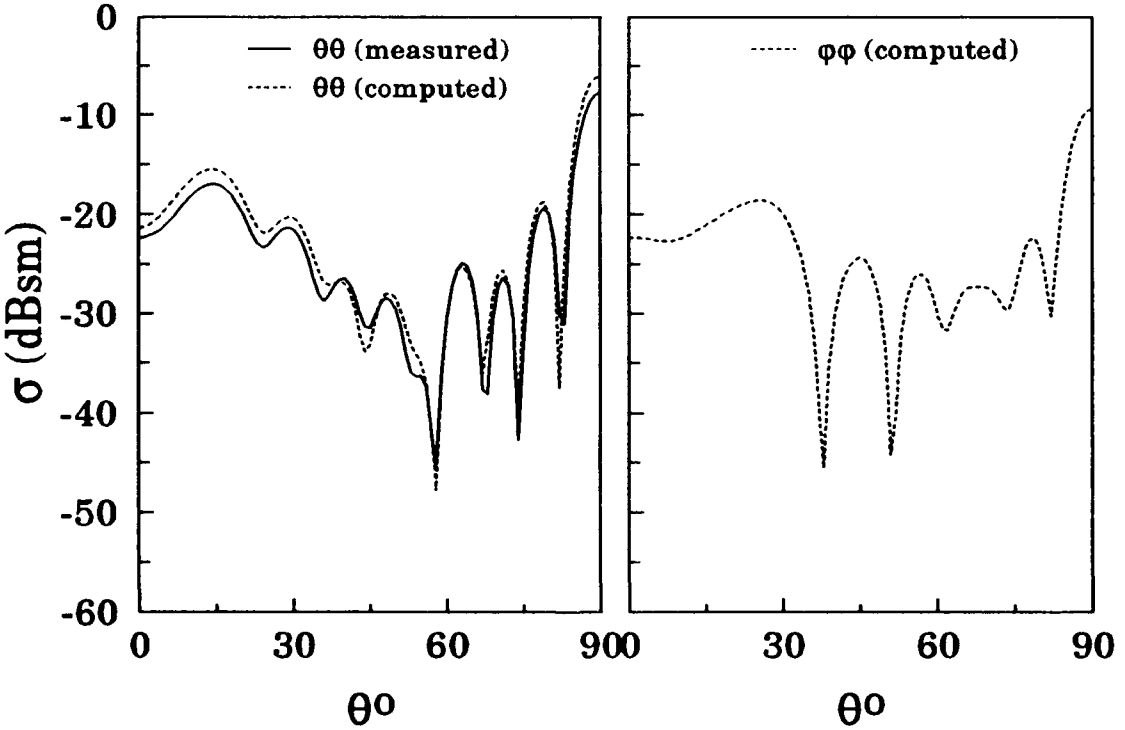

Fig. 16. Computed and measured monostatic RCS of case2 in Table I.

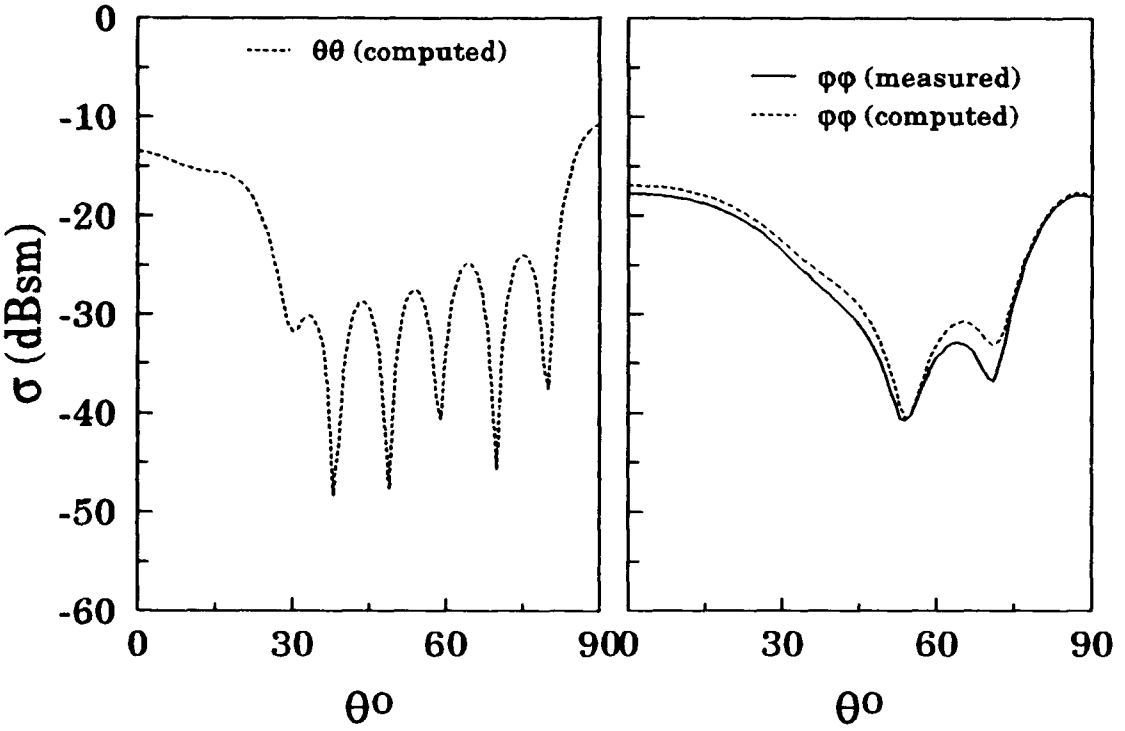

Fig. 17. Computed and measured monostatic RCS of case3 in Table I.

IV CONCLUSION

In this paper, a computer program has been developed to compute the electromagnetic scattering from axisymmetric objects. The method of moments is used to solve the surface-integral equations formulation (E-PMCHW). A number of objects has been analyzed by this program. Each object consisted of arbitrarily arranged homogeneous regions. Both bistatic and monostatic RCS data were presented. The computed data were verified either numerically or experimentally and excellent agreement was demonstrated.

REFERENCES:

[1] L. N. Medgyesi-Mitschang and J. M. Putnam, "Electromagnetic scattering from axially inhomogeneous bodies of revolution," *IEEE Trans. Antennas Propagat.*, vol. AP-32, p. 797, 1984.

[2] W. Zheng, "The null field approach to electromagnetic scattering from composite objects: The case with three or more constituents", *IEEE Trans. Antennas Propagat.*, vol. AP-36, p. 396, 1988.

[3] S. Storm and W. Zheng, "The null field approach to electromagnetic scattering from composite objects," *IEEE Trans. Antennas Propagat.*, Vol. AP-36, p. 376, 1988.

[4] M. A. Morgan and K. K. Mei, "Finite-element computation of scattering by inhomogeneous penetrable bodies of revolution," *IEEE Trans. Antennas Propagat.*, vol. AP-27, p. 202,1979.

[5] D. -S. Wang and P. W. Barber, "Scattering by inhomogeneous nonspheroidal objects," *Appl. Opt.*, vol. 18, p. 1190, 1979.

[6] A. W. Holt, "The Fredholm integral equation method and comparison with the T-matrix approach, " in *Acoustic, Electromagnetic and Elastic Wave Scattering: Focus on the T-matrix Approach*, V. V. and K. V. Varadan, Eds. London, U. K., Pergamon, p. 255, 1980.

[7] J. R. Mautz and R. F. Harrington, "Electromagnetic coupling to a conducting body of revolution with a homogeneous material region," *Electromagn.*, vol. 2, p. 257, 1982.

[8] J. R. Mautz and R. F. Harrington,"H-field E-field and combined field solutions for conducting bodies of revolution," *Arch. Elektron. Ubertragungstech.* vol. 32, pp. 159-164, 1978.

[9] A. A. Kishk and L. Shafai, "Different formulations for numerical solutions of single or multibodies of revolution with mixed boundary conditions," *IEEE Trans. Antennas Propagat.*, vol. AP-37, p. 666, 1986.

[10] M. Kerker, 'The scattering of light and other electromagnetic radiation', *Academic Press Inc.*, 1969 .

Application of Equivalent Edge Currents to Correct the Backscattered Physical Optics Field of Flat Plates

V. Stein

Institute for Radio Frequency Technology
German Aerospace Research Establishment
D-8031 Oberpfaffenhofen

Abstract

In the microwave case the physical optics (PO) method is frequently used for the analysis of complex structures which are modeled by flat plates of triangular or quadrangular shape. The study of the radar cross section (RCS) of an isolated panel, however, reveals deviations from experimental results which are due to edge diffraction effects not considered by PO. In order to correct the PO-field by an additive field term, the equivalent fringe currents (EC) of Michaeli have been used to derive the backscattering matrix of an isolated edge. By adding the matrices of the individual edges to the PO-matrix the RCS of a square flat plate with zero and finite thickness is analysed and the result is compared with measurements. The efficiency of the method is demonstrated for objects modeled by a higher number of panels and edges, namely a cylinder and a double dihedral. All computations were performed with the computer code SIG5 of the Institute.

1. Introduction

Since several years, the computer program SIG5 is applied in the Institute for Radio Frequency Technology for the prediction of the RCS of structures which are complicated in shape and large compared to the wavelength. SIG5, based on PO, is capable of analysing perfectly and imperfectly conducting structures, including double reflections. The targets are modeled by panels of triangular and quadrangular shape, see Fig. 1.1. The hidden surface problem inherent with PO is solved by an exact construction of the shadow boundary for each panel, whose size is only limited by the admissible deviation between the true surface and the model surface. SIG5 is organized in a very similar way to the computer code RECOTA, developed by the Boeing Aerospace Company, Seattle [1]. SIG5 has been successfully tested for a series of perfectly conducting basic structures such as a sphere, cylinder, cube, circular disk and a double dihedral [2-4]. Also, more complex bodies like a periscope structure have been analysed with promising results [5].

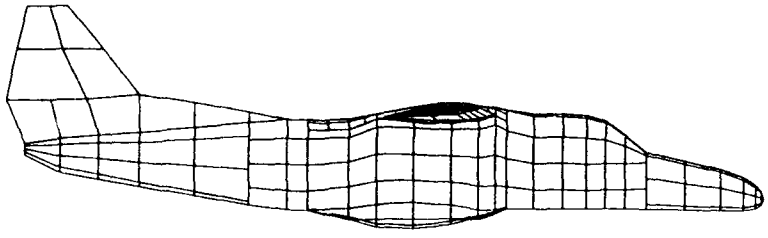

Fig. 1.1
Panel model of an airplane for the application of PO.

Despite the good results which are generally available with PO, there are special cases (certain structures, specific pattern cuts, selected polarizations) where deviations of practical significance between computational and experimental results are observed. They frequently can be explained by the feature of PO to treat the influence of an edge only as the geometrical boundary of a panel thus neglecting physical edge diffraction effects.

The choice of a theory which takes into account edge diffraction effects is influenced by the following viewpoints:

a) Since SIG5 is a very comprehensive computer code each extension should cause a minimum of changes. Therefore, theories are preferred which are able to correct the PO-solution by an additive term.

b) In computing the RCS of large and complex objects modeled by numerous panels the computer effort increases considerably. Therefore, theories which need a high computer effort are not favoured.

c) Since edges of arbitrary length, wedge angle and orientation in space occur in the target model, the theory should not present a solution for a specific panel, rather, the diffracted field of an isolated edge must be described by the specific edge parameters alone.

Bearing these points in mind, only asymptotic theories come into question, which either describe the difference between the total wedge diffracted field and the PO-field directly [6,7] or which evaluate fringe currents flowing along the edge and generating the same difference field by evaluating the radiation integral over the length of the edge [8, 9].

In this paper, the second theory is followed. Here the fringe currents given in [9] are preferred, since they are valid for arbitrary aspects of observation. On the basis of these currents, the backscattering matrix for an isolated edge is derived.

In the following section the theoretical background is discussed. In section 3, the theory is applied for the RCS-analysis of a panel. In section 4, the results for a cylinder and a double dihedral are presented. Section 5, finally, summarizes some conclusions on the basis of the preceeding analysis.

2. Theoretical Background

The results of the theories used in the computer code SIG5 are expressed by the backscattering matrix

$$(2.1) \qquad [T] = \begin{bmatrix} t_{11} & t_{12} \\ t_{21} & t_{22} \end{bmatrix},$$

which relates the cartesian components of the scattered field $\vec{E}_s$ to those of the incident field $\vec{E}_e$:

$$(2.2) \qquad \begin{bmatrix} E_{sx} \\ E_{sy} \end{bmatrix} = [T] \begin{bmatrix} E_{ex} \\ E_{ey} \end{bmatrix}.$$

The propagation direction of the scattered field is given by the z-axis (observer fixed coordinate system). From the complex elements t_{ij} of the scattering matrix the polarization dependent RCS is computed:

$$(2.3) \qquad \sigma_{ij} = \lim_{r\to\infty} (4\pi r^2\, t_{ij}\, t_{ij}^{*}) \ ,$$

where r is the distance between the radar observer and the test object. The RCS referred to 1 square meter and expressed in decibels yields the quantity dBsm, which is used in this paper to compare theoretical and experimental results for the selected transmitting/receiving polarizations.

The total scattering matrix [T] of a complex body can be thought to be composed of a matrix $[T^{PO}]$ which is the sum of the scattering matrices based on PO of the individual N panels and the scattering matrix $[T^{f}]$ which sums up the scattering matrices of the M edges of all panels:

$$(2.4) \qquad [T] = [T^{PO}] + [T^{f}] \ , \quad [T^{PO}] = \sum_{n}^{N} [T_n^{PO}] \ , \quad [T^{f}] = \sum_{m}^{M} [T_m^{f}] \ .$$

The PO-scattering matrix of an individual panel of zero thickness and perfect conductivity is readily evaluated using the radiation integral

$$(2.5) \qquad \vec{E}_s(\vec{r}) = \frac{jk}{4\pi}\frac{e^{-jkr}}{r} Z \int_{F_p} (\vec{s}\times(\vec{s}\times\vec{J}_F(\vec{r}\,'\,)))e^{-jk\vec{s}\cdot\vec{r}\,'} df' \ ,$$

and introducing the surface current

$$(2.6) \qquad \vec{J}_F(\vec{r}\,'\,) = \left\{\begin{matrix} 2\vec{n}\times(\vec{e}\times\vec{p}_e)E_e/Z\ e^{-jk\vec{e}\cdot\vec{r}\,'} \\ 0 \end{matrix}\right\} \text{ on the } \left\{\begin{matrix}\text{illuminated}\\ \text{shadowed}\end{matrix}\right\} \text{ parts of the panel.}$$

The geometrical parameters $\vec{r}$, $\vec{r}\,'$, $\vec{e}$, $\vec{s}$, F_p and $\vec{n}$ are explained in Fig. 2.1, while the electric parameters are given by λ = wavelength, $k = 2\pi/\lambda$ = wave number, Z = wave impedance of the propagation medium, $\vec{p}_e = p_x\,\vec{e}_x + p_y\,\vec{e}_y$ = unit polarization vector and E_e = magnitude of the incident electric field.

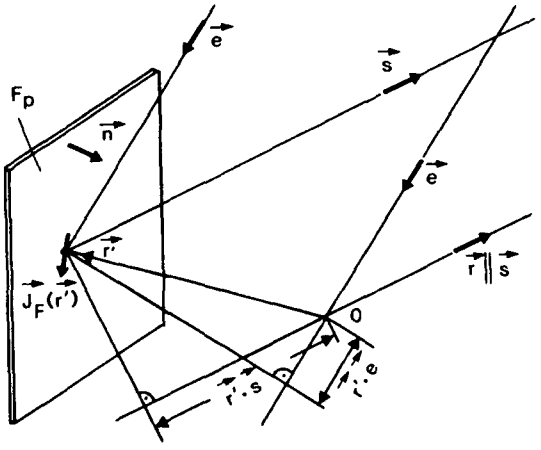

Fig. 2.1
Geometrical scheme for the interpretation of the radiation integral.

The evaluation of the radiation integral for the backscattered ($\vec{e} = -\vec{s}$) field in the observer fixed cartesian coordinate system and the comparison with (2.2) results in the following backscattering matrix:

$$(2.7)\quad [T^{PO}] = -\frac{jk}{2\pi}\frac{e^{-jkr}}{r}\int_{F_p} e^{j2kz'}\,dx'dy' \begin{bmatrix} 1 & 0 \\ 0 & 1 \end{bmatrix} .$$

For a panel of polygonal shape the phase integral can be solved analytically. Details of the integration are given in [4] for panels of triangular and quadrangular shape which are used in the computer program SIG5 to model the target.

Normalizing the scattering matrix to e^{-jkr}/r, the matrix appears purely imaginary. Independent of the orientation of the panel, no differences between xx-polarization and yy-polarization nor any cross-polarization are predicted by PO. This, however, is only true if the panel is perfectly conducting and no double or multiple interactions can occur between pairs or a higher number of panels.

The electric and magnetic fringe currents of Michaeli [9] can be written in a very compact way using the coefficients D_e^f, D_m^f, D_{em}^f (these symbols are proposed by Knott [10]):

$$(2.8)\quad I^f(\psi_e,\psi_s;\beta_e,\beta_s) = -\frac{j2E_{et}}{kZ\sin^2\beta_e} D_e^f(\psi_e,\psi_s;\beta_e,\beta_s) - \frac{j2H_{et}}{k\sin^2\beta_e} D_{em}^f(\psi_e,\psi_s;\beta_e,\beta_s) ,$$

$$(2.9)\quad M^f(\psi_e,\psi_s;\beta_e,\beta_s) = \frac{j2ZH_{et}}{k\sin\beta_e\sin\beta_s} D_m^f(\psi_e,\psi_s;\beta_e,\beta_s) .$$

$E_{et} = \vec{t}\cdot\vec{E}_e$ or $H_{et} = \vec{t}\cdot\vec{H}_e$ is the component of the incident electric or magnetic field parallel to the edge with unit tangent vector $\vec{t}$. The geometrical parameters ψ_e, ψ_s, β_e, β_s and n are explained in Fig. 2.2. The formulas for D_e^f, D_m^f and D_{em}^f are given in the appendix for the backscattering case ($\psi_e = \psi_s$, $\beta_s = \pi - \beta_e$).

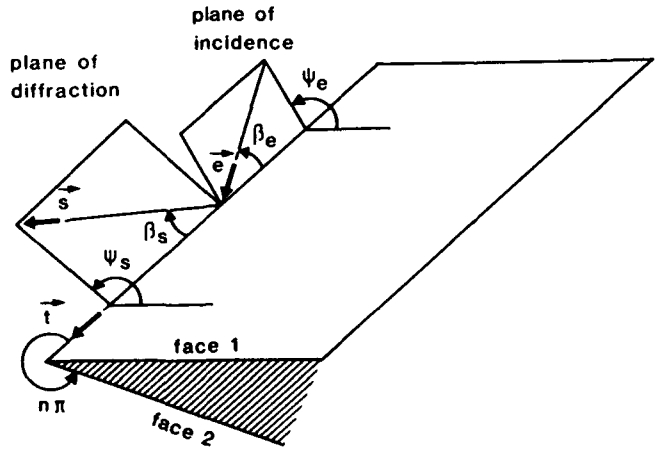

Fig. 2.2
Wedge geometry.

Before choosing the fringe currents of Michaeli, it was necessary to relate this theory to other theories, which, in principle, could be used to solve edge diffraction problems observing the viewpoints given in the introduction.

Though there are several papers [10 - 15] dealing with the relationships between asymptotic diffraction theories, it is useful to summarize the results with the aid of a few statements. Thereby the output of the different theories are given in the form of currents. For mathematical details see [15].

The fringe currents of Michaeli can be written in the following way:

(2.8a) $I^f = I^t - I^{PO}$,

(2.9a) $M^f = M^t - M^{PO}$,

where I^t, M^t are the equivalent electric and magnetic total currents, responsible for the total wedge diffracted field while I^{PO} and M^{PO} are the equivalent PO-components responsible for the PO-field of the wedge. The expressions derived by Michaeli are obtained by asymptotic end-point evaluation of the fringe current radiation integral over the ray coordinate measured along the diffracted ray grazing the surface of the local wedge. The resulting expressions are finite for all aspects of illumination and observation, except for the special case where the direction of observation is the continuation of a glancing incident ray coming from outside the wedge. This situation occurs only in forward scattering.

Choosing the coordinate for the radiation integral in a traditional way normal to the edge, expressions for the fringe currents are obtained [16] which display infinities for certain combinations of observation and incidence directions. These fringe currents are identical to those which can be evaluated [15] from the fringe diffracted fields of Mitzner [7]. Now adapting the fringe currents to the cone of diffracted rays one would expect that these would be identical to those which can be derived from the fringe field expressions of Ufimtsev [6] and which are used in [1]. This is the case for the electric total current, for the magnetic total and PO-current but in general not for the electric PO-current.

The total currents are identical to the filamentary currents of Keller's GTD-field [17], represented by Knott and Senior in a compact manner [18] and denoted as equivalent currents by Ryan and Peters [19] who applied the concept to compute the edge diffracted field in caustic regions. Evaluating the equivalent currents of the GTD for vertical incidence ($\beta_e = 90°$) on a half-plane ($n = 2$) one receives the filamentary currents of the diffracted field derived by Sommerfeld [20].

The difference in the electric PO-currents is given by a coupling term between the incident electric field, being perpendicular to the plane of incidence, and the PO-field having a component parallel to the plane of diffraction. This coupling term is not taken into account by the theory of Ufimtsev as was pointed out in [14]. Only in the case that both faces of the wedge are illuminated by the incident wave does the coupling term become identical to zero [15] and the fringe currents extracted from the theory of Ufimtsev become identical to the fringe currents of Michaeli.

Introducing now the fringe currents (2.8) and (2.9) in the radiation integral over a filamentary current with length L

$$(2.10)\quad \vec{E}_s^f(\vec{r}) = \frac{jk}{2\pi}\frac{e^{-jkr}}{r}\int_L \left(Z\, I^f(\vec{r}')\,(\vec{s}\times(\vec{s}\times\vec{t})) + M^f(\vec{r}')\,(\vec{s}\times\vec{t})\right) e^{jk\vec{s}\cdot\vec{r}'}\, dl' ,$$

one arrives at the backscattering matrix

$$(2.11)\quad [T^f] = -\frac{1}{2\pi}\frac{e^{-jkr}}{r}\int_L e^{j2k\vec{s}\cdot\vec{r}'}\, dl' \times$$

$$\times \begin{bmatrix} D_e^f\, t_x^2 + D_m^f\, t_y^2 - D_{em}^f\, t_x\, t_y & (D_e^f - D_m^f)\, t_x\, t_y + D_{em}^f\, t_x^2 \\ (D_e^f - D_m^f)\, t_x\, t_y - D_{em}^f\, t_y^2 & D_m^f\, t_x^2 + D_e^f\, t_y^2 + D_{em}^f\, t_x\, t_y \end{bmatrix} .$$

The geometrical parameters are explained in Fig. 2.3.

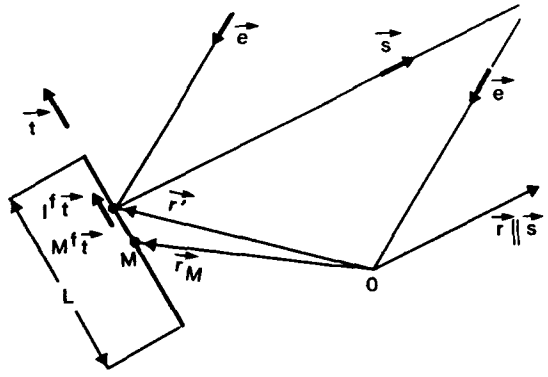

Fig. 2.3
Geometrical sketch to evaluate the radiation integral.

As in the case of the PO-scattering matrix the phase integral can be solved analytically. Introducing the mid-point vector $\vec{r}_M$ of the edge one obtains

$$(2.12)\quad \int_L e^{j2k\vec{s}\cdot\vec{r}'}\, dl' = L\,\frac{\sin(kLt_z)}{kLt_z}\,\frac{e^{j2kr_{Mz}}}{1-t_z^2} ,$$

with $t_z = -\cos\beta_e$.

Normalizing the backscattering matrix $[T^f]$ by e^{-jkr}/r it appears purely real. In general differences between HH- and VV-polarization are predicted. Also, since $[T^f]$ is asymmetric, differences between HV- and VH-polarization are predicted which is not correct for monostatic scattering processes. This is due to corner diffraction effects which arise with an edge of finite length and which are not considered in the theory. Symmetry is observed for the special case of normal wave incidence ($\beta_e = 90°$). Further, if the contour of a panel is a smooth curve, the matrix $[T^f]$ would be symmetric.

For the discussions in the next section, some properties of the coefficients D_e^f, D_m^f, D_{em}^f are needed, which are summarized in the following. Fig. 2.4 shows

the coefficients for normal incidence (β_e = 90°) and a half-plane (n = 2) depending on the angle ψ_e. In Fig. 2.5 the coefficients for a step (n = 1.5) are represented where D^f_{em} is identical to zero. In both cases, mirror symmetries for each coefficient become relevant about ψ_e = 180° for the half-plane and ψ_e = 135° for the step. Further symmetries, now radial symmetries, occur for the half-plane between coefficient D^f_e and D^f_m about ψ_e = 90° and ψ_e = 270°.

Fig. 2.6 shows the coefficients D^f_e, D^f_m and D^f_{em} for ψ_e = 270° and a half-plane now dependent of the angle β_e. One also finds symmetries, namely mirror-symmetry for D^f_e and D^f_m and radial-symmetry for D^f_{em} about β_e = 90°. These symmetries occur for all ψ_e = const.

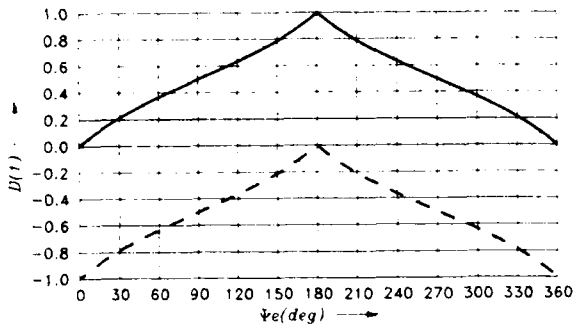

Fig. 2.4
Coefficients D^f_e (——) and D^f_m (---) for a half-plane (n=2) depending on ψ_e; β_e=90°.

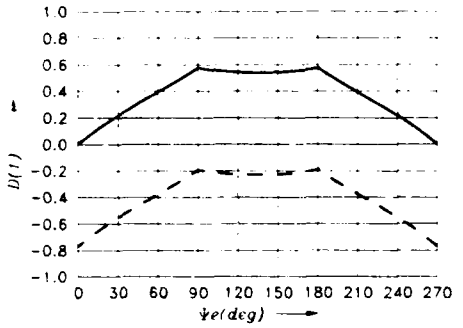

Fig. 2.5
Coefficients D^f_e (——) and D^f_m (---) for a step (n=1.5) depending on ψ_e; β_e=90°.

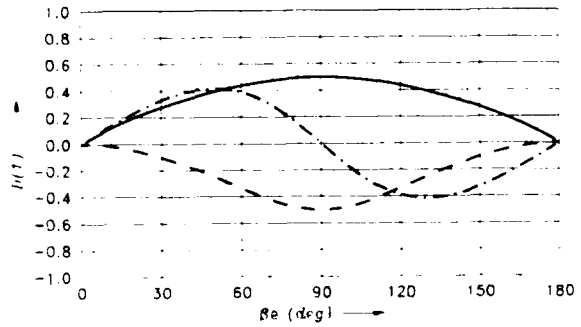

Fig. 2.6
Coefficients D^f_e (——), D^f_m (---) and D^f_{em} (-.-) for a half-plane depending on β_e; ψ_e = 270°.

3. Analysis of the RCS of a Square Test Panel by the PO- and EC-Method

Studies similar to the ones reported here were performed by Ross [21], Sikta, Burnside, Chu and Peters [22], Balanis, Griesser and Marsland [23], Volakis and Ricoy [24], Pelosi, Tiberio, Puccini and Maci [25], Ivrissimtzis and Marhefka [26]. Ross applied the GTD up to triple diffraction to compute the RCS of rectangular flat plates. Sikta et al. used a modified equivalent current concept based on GTD and a corner diffraction analysis to study the RCS of flat plate structures such as a square flat plate, a finlike plate and a disc. Balanis et al. used GTD up to third order diffraction for principal

plane and EC-currents of Michaeli for off-principal plane backscattering of plates. The angular spectrum method along with the generalized matrix formulation were employed for the diffraction analyses of a thick perfectly conducting half-plane by Volakis and Ricoy. Pelosi et al. applied GTD to calculate the RCS of a square plate. Ivrissimtzis and Marhefka used a uniform ray approximation including higher order terms for the analysis of polyhedral structures.

The procedure presented in the previous section is not limited to the simple structure of a flat plate as will be demonstrated in the next section. However, in this section the scattering from a square test plate is investigated in great detail to estimate the efficiency and the limits of application of the chosen method.

The square test panel is analysed at a frequency of 16.66 GHz which results in a wavelength of 17.995 mm. The edge length is 91.4 mm (5.08 λ) and the thickness is 0.8 mm (0.044 λ). In order to have an independent external accuracy check for the following computations, the test panel was chosen to be equal to one of the panels investigated by Ross [21]. The panel is defined in the observer-fixed coordinate system, see Fig. 3.1. The rotations around the x, y and z-axis are defined by the angles φ_x, φ_y, φ_z. An incident wave with electric field vector parallel to the x-axis is designated as horizontally polarized while a field vector parallel to the y-axis describes a vertically polarized field, if the object is rotated around the y-axis for instance.

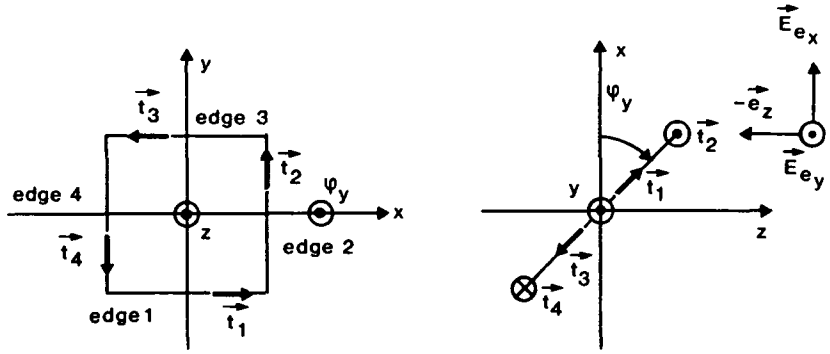

Fig. 3.1 Orientation of the panel in the observer-fixed coordinate system and numbering of the edges for a panel with zero thickness.

Fig. 3.2 resp. Fig. 3.3 shows the experimental RCS-result for horizontal resp. vertical polarization and for the principal plane (φ_x=0, φ_y=α, φ_z=0). For α = 0° one has normal incidence, for α = 90° the panel is seen under grazing incidence. The PO-result for a panel with zero thickness, which is usually compared with experimental results, is shown in Fig. 3.4. The maximum RCS-value amounts to 4.33 dBsm.

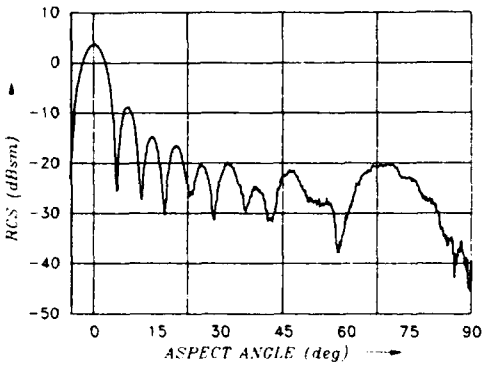

Fig. 3.2
Experimental result for horizontal polarization.

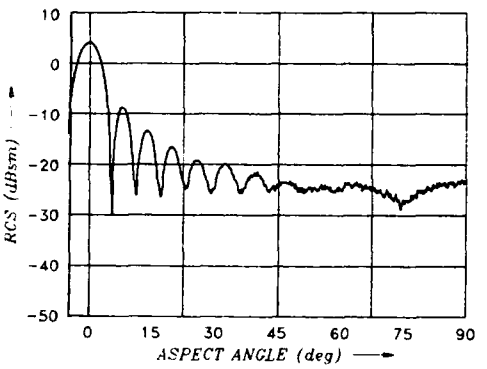

Fig. 3.3
Experimental result for vertical polarization.

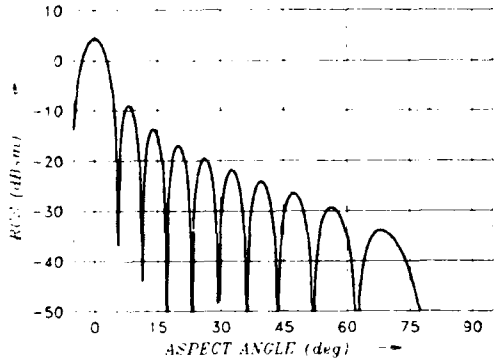

Fig. 3.4
PO-result for the test panel with zero thickness.

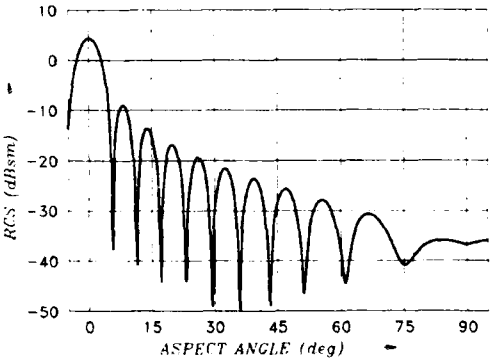

Fig. 3.5
PO-result for the test panel with thickness 0.044 λ.

Besides the smoothing of the deep nulls of the PO-result, the sidelobe peaks far from the mainlobe are significantly higher in the experiment than in the theory. At grazing incidence a deep null of $-\infty$ dB is predicted from theory. In the experiment this null occurs only for horizontal polarization, while for vertical polarization a level of about -27 dB under the main lobe peak can be observed. In view of the experimental results the theoretical results need improvement.

However, it must be emphasized, that for the experiment a panel with a thickness of 0.044 λ was used while for the theory the panel was assumed with zero thickness. Thus far the comparison is a little unfair. If one models the flat plate with the same thickness as was used for the experiment, then it consists of six faces. Each of them can contribute to the total scattered field if it is illuminated by the incident field. The result is presented in Fig. 3.5. One can see that the deep nulls are filled up, that the peaks of the distant sidelobes are higher than in the case of zero thickness, and that, at grazing incidence, an RCS on the order of -41 dB under the peak is predicted compared to $-\infty$ dB for the zero thickness panel and the -27 dB of the experiment.

In the following the influence of the edges is considered. First the panel with zero thickness is analysed.

Edges 2 and 4 make an angle $\beta_e = 90°$ with the incident ray independent from φ_y, see Fig. 3.1, while β_e of edges 1 and 3 varies with $\beta_e = 90° + \varphi_y$. From Eq. (2.11) and Eq. (2.12), one can expect an oscillating behaviour of the RCS of edges 1 and 3 and a monotonic function for edges 2 and 4 with respect to the rotation angle φ_y. For rotation angles $0° < \varphi_y < 180°$, edge 2 is nearer to the radar observer than edge 4, therefore, it is sometimes called the leading edge while edge 4 is the trailing edge.

First the influence of edges 1 and 3 on the RCS computed by PO is considered. The scattering matrix of edge 1 is given by

$$(3.1)\quad [T_1^f] = -\frac{1}{2\pi}\frac{e^{-jkr}}{r} L \frac{\sin(kL\sin\varphi_y)}{kL\sin\varphi_y} \begin{bmatrix} D_e^f & D_{em}^f \\ 0 & D_m^f \end{bmatrix},$$

with arguments $\psi_e = 90°$, $\beta_e = 90° + \varphi_y$ for D_e^f, D_m^f and D_{em}^f. For edge 3 the following formula is obtained:

$$(3.2)\quad [T_3^f] = -\frac{1}{2\pi}\frac{e^{-jkr}}{r} L \frac{\sin(kL\sin\varphi_y)}{kL\sin\varphi_y} \begin{bmatrix} D_e^f & D_{em}^f \\ 0 & D_m^f \end{bmatrix},$$

with $\psi_e = 90°$, $\beta_e = 90° - \varphi_y$.

We can make the following observations:

1. Both scattering matrices are purely real, after normalizing by the factor e^{-jkr}/r.
2. The maximum value is reached for $\varphi_y = 0°$ (the incident ray hits the plate normally). The maximum value amounts to about -32 dBsm which is about -36 dB under the PO-value. This means that the peak value computed by the PO-method is negligibly influenced by the diffraction effects of edges 1 and 3. Since, further, the RCS decreases with increasing angle φ_y in an oscillating manner, both edges have practically no influence on the PO-result.
3. Since mirror symmetries for D_e and D_m hold, see Fig. 2.6, the copolar scattered fields of each edge are equal in amplitude and phase.
4. Both matrices indicate a cross-polarization term and, therefore, are asymmetric. Since, however, for the edge coefficient D_{em}^f a radial symmetry, see Fig. 2.6, holds, the sum matrix $[T_{1,3}^f] = [T_1^f] + [T_3^f]$ is symmetric and is given by

$$(3.3)\quad [T_{13}^f] = -\frac{1}{\pi}\frac{e^{-jkr}}{r} L \frac{\sin(kL\sin\varphi_y)}{kL\sin\varphi_y} \begin{bmatrix} D_e^f & 0 \\ 0 & D_m^f \end{bmatrix},$$

with arguments $\psi_e = 270°$, $\beta_e = 90° - \varphi_y$. The sum matrix predicts differences between horizontal and vertical polarization. However, this effect has practically no influence on the final result.

Fig. 3.6 shows the RCS of edge 1 and 3 for horizontal polarization and Fig. 3.7 for vertical polarization. Fig. 3.8 shows the sum RCS of edges 1 and 3 for horizontal polarization. For vertical polarization only negligible differences exist.

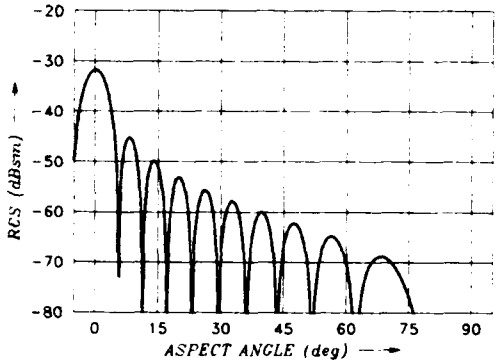

Fig. 3.6
RCS of edge 1 resp. edge 3 for horizontal polarization.

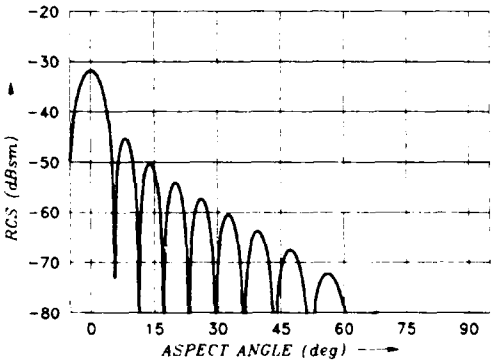

Fig. 3.7
RCS of edge 1 resp. edge 3 for vertical polarization.

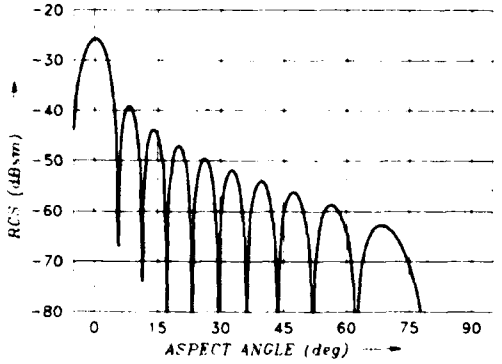

Fig. 3.8
RCS of edges 1 and 3, horizontal polarization.

Contrary to edges 1 and 3, edges 2 and 4 generate contributions of significant practical interest. Bearing in mind that $D^f_{em}(\beta_e = 90°) = 0$, one obtains for edge 2

$$(3.4)\quad [T^f_2] = -\frac{1}{2\pi}\,\frac{e^{-jkr}}{r}\,L\,e^{jka\sin\varphi_y}\begin{bmatrix} D^f_m & 0 \\ 0 & D^f_e \end{bmatrix}.$$

The arguments of the edge coefficients are $\psi_e = 270° - \varphi_y$, $\beta_e = 90°$. For edge 4, we get for the parameters $\psi_e = 270° + \varphi_y$, $\beta_e = 90°$

$$(3.5)\quad [T^f_4] = -\frac{1}{2\pi}\,\frac{e^{-jkr}}{r}\,L\,e^{-jka\sin\varphi_y}\begin{bmatrix} D^f_m & 0 \\ 0 & D^f_e \end{bmatrix}.$$

The following observations can be made:

1. After normalization both scattering matrices appear to be complex.
2. The RCS contributions of both matrices vary monotonically with respect to the rotation angle and are significant compared to the PO-solution.
3. The individual RCS contributions are different from each other and show differences for horizontal and vertical polarization.
4. For horizontal polarization, the contribution of edge 4 dominates, while, for vertical polarization, the contribution of edge 2 dominates.
5. Since symmetry, see Fig. 2.4, is given, the RCS of edge 2 for horizontal (vertical) polarization is identical to the RCS of edge 4 for vertical (horizontal) polarization. For the sum matrix one obtains

$$(3.6)\quad [T^f_{2,4}] = -\frac{1}{2\pi}\frac{e^{-jkr}}{r} L \cos(ka\sin\varphi_y)(D^f_m - D^f_e) \begin{bmatrix} 1 & 0 \\ 0 & -1 \end{bmatrix} - j\frac{1}{2\pi}\frac{e^{-jkr}}{r} L \sin(ka\sin\varphi_y)(D^f_m + D^f_e) \begin{bmatrix} 1 & 0 \\ 0 & 1 \end{bmatrix},$$

where the edge coefficients have the arguments $\psi_e = 270° - \varphi_y$, $\beta_e = 90°$.

The individual RCS contribution of edges 2 and 4 is represented in Fig. 3.9 and Fig. 3.10. The sum RCS of edges 2 and 4 is given in Fig. 3.11.

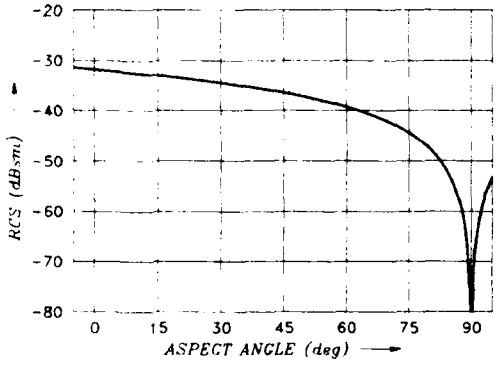

Fig. 3.9
RCS of edge 2 (leading edge) for horizontal polarization and of edge 4 (trailing edge) for vertical polarization.

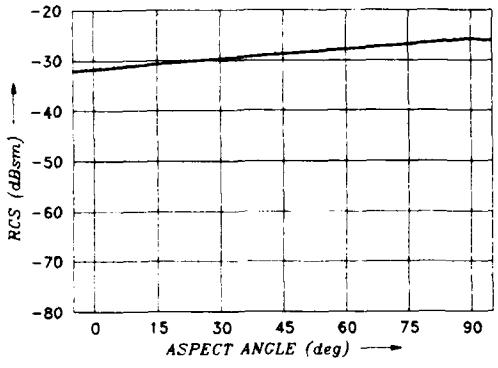

Fig. 3.10
RCS of edge 2 for vertical polarization and of edge 4 for horizontal polarization.

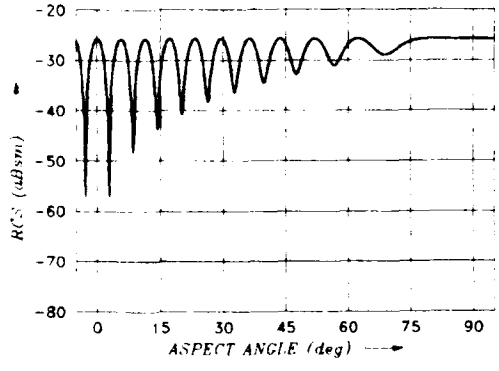

Fig. 3.11
RCS of edges 2 and 4 for both polarizations.

Fig. 3.12 finally shows the PO-result plus the contribution of all four edges which is identical for horizontal and vertical polarization. One can confirm excellent agreement with the experimental results for vertical polarization. It is, however, unsatisfactory that the theoretical solution doesn't indicate any polarization dependence.

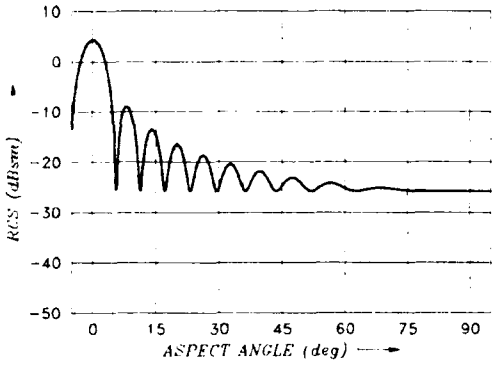

Fig. 3.12
RCS of the test panel with zero thickness for horizontal and vertical polarization computed by PO- and EC-method.

Mathematically this can be explained by discussing the scattering matrix $[T_{2,4}]$. The imaginary part has identical elements for horizontal and vertical polarization. The real part has elements of equal magnitude but opposite sign, so that, with the additive correction of the purely imaginary PO-solution, the matrix behaves like -a-jb for horizontal and +a-jb for vertical polarization. This means that the final RCS result (PO-solution + EC-solution) presents identical values for horizontal and vertical polarization. This is not in agreement with measurements. Physically the effect is explained by the fact that the theory used does not take into account second and higher order diffraction effects. For horizontal polarization, the fields associated with double diffraction e.g. are 4 kL greater than the corresponding vertical polarization contribution [21]. Polarization dependent effects, however, are predicted by the theory for other diagram cuts, other panel shapes (e.g. triangle) or other wedge angles.

The latter is demonstrated for a flat plate with dimensions of the square panel, however, with the same thickness, namely 0.044 λ, as in the experiment. This plate is modeled now by 6 panels and 12 edges (n = 1.5). Without discussion if it is allowed to use the theory for close adjacent edges the result

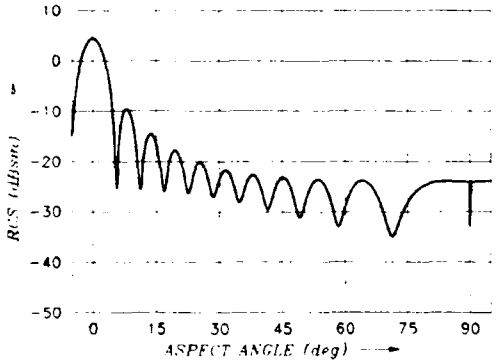

Fig. 3.13
RCS of the test panel with 0.044 λ thickness for horizontal polarization.

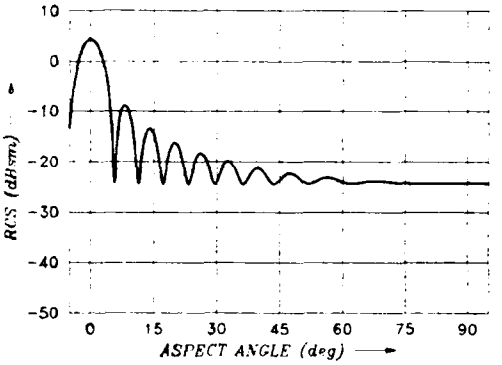

Fig. 3.14
RCS of the test panel with 0.044 λ thickness for vertical polarization.

of the computations is presented in Fig. 3.13 and Fig. 3.14. For horizontal polarization, the discrepancies between theory and experiment have become minor, but the deep null for grazing incidence again is not predicted by the theory.

If the plate is rotated around the z-axis by an angle of $\varphi_z = 45°$ a diagonal cut can be achieved by a following rotation with φ_y. The theoretical results are presented in Figs. 3.15 and 3.16. Again no cross-polarization occurs which is in agreement with symmetrical properties. The experimental results are presented in Figs. 3.17 and 3.18. Since the RCS-values drop very quickly down to levels of about -40 dB under the mainlobe it is not very meaningful to discuss minor deviations between experimental and theoretical results.

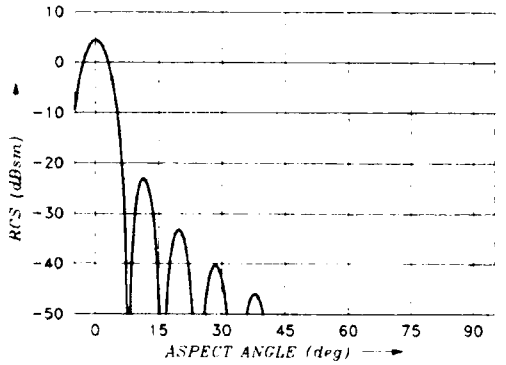

Fig. 3.15
Theoretical RCS of the test panel for a diagonal cut, horizontal polarization.

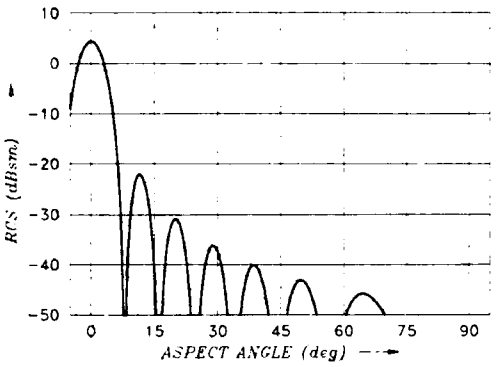

Fig. 3.16
Theoretical RCS of the test panel for a diagonal cut, vertical polarization.

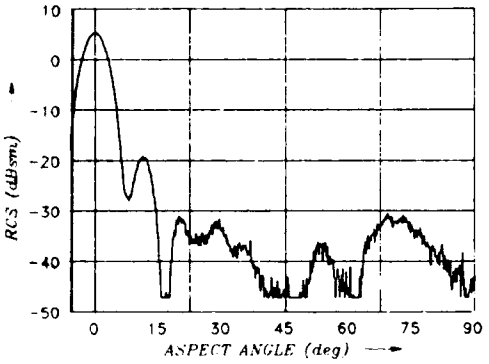

Fig. 3.17
Experimental RCS of the test panel for a diagonal cut, horizontal polarization.

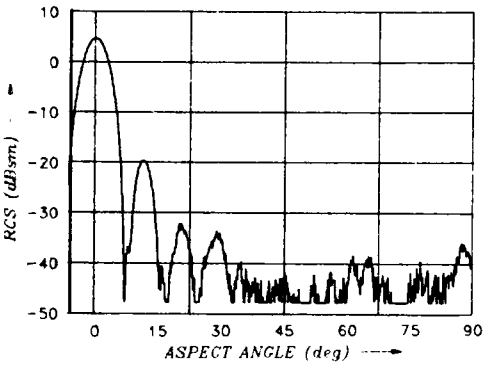

Fig. 3.18
Experimental RCS of the test panel for a diagonal cut, vertical polarization.

Finally, the RCS has been computed for a cut where the rotation axis makes an angle of $\varphi_z = 30°$ with the main axis (15° with the diagonal) of the plate. In this case no symmetry occurs and the theory predicts cross-polarization. Because of the asymmetry in the scattering matrix, the cross-polarization HV, see Fig. 3.19, is slightly different from the cross-polarization VH, see Fig. 3.20. No experiments could be carried out at this time in our institute; see however [27].

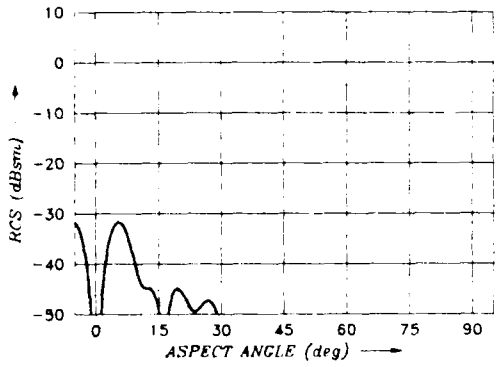

Fig. 3.19
Theoretical RCS of the test panel for a 30°-cut, HV-polarization.

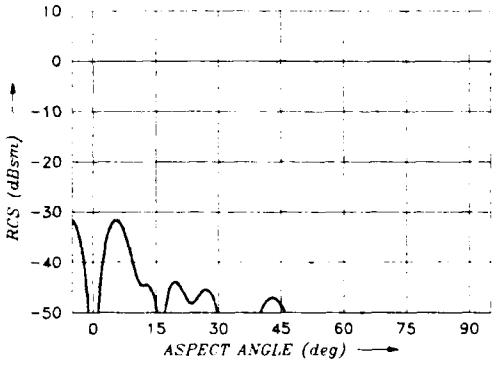

Fig. 3.20
Theoretical RCS of the test panel for a 30°-cut, VH-polarization.

This section is closed with simple formulas derived from the above matrices to estimate the effect of a single edge in relation to the RCS peak value of a panel computed by PO. The panel may be of arbitrary polygonal structure with size A. The edge under consideration has the length L, is hit normally by the incident wave and is rotated around the y-axis by the angle φ_y (this is just the situation of edge 2 in Fig. 3.1). Relating the magnitude of the elements of the scattering matrix given by Eq. (3.4) to the peak value of the PO-scattering matrix, one obtains for horizontal polarization

$$r_{HH} = 20 \log \frac{L\,|D_m^f|}{kA}\,, \tag{3.7}$$

and for vertical polarization

$$r_{VV} = 20 \log \frac{L\,|D_e^f|}{kA}\,. \tag{3.8}$$

The arguments of D_m^f, D_e^f are $\psi_e = 270° - \varphi_y$, $\beta_e = 90°$.

Using the values for D_m^f and D_e^f given in Fig. 2.4 for a half-plane (n = 2) and in Fig. 2.5 for a step (n = 1.5), the following table may be established choosing the test panel of this section as an example.

	φ_y	0°	45°	90°	135°	180°	225°	270°
half-plane (n=2)	r_{HH} [dB]	-36.1	-40.8	-∞	-40.8	-36.1	-33.1	-30.1
	r_{VV} [dB]	-36.1	-33.1	-30.1	-33.1	-36.1	-40.8	-∞
step (n=1.5)	r_{HH} [dB]	-32.3	-36.8	-44.5	-42.8	-44.5	-36.8	-32.3
	r_{VV} [dB]	-∞	-40.3	-34.8	-35.4	-34.8	-40.3	-∞

Table 3.1 Level of edge diffraction effects related to the PO-peak value for the square test panel with edge length L=5.08 λ.

4. Application of the EC-Method for a Circular Cylinder and a Double Dihedral

4.1 Circular Cylinder

The test cylinder has a length of 5 λ and a diameter of 1 λ. The wave length is 1128 mm. The broadside RCS amounts to 20 dBsm and the front face RCS to 9.9 dBsm. The cylinder is rotated around an axis vertically to its own axis. Theoretical results for the smooth cylinder based on PTD are published together with experimental results by Ufimtsev in [6]. The circumference of the cylinder was modeled (see Fig. 4.1) by 14 rectangular panels with dimensions 5 λ × 0.22 λ. The deviation from the true cylinder surface was about λ/80. Each of the front faces was modeled with 14 triangles. In the geometrical model artificial edges (n = 1.29) arise between the rectangular panels. The natural circular edges (n = 1.5) between the cylinder circumference and the front faces are approximated by straight lines of length 0.22 λ. Both types of edges are treated in the same way by the theory.

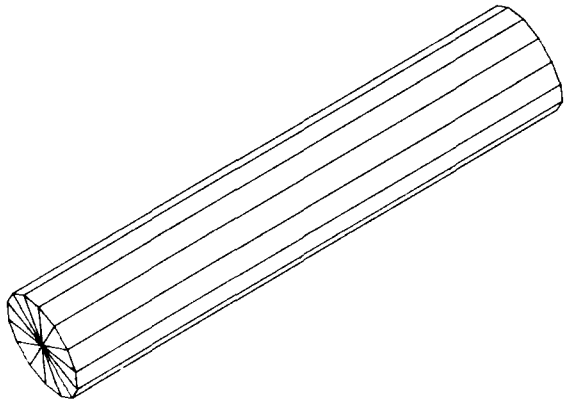

Fig. 4.1
Panel model of the test cylinder.

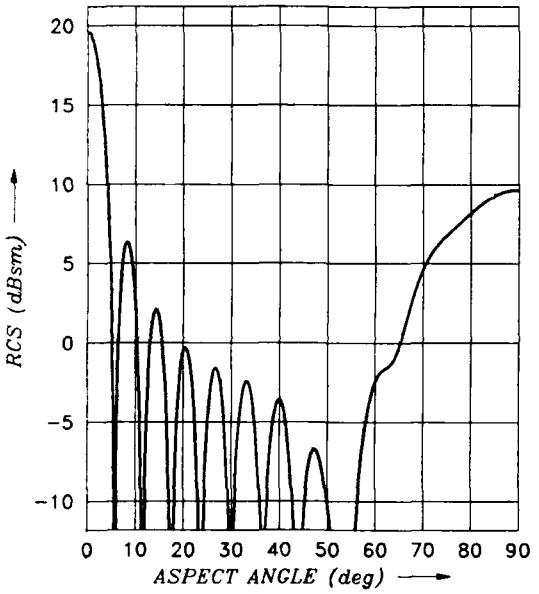

Fig. 4.2
RCS of the clinder modeled by panels, PO-solution.

The PO-solution, insensitive to polarization, is presented in Fig. 4.2. The results of the experiment and of the PTD-theory for horizontal and vertical polarization are given in Fig. 4.3. The broadside peak of the theoretical curves, however, should not exceed 20 dBsm. The pictures of Fig. 4.4, finally present the results of the procedure outlined in this paper. For this special cut they should be identical to the results of Ufimtsev. This is the case except for the difference at broadside incidence and some deviations of minor practical interest.

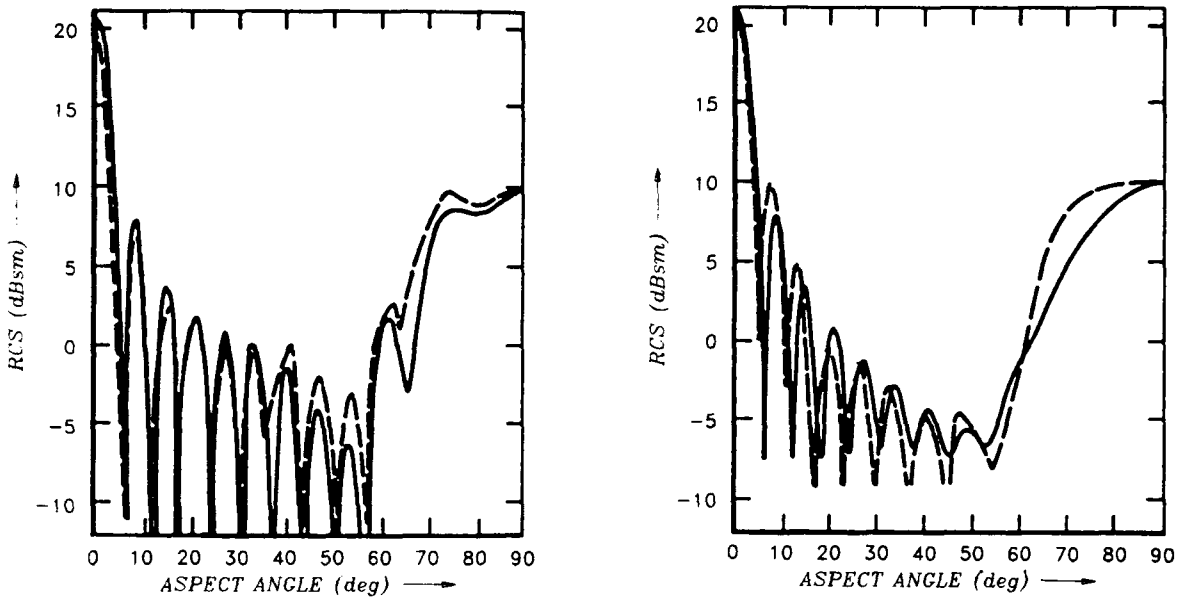

Fig. 4.3 RCS of the smooth cylinder, experiment (---) and PTD-solution (——), left side: HH-polarization, right side: VV-polarization.

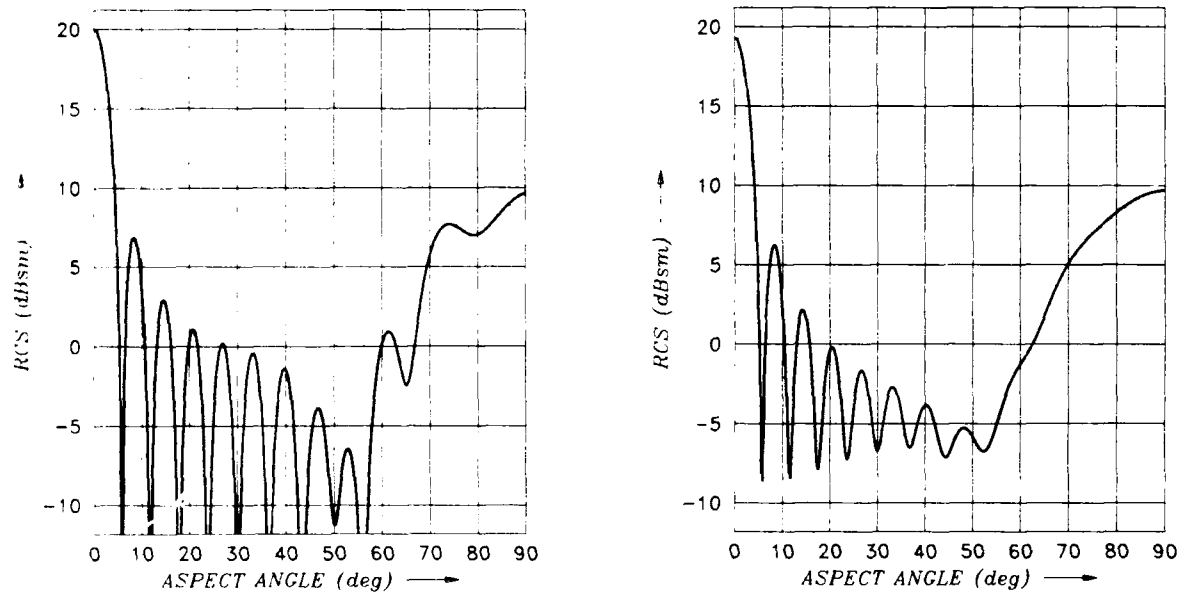

Fig. 4.4 RCS of the cylinder modeled by panels, PO- and EC-solution, left side: HH-polarization, right side: VV-polarization.

4.2 Double Dihedral

A double dihedral constructed on the basis of a cube with additional shadowing surfaces, see Fig. 4.5, is rotated in an unconventional way as shown by Fig. 4.6. For $\alpha = 0°$ the edges of the double dihedral make an angle of 45° with the axis of rotation. The purpose was to generate a strong depolarized backscattered field. Previous PO-results are published for the main cut in [2] and for the diagonal cut within a restricted range of aspect angles in [4].

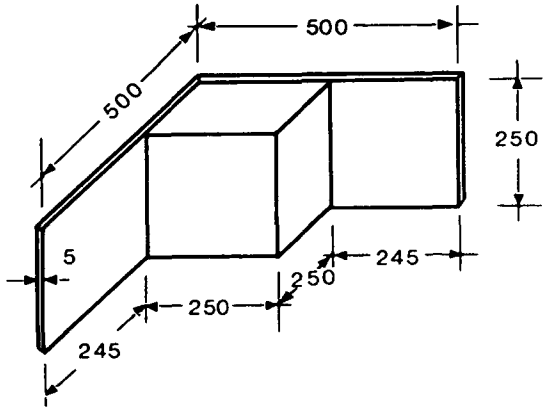

Fig. 4.5
Cube with additional shadowing faces forming a double dihedral, dimensions in mm.

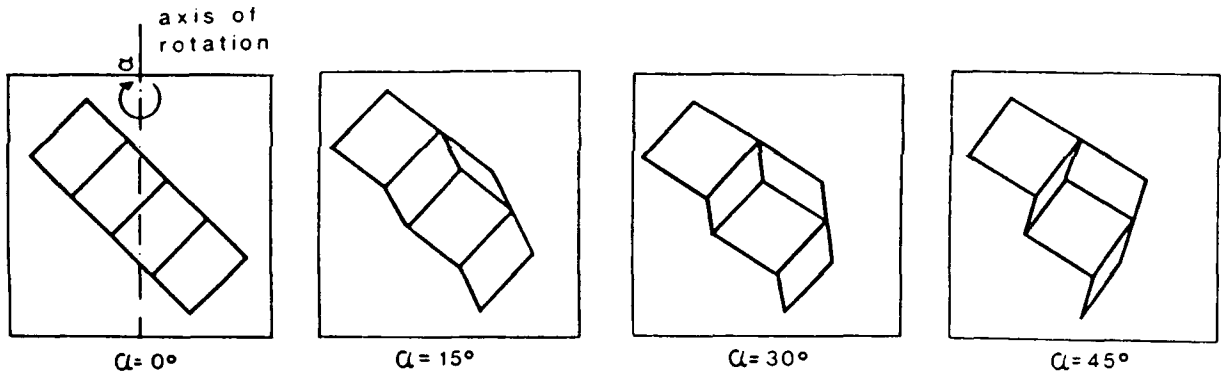

Fig. 4.6 Geometry and axis of rotation.

Figs. 4.7, 4.8 and 4.9 present the results for VH-polarization of experiment, of PO including double reflection and of PO + EC for the full range of aspect angles and a frequency of 15.5 GHz (λ = 19.4 mm). The measurements had to be arranged with great care since a wide dynamic range was needed. In addition, the exact positioning of the double dihedral according Fig. 4.6 caused major problems.

The structure of the pattern around 0° is well represented by PO alone but the decrease is too rapid with increasing aspect angles. In addition, the spikes at -235°, -180°, -125°, -55° and +55° are not predicted by PO. This, however, is the case when the EC-field is added to the PO-field. The spikes, therefore, are due to edge diffraction only.

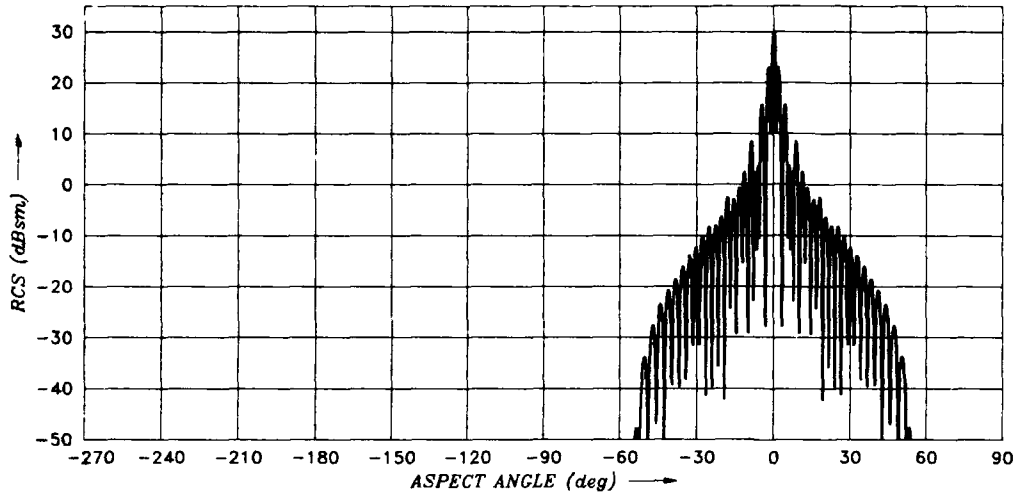

Fig. 4.7 PO-result for the double dihedral, VH-polarization.

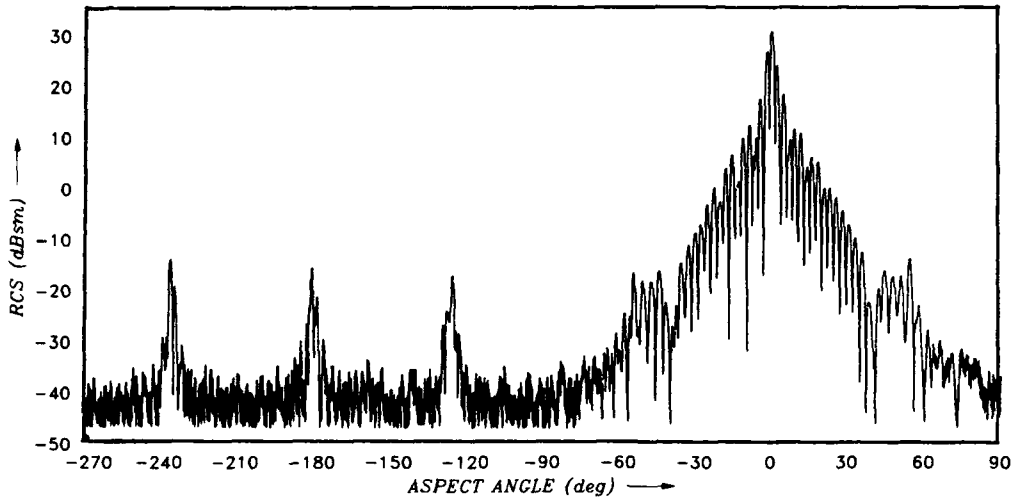

Fig. 4.8 Experimental result.

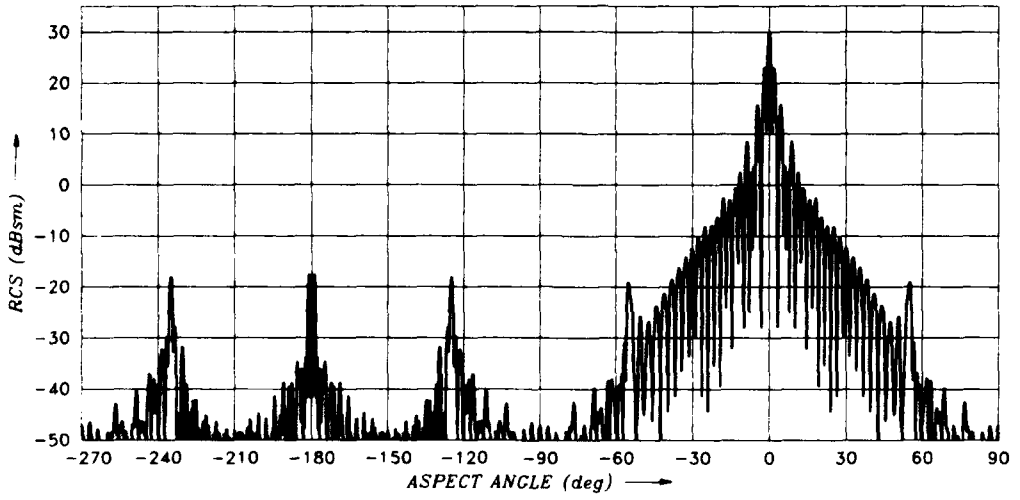

Fig. 4.9 PO- and EC-result.

5. Conclusion

The PO-method is frequently applied with good success to predict the RCS of large and complicated structures modeled by a collection of quadrangular and triangular panels. However, there are certain situations (specific structures, pattern cuts, polarizations) for which a correction of the PO-field by an edge diffracted field is required.

In this paper the concept of equivalent currents (EC) is applied. The fringe currents of Michaeli are used to derive the scattering matrix of an isolated edge with arbitrary length and orientation in an observer fixed coordinate system. The relationship of the method to other theories which are concerned with edge diffraction are summarized by some statements. The theory is applied for the analysis of a square flat plate, of a cylinder and of a double dihedral. All theoretical results are compared with measurements.

The square flat plate with edge length 5.08 λ is analysed in great detail. The results for the principal plane pattern are in excellent agreement for vertical polarization, independent of whether the plate was assumed with zero thickness or with 0.044 λ thickness (as used for the measurements). For horizontal polarization the agreement is unsatisfactory. In the case of zero thickness beyond that identical results for vertical and horizontal polarization are obtained. These effects are due to second order diffraction effects neglected in the EC-theory. This means that further effort is required if one is interested in the improvement of RCS calculations of an isolated plate.

The method is further applied for a cylinder with length 5 λ and diameter 1 λ. The circumference was modeled by 14 rectangular panels, thus introducing artificial edges. Each of the front faces consisted of 14 triangular panels, thus modeling a circular edge by short straight edges. The RCS-results of the EC-method are in good agreement with those of the PTD-method and experiment, both applied for a smooth cylinder.

Finally the concept is used for a double dihedral which was positioned in such a way that strong depolarizations could occur during rotation. Also in this case the correction of the PO-field by the fringe current field was very efficient. The calculated RCS-values are again in good agreement with experimental results.

So one can conclude that the implementation of the presented procedure in a computer program would be efficient enough to treat edge diffraction effects with sufficient accuracy under practical viewpoints.

Acknowledgement

The author thanks Dr. Röde and Dr. K.H. Bethke for the RCS-measurements, Mr. D. Klement for the RCS-computations of the panel with finite thickness and Mrs. M. Malchow for typing the manuscript. Special thanks are expressed to Dr. A. Michaeli whom I was able to contact during the work.

6. References

[1] Youssef, N.N. "Radar Cross Section of Complex Targets". *Proc. IEEE*, Vol. 77, N. 5, May 1989, pp. 722-734.

[2] Klement, D. Preißner, J. Stein, V. "Computation of the Scattering Matrix of Radar Targets: Concept of the Method and First Results". *AGARD-Symposium on Target Signatures*, London, Oct. 1984, CP 364, pp. 20-1 to 20-23, NATO unclassified.

[3] Stein, V. "Physical Optics Method: Prediction of Radar Signatures". *AGARD Lecture Series on Theoretical Aspects of Target Classification*, AGARD-LS-152, 1987.

[4] Klement, D. Preißner, J. Stein, V. "Special Problems in Applying the Physical Optics Method for Backscatter Computations of Complicated Objects". *IEEE Trans. on Ant. and Prop.*, Vol. 36, No. 2, Febr. 1988, pp. 228-237.

[5] Stein, V. "RCS Prediction Models Based on PO and PTD and State of Validation". *AGARD Conference Proceedings 501*, pp. 12-1 to 12-14, 1991.

[6] Ufimtsev, P.Ya. *Method of Edge Waves in the Physical Theory of Diffraction.* Foreign Technology Division, FTD-HC-23-259-71, Translation, AD 733203, Reproduced by National Technical Information Service, Springfield, Va. 22151, 1962.

[7] Mitzner, K.M. *Incremental Length Diffraction Coefficient.* Aircraft Division Northrop Corp., Tech.Rep. No. AFAL-TR-73-296, Apr. 1974.

[8] Chiavetta, J.R. *A Physical Theory of Diffraction for Impedance Wedge.* Boeing Aerospace Co., Doc. D180-26576-1, July 1981.

[9] Michaeli, A. "Elimination of Infinities in Equivalent Edge Currents, Part I: Fringe Current Components". *IEEE Trans. on Ant. and Prop.*, Vol. AP-34, No. 7, July 1986, pp. 912-918.

[10] Knott, E.F. "The Relationship Between Mitzner's ILDC and Michaeli's Equivalent Currents". *IEEE Trans. on Ant. and Prop.*, Vol. AP-33, No. 1, Jan. 1985, pp. 112-114.

[11] Breinbjerg, O.
Rahmat-Samii, Y.
Appel-Hansen, J.
A Theoretical Examination of the Physical Theory of Diffraction and Related Equivalent Currents. Electromagnetics Institute, Technical University Denmark, Lyngby, R 339, May 1987.

[12] Marhefka, R.J.
Brinkley, T.J.
"Comparison of Methods for Far Zone Scattering from Flat Plate and Cube".
ACES Journal, Fall 1988, Vol. 3, No. 2, pp. 57-78.

[13] Ufimtsev, P.Y.
"Theory of Acoustical Edge Waves".
J. Acoustical Soc. Am., 86(2), Aug. 1989.

[14] Breinbjerg, O.
"Prediction of Bistatic Scattering from Perfectly Conducting Flat Plates by the Method of Equivalent Currents".
1990 URSI Digest, May 7-11, 1990, Dallas, Texas, p. 390.

[15] Stein, V.
Beziehungen zwischen bekannten Theorien zur Behandlung der Beugung an der Kante im Hochfrequenzfall.
DLR-FB 89-49 (1989).

[16] Michaeli, A.
"Equivalent Edge Currents for Arbitrary Aspects of Observation".
IEEE Trans. on Ant. and Prop., Vol. AP-32, No. 3, March 1984, pp. 252-258.

[17] Keller, J.B.
"Geometrical Theory of Diffraction".
Journal of the Optical Society of America, Vol. 52, N. 2, Febr. 1962.

[18] Knott, E.F.
Senior, Th.B.A.
"Comparison of Three High-Frequency Diffraction Techniques".
Proc. IEEE, Vol. 62, No. 11, Nov. 1974, pp. 1468-1473.

[19] Ryan, C.E.
Peters, L., Jr.
"Evaluation of Edge-diffracted Fields Including Equivalent Currents for the Caustic Regions".
IEEE Trans. on Ant. and Prop., Vol. AP-17, pp. 292-299, May 1969.

[20] Sommerfeld, A.
Optik.
Akademische Verlagsgesellschaft, Geest + Portig, Leipzig, 1964, S. 215-238.
see also: "Mathematische Theorie der Diffraction", *Math. Annalen* 4, 1986, S. 317-374.

[21] Ross, R.A.
"Radar Cross Section of Rectangular Flat Plates as a Function of Aspect Angle".
IEEE Trans. on Ant. and Prop., Vol. AP-14, No. 3, 1966, pp. 329-335.

[22] Sikta, F.A.
Burnside, W.D.
Chu, T.T.
Peters, L. jr.
"First-Order Equivalent Current and Corner Diffraction Scattering from Flat Plate Structures".
IEEE Trans. on Ant. and Prop., Vol. AP-31, July 1983, pp. 584-589.

[23] Balanis, C.A.
Griesser, T.
Marsland, D.A.
Electromagnetic Backscattering by Plates and Discs.
Department of Electrical and Computer Engineering, Arizona State University, NASA-CR-180643, 1987.

[24] Volakis, J.L.
Ricoy, M.A.
"Diffraction by a Thick Perfectly Conducting Half-Plane".
IEEE Trans. on Ant. and Prop., Jan. 1987, Vol. AP-35, No. 1, pp. 62-72.

[25] Pelosi, G.
Tiberio, R.
Puccini, S.
Maci, S.
"Applying GTD to Calculations of the RCS of Polygonal Plates".
IEEE Trans. on Ant. and Prop., Vol. AP-38, N. 8, Aug. 1990, pp. 1294-1298.

[26] Ivrissimtzis, L.P.
Marhefka, R.J.
"A Uniform Ray Approximation of the Scattering by Polyhedral Structures Including Higher Order Terms".
IEEE Trans. on Ant. and Prop., accepted for publication.

[27] Young, J.D.
"A Study of Scattering from Edge Waves Using High Resolution Radar Images".
1990 URSI Digest, May 7-11, 1990, Dallas, Texas, p. 49.

Appendix

The coefficients D_e^f, D_m^f, D_{em}^f of the backscattering matrix are given by the theory of Michaeli [9]. For more details see also [15].

$$(A1) \quad D_v^f = D_{1v} - D_{1v}^{po} + D_{2v} - D_{2v}^{po} \ , \ v = e,m,em \ ,$$

$$(A2) \quad D_{1e} = \frac{\sin\frac{\psi_e}{n}}{n} \frac{1}{\cos\frac{\pi-\alpha_1}{n} - \cos\frac{\psi_e}{n}} \ ,$$

$$(A3) \quad D_{1m} = \frac{\sin\psi_e}{n} \frac{\sin\frac{\pi-\alpha_1}{n}}{\sin\alpha_1} \frac{1}{\cos\frac{\pi-\alpha_1}{n} - \cos\frac{\psi_e}{n}} \ ,$$

$$(A4)\quad D_{1em} = \frac{1}{n}\cos\beta_e\,(\mu_1 + \cos\psi_e)\,\frac{\sin\frac{\pi-\alpha_1}{n}}{\sin\alpha_1}\,\frac{1}{\cos\frac{\pi-\alpha_1}{n} - \cos\frac{\psi_e}{n}}\,,$$

$$(A5)\quad D^{po}_{1e} = -\,U(\pi-\psi_e)\,\frac{\sin\psi_e}{\mu_1 + \cos\psi_e}\,,$$

$$(A6)\quad D^{po}_{1m} = D^{po}_{1e}\,,$$

$$(A7)\quad D^{po}_{1em} = 0\,.$$

$$(A8)\quad \mu_1 = \cos\psi_e - \frac{2}{\tan^2\beta_e}\,,$$

$$(A9)\quad \alpha_1 = \arccos\mu_1\,,$$

$$(A10)\quad U(x) = \begin{cases} 1 \\ 0 \end{cases} \quad \text{for} \quad \begin{cases} x > 0\,, \\ x < 0\,. \end{cases}$$

The coefficients D_{2v}, D^{po}_{2v} result from D_{1v}, D^{po}_{1v} by the following transformations:

$$(A11)\quad \psi_e \to n\pi-\psi_e\,, \qquad \beta_e \to \pi-\beta_e\,.$$

Application of Parallel Processing to a Surface Patch / Wire Junction EFIE Code

L. C. Russell, J. W. Rockway
Naval Ocean Systems Center
San Diego, California 92152

ABSTRACT

A surface patch / wire junction EFIE method of moment algorithm, JUNCTION, developed by the University of Houston has been implemented in a transputer based parallel processing environment installed in a personal computer. This paper addresses transputer hardware and software options, the JUNCTION algorithm, techniques for parallelizing matrix analysis algorithms, and performance results. The transputer array was found to provide a flexible, low-cost, high performance desktop computing environment for method of moment analysis.

1.0 INTRODUCTION

This paper presents the application of parallel processing techniques to an existing computational electromagnetic (CEM) code. The goal was to demonstrate that high performance computing (HPC) can improve the utility and efficiency of computational techniques used in electromagnetic ship analysis [Li, 1988]. The parallel processing platform was an array of four transputers on a board inside an IBM-compatible PC. The transputers were run using the ParaSoft EXPRESS operating environment [ParaSoft, 1990]. This operating environment was chosen to allow portability of the code to other HPC platforms and minimize the number of required programming changes to the CEM code. The selected CEM code was the method of moment (MoM) algorithm JUNCTION developed by the University of Houston [Hwu et al, 1988; Wilton et al, 1988].

2.0 PARALLEL PROCESSING

The concept of parallel processing has been around for a long time but only recently was its utility generally recognized. By 1986 more than a dozen companies were either selling or in the process of building parallel processors [Tazelaar, 1988].

2.1 Transputer hardware

The hardware platform chosen was an array of four transputers on a motherboard which could be installed inside a PC. This decision was based on the low cost, ease of use, and flexibility of a transputer based system. Transputer systems provide an inexpensive entry into the world of parallel processing. For this entry level application a decision was made to purchase only four floating point transputer modules (TRAMs) each with one Megabyte of external RAM. These size 1 TRAMs are an industry standard and provide sufficient memory for most applications at a reasonable cost and in a compact package. The T800 transputer used has a peak performance of 1.5 Mflops.

2.2 Transputer Software

There are several different ways to program an array of transputers. Each method has trade-offs in portability, performance, and ease of use. The parallel language, Occam, was developed concurrently with the transputer. Parallel versions of high level languages such as Fortran, C, Pascal, and Modula 2 can be obtained. The parallel operating environment EXPRESS (ParaSoft Corporation) is available for transputer systems.

2.2.1 Occam

There are a number of advantages to using Occam for programming a transputer system. Since Occam was developed simultaneously with the transputer, it is one of the few languages designed for concurrency. Occam has the performance and efficiency of assembly language. Occam can be used as a harness to link modules written in other industry standard languages. Its other features include: well implemented timing capabilities, straightforward control of process scheduling, and a high level of structure.

The main disadvantage to using Occam is that programs written in Occam are not portable to other parallel computers. Existing codes written in other languages need to be completely recoded. Occam works only with the transputer. Other disadvantages are that Occam does not support many features of other high level languages (no recursion or dynamic memory allocation), use of it requires learning a new language, and Occam may not be supported in the future. In the trade-off space (portability versus performance versus ease of use) Occam scores high only in performance.

2.2.2 High Level Languages

The advantage of using a parallel version of a high level language such as Fortran, C, Pascal, or Modula 2 is that one can use a language with which one is already familiar. All that is required is to learn the parallel extensions. Existing sequential code can be ported over.

There are, however, a number of disadvantages to using a parallel version of a high level language. Programming an array of transputers requires the user to develop both a host program and a node program. The host program runs on the host processor and handles I/O calls and manages the other processors. The node program runs on all the other processors and does the bulk of the computations. The user is required to maintain two programs instead of the usual one program. This can make program development and maintenance somewhat complex. Performing I/O, making system calls, and measuring timing can be very difficult. Debuggers for parallel versions of high level languages are starting to appear, but they are not widely available. Debugging parallel programs is very difficult. In addition to all this, parallel versions of high level languages do not offer the performance that one can get from Occam.

2.2.3 ParaSoft EXPRESS

Parallel operating environments such as ParaSoft's EXPRESS allow the user the convenience of using a familiar high level language while mitigating some of the disadvantages to parallel high level languages which were mentioned in the previous section. EXPRESS is based on the CUBIX programming model which was developed at CalTech. EXPRESS is available for both Fortran and C. There is no need to develop both a host and node program. Instead only one program (which runs on all processors) needs to be developed and maintained. EXPRESS does not include a compiler so one of the parallel high level language compilers mentioned above is still needed to compile and link the code. During linking the EXPRESS library is linked into the user's source code. The EXPRESS library provides simple Fortran or C language function calls to handle I/O and system calls. EXPRESS also provides timing capabilities, a source level debugger, and a performance monitor. The number of processors being used does not have to be hardwired into the code. Instead this is specified at runtime by a switch in the run command. In addition, EXPRESS is available for a wide variety of parallel machines, not just the transputer. Currently EXPRESS is available for: the multi-headed IBM 3090 (AIX) and the multi-headed CRAY (UNICOS) mainframes; the Intel iPSC 2 and iPSC 860; the nCUBE 1 and 2; PC, MAC, and SUN hosts for transputers; and the IBM RS/6000, Silicon Graphics, and SUN workstations. All this leads to very portable source code.

The only significant disadvantage to EXPRESS is that it possibly degrades system performance to some extent. However, this disadvantage is more than offset by the advantage of having portable code. For these reasons EXPRESS by ParaSoft was chosen for the operating environment. Portability was the key feature since the ultimate goal of this effort was to run the code on a high performance computer. The language chosen was Fortran since this is the principal language of the JUNCTION method of moments code. For obvious reasons, it was desirable to make as few changes to the existing code as possible.

3.0 The JUNCTION METHOD OF MOMENTS CODE

The JUNCTION computer code invokes the method of moments to solve a coupled electric field integral equation (EFIE) for the currents induced on an arbitrary configuration of perfectly conducting bodies and wires [Wilton et al, 1989]. There are three principal advantages to the JUNCTION formulation. First, the EFIE formulation for the surfaces of bodies, in contrast to the magnetic field integral equation (MFIE), applies to open bodies. Second, JUNCTION allows voltage and load conditions to be easily specified at terminals defined on the structure. Third, the triangular patches of JUNCTION are the simplest planar surfaces which can be used to model arbitrary surfaces and boundaries, and triangular patches permit patch densities to be varied locally so as to model a rapidly varying current distribution.

The method of moments is a numerical procedure for solving field integral equations [Harrington, 1968]. Basis functions are chosen to represent the unknown currents. Testing functions are chosen to enforce the integral equation on the surface of the conducting structure. With the choice of basis and testing functions a matrix approximating the integral equation is derived. In JUNCTION a system of N linear equations results, where $N = N_B + N_W + N_J$.

$$\begin{bmatrix} [Z^{BB}] & [Z^{BW}] & [Z^{BJ}] \\ [Z^{WB}] & [Z^{WW}] & [Z^{WJ}] \\ [Z^{JB}] & [Z^{JW}] & [Z^{JJ}] \end{bmatrix} \begin{bmatrix} [I^B] \\ [I^W] \\ [I^J] \end{bmatrix} = \begin{bmatrix} [E^B] \\ [E^W] \\ [E^J] \end{bmatrix}$$

where Z is the impedance matrix, I is the current vector, and E is the excitation vector. The superscripts are B for body elements, W for wire elements, and J for junctions between wires and bodies. The analytical expressions for each of the individual submatrices are different. Solution of the linear system of equations yields the set of unknown coefficients used in the representation of the surface, wire, and junction currents. Once these currents are known, the scattered field or any other electromagnetic quantity of interest may be determined.

4.0 IMPLEMENTATION OF SEQUENTIAL PROGRAM

The first step in parallelizing an existing program is to verify the sequential version of the program. This is done by running the program on a serial computer. Once this has been successfully done, the next step is to get the program to run on a single processor on the parallel computer. This is necessary to eliminate any problems caused by compiler differences between the serial compiler and the parallel compiler and also to "check out" the hardware. Only after this has been completed can the parallelization of the program be considered.

JUNCTION was broken into four separate programs: DATGN, GEOMETRY, CURRENT, and FIELD. DATGN creates input data set files. GEOMETRY calculates the geometrical parameters. CURRENT computes the currents and impedance. FIELD computes charges, near fields, far fields, radar cross sections, and power gain. The computationally intensive programs are CURRENT and FIELD. This paper is concerned with the parallelizing of CURRENT.

From a computational standpoint CURRENT consists of filling the impedance matrix and the excitation vector, and then solving for the current vector. The current vector gives the currents on the bodies. wires and junctions. The methods used are standard matrix manipulation techniques. Once the matrix is filled, Gaussian elimination is performed using LU decomposition with partial pivoting to factor the matrix. Finally, the current vector is solved for by using backward and forward substitution. The library subroutines used are the LINPACK routines CGEFA and CGESL [Dongarra et al, 1979]. CGEFA factors a general complex matrix. CGESL solves a complex matrix equation using the output from CGEFA.

5.0 PARALLEL MATRIX FACTOR AND SOLVE

5.1 Parallel LINPACK

When this effort was initiated, general parallel versions of the LINPACK subroutines were not available. This is because parallel subroutines are by their nature very machine specific and one of the goals of the LINPACK project was for the subroutines to be machine independent.

On sequential computers the number of computations required to factor a matrix into a product of triangular matrices is of the order (n^3) where n is the dimension of the matrix. In comparison, the number of computations required for the triangular solution are of the order (n^2). Because of this, unless multiple solutions are required, most effort has focused on optimizing the factorization algorithm.

On parallel computers good efficiency is more difficult to obtain for matrix solving compared to matrix factoring. This is because much more interprocessor communication is required during solving. Solving is inherently a finer grain process than factoring. Various parallel algorithms have been proposed. Each one has its advantages and disadvantages which are dependent on the number of processors being used, the size of the problem being solved, and the relative cost of communication and computation.

The matrix columns were distributed onto the processors using an interleaving technique known as column wrap mapping. Column wrap mapping has good load balancing properties and gives excellent performance when doing LU decomposition.

Intel Corporation provided the source code for Intel's parallel versions of DGEFA and DGESL from LINPACK. DGEFA and DGESL are double precision non-complex versions of CGEFA and CGESL, respectively. Included were two different matrix solving routines: a cyclic version and a wavefront version of DGESL. The differences between these versions are described below. These routines were all developed for Intel's iPSC parallel computer so a number of modifications were needed to implement them under EXPRESS on the transputer array. The matrix factoring routine was straightforward to parallelize and provided very high efficiencies.

The difficult problem was the solution of the lower triangular linear system

$$Lx = b,$$

where L is a lower triangular matrix of order n, b is a known vector of dimension n, and x is the unknown solution vector of dimension n. The sequential version of LINPACK solves this by forward substitution using the following doubly nested loop:

for $j = 1$ to n
  $x_j = b_j / L_{jj}$
  for $i = j+1$ to n
    $b_i = b_i - x_j L_{ij}$

There are a number of ways to parallelize this problem on a distributed memory parallel computer. Several algorithms have been developed. Two of the most popular are the *wavefront* algorithm and the *cyclic* algorithm [Heath et al, 1988]. These algorithms assume the matrix is column wrap mapped onto the processors.

The wavefront algorithm breaks the updating of b into segments and pipelines the segments through the processors in a wavefront fashion. The n-vector z is used to accumulate the updates of b so that the components of b remain distributed among the processors. The size of the circulated segments is an adjustable parameter that controls the granularity of the algorithm and therefore affects performance. The optimal value of the segment size depends on the characteristics of the hardware.

The wavefront algorithm is written in pseudo-code as:

for $j \in$ *mycols*
  for $k = 1$ to # *segments*
    receive *segment*
    if $k = 1$ then
      $x_j = (b_j - z_j)/L_{jj}$
      segment = *segment* - $\{z_j\}$
    for $z_i \in$ *segment*
      $z_i = z_i + x_j L_{ij}$
    if |*segment*| > 0 then
      send *segment* to processor *map*(j + 1)

The cyclic algorithm is similar to the wavefront algorithm in that they both send a segment z between processors. However, the cyclic algorithm circulates a single segment of the fixed size p-1, where p is the number of processors. The name *cyclic* comes from the segment cycling through all other processors before returning to a given processor. The updates computed by the processor while the segment is circulating elsewhere are stored in the vector t. The cyclic algorithm is written in pseudo-code as:

for $j \in$ *mycols*
  receive *segment*
  $x_j = (b_j - z_j - t_j)/L_{jj}$
  segment = *segment* - $\{z_j\}$
  for $z_i \in$ *segment*
    $z_i = z_i + t_i + x_j L_{ij}$
  $z_{j+p-1} = t_{j+p-1} + x_j L_{j+p-1,j}$

$segment = segment \cup \{z_{j+p-1}\}$
send *segment* to processor *map*(*j*+1)
for $i = j + p$ to n
  $t_i = t_i + x_j L_{ij}$

Theoretical analysis shows that the cyclic algorithm performs best on a small number of processors whereas the wavefront algorithm performs best on a large number of processors.

5.2 Implementation of parallel LINPACK under EXPRESS

A number of modifications were needed to the Intel parallel LINPACK routines in order to implement them on the transputer array operating under ParaSoft EXPRESS. These modifications fell into three categories:

1. converting double precision variables to complex variables,
2. using complex LINPACK routines instead of the equivalent double precision LINPACK routines,
3. using EXPRESS communication functions/routines instead of iPSC communication functions/routines.

5.3 Results

Performance measurements were made of both the parallel matrix factor routine and the two parallel matrix solve routines. Timings were made using one, two, three and four processors. The timing measurements were converted to the standard performance measurement parameters, speed-up and efficiency. Speed-up is the ratio of the execution time of the algorithm on a single processor to the execution time of the parallel algorithm on the n processors. Efficiency is the speed-up divided by n and expressed as percent.

Due to memory limitations, examples with more than 200 unknowns could not be run on a single transputer. Several sample problems were developed to test out the parallel factor and solve routines. The four sample problems had the following number of unknowns: 104, 116, 155, and 189.

5.3.1 Factor

Figure 5-1 shows the timing results on the parallel version of CGEFA for the four sample problems. Figure 5-2 shows speed-up and figure 5-3 shows efficiency. The important issue is that as the number of unknowns increases the parallel matrix factoring routine becomes more efficient. This is expected since small problems do not achieve good load balancing and cannot benefit greatly from parallel computation. An efficiency of over 90% is considered very good.

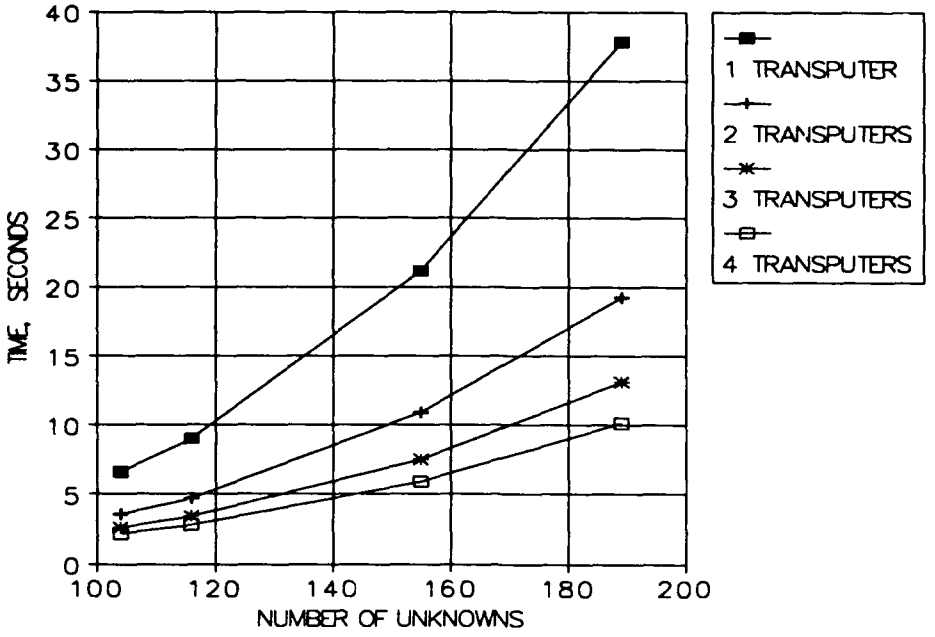

Figure 5-1. Timing for parallel matrix factoring routine.

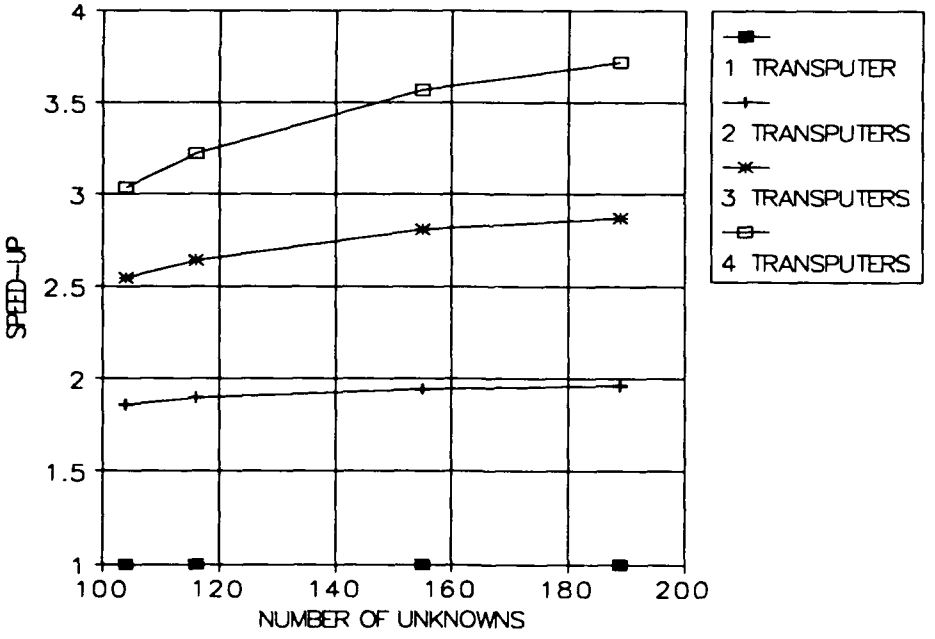

Figure 5-2. Speedup achieved for parallel matrix factoring routine.

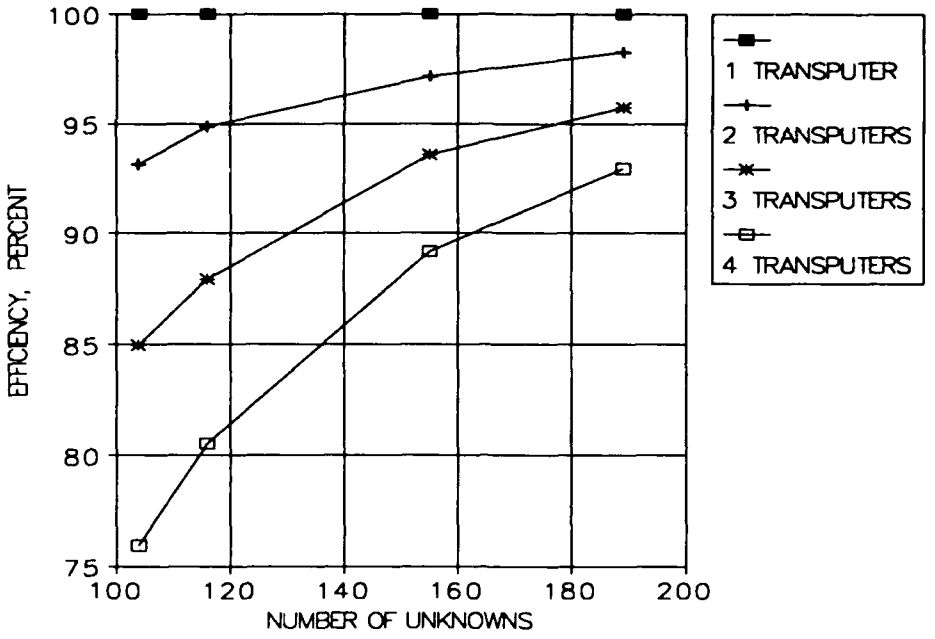

Figure 5-3. Efficiency achieved for parallel matrix factoring routine.

5.3.2 Solve

The performance of the two parallel matrix solve routines were measured for all the example problems. The results are shown here for the largest problem, the one with 189 unknowns. Table 5-1 shows the results for the cyclic algorithm.

Table 5-1. Performance results for cyclic algorithm for 189 unknowns.

Number of Processors	Time, seconds	Speedup	Efficiency
1	0.621	1.00	100%
2	0.367	1.69	84.5%
3	0.257	2.42	80.7%
4	0.207	3.00	75.0%

The performance results for the wavefront algorithm are complicated by the presence of the adjustable segment size parameter. This segment size parameter can range from 1 to the number of unknowns. Table 5-2 shows the optimal performance segment size and time. The optimal performance segment size is a function of the number of processors (as well as the number of unknowns). In addition, by comparing the timing results for the wavefront algorithm with the results for the cyclic algorithm it can be seen that even with the optimum segment size the performance for the wavefront algorithm is much worse than the cyclic algorithm. For these two reasons the wavefront algorithm was rejected for use on the size of problem which could be run on the four

processor transputer array. However, it must be noted that the performance results could turn out to be very different on a high performance computer with many more processors running larger problems.

Table 5-2. Performance results for wavefront algorithm for 189 unknowns.

Number of Processors	Optimal segment size	Time, seconds
1	95	0.741
2	72	0.555
3	34	0.448
4	24	0.380

6.0 PARALLEL MATRIX FILLING

Developing a highly efficient general routine for parallel matrix filling was much more difficult in comparison to the work required to parallelize the matrix factor and solve routines. This was due to several reasons: the large variety of problem geometries being solved, shared calculations between matrix columns, memory limitations, and concurrent filling of the excitation vector.

6.1 Sequential matrix filling

In JUNCTION the columns of the matrix correspond to source points on the structure. The rows of the matrix correspond to observation points on the structure. The body columns/rows come before the wire columns/rows, but otherwise the ordering of the columns/rows depends on how the problem was specified in the input data portion of the code. The junction points are scattered within the wire portion of the matrix. Wire columns correspond to nodes on the wires whereas body columns correspond to sides of triangular patches on the surfaces. A junction is a node on a wire, hence its location is in the wire portion of the matrix.

6.2 Column mapping techniques

There are a wide variety of techniques which can be used to map the columns of the matrix onto the processors. A column wrap mapping technique was used for matrix factoring and solving as described in the previous chapter.

It quickly became apparent that column wrap mapping was not necessarily the best method to use for parallelizing the matrix filling portion of the code. Adjacent columns of the matrix are often associated with each other. For bodies adjacent columns are usually either on the same face or on an attached face. For wires adjacent columns often refer to nodes which are joined by the same segment. In JUNCTION calculations are made with respect to faces and segments, not edges and nodes. This avoids duplication of work in a serial computation. Alternative methods for mapping the columns onto the processors were needed. (Note: mapping the rows onto the processors, instead of the columns, was never considered since matrix factoring required the columns to be already mapped onto the processors).

Alternative mapping techniques were devised and evaluated. The techniques and performance results are described below in the section on structural dependencies. It was found that using a different mapping technique to fill the matrix did not compromise the output from matrix solving. The only effect was to scramble the output vector. The output vector is easily and rapidly unscrambled at the end of the matrix solve routines. Unscrambling the output vector at the end is much faster than unscrambling the matrix before the matrix factor routine, since much less inter-processor communication is required for the former.

6.3 Structural dependencies

The performance of the parallel matrix filling algorithm was found to be very dependent on the structure being analyzed. The first types of problems analyzed were for *homogeneous* structures. Homogeneous structures are defined as having either all body elements or all wire elements. Next, *heterogeneous* structures were evaluated. Heterogeneous structures are defined as having a mixture of body, wire, and junction elements.

6.3.1 Homogeneous structures

Six types of structures were considered: straight wires, cylinders, plates, cones, disks, or spheres. The performance of the parallel matrix filling routines was evaluated for homogeneous problems made up of each of these types of structures. Two column mapping techniques were compared for each structure type. The two techniques used were *column wrap mapping* and *column block mapping*. Column wrap mapping consists of interleaving the columns onto the processors. It is described in detail in Section 6.2. Column block mapping consists of distributing the columns onto the processors using contiguous blocks of columns rather than individual columns. As an example, if 4 processors were being used to fill a matrix with 100 columns, using column block mapping would mean that the first processor would fill the first 25 columns, the second processor would fill the second 25 columns, and so on.

Four sample problems were developed for each structure type. The number of unknowns ranged from 40 to 200. Each sample problem was run on both a single transputer and four transputers. Measurements were made of both matrix filling time and matrix solving time for both column wrap mapping and column block mapping.

Table 6-3 shows the measured times and calculated efficiencies for matrix filling for the different structures using wrap and block mapping.

For a single processor it is seen that an all wire homogeneous matrix takes longer to fill than an all body homogeneous matrix of the same size. On average an all wire matrix took about 38% longer to fill than the same size all body matrix. Improvements are being been made in JUNCTION to improve the speed of calculation for wires. The cylinder, plate, cone, disk and sphere matrices all took about the same time to fill a given size matrix.

When the sample problems were run on four processors, distinct structural dependencies emerged for filling times and efficiencies. It is important to note that column block mapping always performed better than column wrap mapping. Column block mapping filling efficiencies were almost always greater than 70%, whereas column wrap mapping filling efficiencies were always between 40 and 60%. It is also interesting to note that the different structures performed differently in filling efficiencies. For column wrap mapping wires performed best followed by plates, cones, spheres, disks, and, then, cylinders. For column block mapping wires again performed best followed by cylinders, plates, cones, spheres, and, then, disks. These results are due to the nature of the physical connectivity of the various structures and how their elements are distributed to the columns

Table 6-3. Matrix filling times/efficiencies for various structures.

Structure Type	Number of Unknowns	1 Processor	4 Processors			
			Wrap Mapping		Block Mapping	
		TIME,sec	TIME	EFFIC	TIME	EFFIC
WIRE	47	7.38	3.32	55.6%	1.97	93.7%
	97	30.78	14.06	54.7%	8.08	95.2%
	147	70.51	31.54	55.9%	17.95	98.2%
	197	126.06	56.91	55.4%	32.22	97.8%
CYLINDER	56	8.56	4.97	43.1%	2.80	76.4%
	104	27.04	15.78	42.8%	7.94	85.1%
	152	55.95	32.69	42.8%	15.68	89.2%
	200	95.17	55.62	42.8%	25.99	91.5%
PLATE	40	5.12	2.66	48.1%	1.66	77.1%
	96	25.11	12.69	49.5%	7.88	79.7%
	133	45.7	25.95	44.0%	14.01	81.5%
	176	76.87	39.15	49.1%	21.92	87.7%
CONE	52	7.15	4.08	43.8%	2.54	70.4%
	100	24.09	13.88	43.4%	7.36	81.8%
	155	55.85	29.12	47.9%	16.56	84.3%
	200	90.52	46.58	48.6%	25.31	89.4%
DISK	49	6.60	3.77	43.8%	2.77	59.6%
	98	25.19	13.7	46.0%	10.42	60.4%
	150	55.65	29.84	46.6%	20.05	69.4%
	200	97.01	53.12	45.7%	34.33	70.6%
SPHERE	60	9.06	4.82	47.0%	3.23	70.1%
	90	19.75	10.65	46.4%	6.85	72.1%
	168	66.56	37.98	43.8%	20.27	82.1%
	198	91.84	47.99	47.8%	28.96	79.3%

of the matrix. Again, in JUNCTION calculations are made with respect to faces and segments. To avoid duplication of computation on the processors it is advantageous to have all the edge computations for a given face to be on the same processor. For a wire both nodes of a given segment should be on the same processor.

Table 6-4 shows the measured times and calculated efficiency for matrix factoring and solving for the different structures.

In matrix factoring and solving there are no structural dependencies. It should also be noted that as the number of unknowns increases, the factoring and solving efficiencies increase. For 200 unknowns factoring and solving efficiency is greater than 95% percent. Matrix filling efficiency also increases as the number of unknowns increases.

Table 6-4. Matrix factor and solve times/efficiency for various structures.

Structure Type	Number of Unknowns	1 Processor	4 Processors	
		TIME,sec	TIME	EFFIC
WIRE	47	0.66	0.22	75.0%
	97	5.34	1.48	90.2%
	147	18.09	4.81	94.0%
	197	42.94	11.19	95.9%
CYLINDER	56	1.13	0.35	80.7%
	104	6.70	1.81	92.5%
	152	20.22	5.34	94.7%
	200	45.36	11.79	96.2%
PLATE	40	0.42	0.15	70.0%
	96	5.12	1.44	88.9%
	133	13.35	3.58	93.2%
	176	30.55	8.04	95.0%
CONE	52	0.92	0.29	79.3%
	100	5.97	1.63	91.6%
	155	21.45	5.63	95.2%
	200	45.41	11.79	96.3%
DISK	49	0.78	0.25	78.0%
	98	5.60	1.54	90.9%
	150	19.48	5.11	95.3%
	200	45.32	11.78	96.2%
SPHERE	60	1.37	0.41	83.5%
	90	4.38	1.21	90.5%
	168	27.10	7.11	95.3%
	198	44.02	11.41	96.5%

6.3.2 Heterogeneous structures

The heterogeneous structures that were evaluated consisted mostly of square plates with numerous attached wires. This allowed the evaluation of matrices with various numbers of body, wire, and junction columns.

After evaluating a large number of heterogeneous problems a number of observations were made. These observations are summarized below:

- The junction columns are scattered within the wire portion of the matrix. The distribution of the junction columns depends on how the problem is initially specified. Fortunately, it is fairly straightforward to convert from junction number to matrix column number.
- A junction can connect to between one and six faces on a body. A quirk of JUNCTION is that the code will only recognize a maximum of one junction attached to a given face.

- To achieve maximum efficiency the filling of a junction column should be done by the same processor which is filling the columns associated with the faces to which the junction is attached, since a large part of the calculations are in common. The problem is that the associated body columns are sometimes scattered all through the matrix.
- The time to fill a matrix is a function of many factors including: relative/absolute number of wire, body and junction unknowns; number of separate wires; number of segments on each wire; locations of wires and junctions relative to a body; number of faces connected to each junction.
- Developing a general method for balancing the work load and achieving optimum efficiency for a heterogeneous problem is very complicated, even for the simple problems studied involving a single plate with various attached wires. If the choice is between block and wrap mapping, block mapping gives better results. (For the problems studied, block mapping was 62 - 93% efficient, whereas wrap mapping was 41 - 52% efficient).

Based on the above observations a decision was made to implement two additional column mapping techniques. Both techniques are modifications of the standard block mapping technique.

The first technique is called *random mapping*. Random mapping is block mapping with one twist: instead of the junction columns staying grouped with the wire columns, the junction columns are filled by the processors which are filling the body columns of the matrix. The columns are redistributed to keep a balanced number of columns on each processor. As an example, suppose a matrix has 50 body columns, 50 wire columns, and 6 junctions, and the problem is being run on 4 processors. Under standard column block mapping the first 25 body columns would be filled by the first processor, the second 25 body columns would be filled by the second processor, the first 25 wire columns would be filled by the third processor, and the second 25 wire columns would be filled by the fourth processor. The junction columns, being wire columns also, would be distributed on the third and fourth processors. Under random mapping the six junction columns would first be distributed to the first two processors in the following manner: junction 1 column to first processor, junction 2 column to second processor, junction 3 column to first processor, junction 4 column to second processor, and so on. The first and second processors would each have 3 junction columns. Block processing would then be used to distribute the body and remaining wire columns, so that each processor would finish up with 25 total columns as before.

The second technique is called *1st order mapping*. This is similar to the random mapping described above except now the junction columns are assigned to the body processors using knowledge of which processor will be calculating the majority of columns associated with the faces to which that junction is attached. This could potentially cause more junction columns to end up on one of the body processors than another, but the improvement in performance could be significant.

An analysis of matrix filling efficiency was run on four processors for the problem of a square plate with 8 wires attached to it. The problem involved 96 body unknowns, 96 wire unknowns, and 8 junctions. The four different column mapping techniques were used. The results are shown in table 6-5.

The results show that random mapping only gives a slight improvement over block mapping, but 1st order mapping gives a significant improvement over block mapping.

Table 6-5. Efficiencies of various mapping techniques.

Mapping Technique	Efficiency
WRAP	40.5%
BLOCK	61.8%
RANDOM	63.9%
1ST ORDER	76.9%

7.0 RESULTS AND CONCLUSIONS

7.1 Performance Comparisons

Comparisons were run for the micro-Vax, a single transputer, the four transputer array, and the Convex Model C-220. The Convex is a mini-supercomputer which can do some automatic vectorization.

Sample data sets were generated for both bodies and wires. Eight body data sets were generated with 104, 152, 200, 248, 296, 356, 404, and 452 unknowns. Eight wire data sets were generated with 47, 97, 147, 197, 247, 297, 347, and 397 unknowns. For each data set and each hardware platform timing measurements were made for both matrix filling and matrix factoring and solving. On the four transputer array the data sets were run using both column wrap mapping and column block mapping. On the Convex measurements were made of both CPU time and actual elapsed time. At the time the measurements were made there were 13 other users on the Convex and elapsed time averaged about 3.5 times longer than CPU time. This should be kept in mind when making comparisons between the various hardware platforms. Results are shown in tables 7-1 through 7-4.

Table 7-1. Time to fill all-body matrix, seconds.

Number of Unknowns	COMPUTER PLATFORM					
	Micro-Vax	1 Xputer	4 Xputer		CONVEX	
			Wrap Map	Block Map	CPU	Elapsed
104	73.7	26.6	16.7	8.8	5.1	20
152	151.7	55.0	33.4	16.5	10.7	26
200	257.5	93.8	56.1	26.6	18.3	69
248	394.0		85.4	39.7	27.9	105
296	555.9		120.1	54.9	39.4	145
356	801.6		172.8	78.0	56.9	201
404	1027.8		221.4	99.1	73.1	260
452	1282.3		276.1	122.9	91.4	329

Table 7-2. Time to factor & solve all-body matrix, seconds.

Number of Unknowns	COMPUTER PLATFORM					
	Micro-Vax	1 Xputer	4 Xputer		CONVEX	
			Wrap Map	Block Map	CPU	Elapsed
104	15.1	6.7	1.8	1.8	0.5	2
152	45.5	20.2	5.3	5.3	1.3	4
200	101.8	42.7	11.7	11.8	2.8	7
248	191.9		21.9	22.1	5.1	32
296	323.7		36.9	37.1	8.5	30
356	559.9		63.6	63.9	14.5	55
404	814.3		92.5	92.8	21.0	79
452	1137.2		129.0	129.4	29.1	102

Table 7-3. Time to fill all-wire matrix, seconds.

Number of Unknowns	COMPUTER PLATFORM					
	Micro-Vax	1 Xputer	4 Xputer		CONVEX	
			Wrap Map	Block Map	CPU	Elapsed
47	19.1	7.3	3.3	2.0	0.9	1
97	78.9	30.6	14.0	8.0	3.6	9
147	180.5	70.1	31.4	17.9	8.3	23
197	322.4	125.4	56.7	32.0	14.9	54
247	505.3		88.0	49.6	23.4	112
297	729.3		127.8	71.9	33.8	154
347	993.7		173.1	97.2	46.0	166
397	1302.1		227.8	127.8	60.2	172

The results show that the micro-Vax fills a wire matrix 32% slower than it fills a body matrix of the same size. Using column wrap mapping the four transputers fill a wire matrix 8% slower than they do a body matrix. In contrast, the Convex fills a wire matrix 15% faster than it does a body matrix! This may be due to the Convex's automatic vectorizing abilities. For comparison, a single transputer fills a wire matrix 36% slower than it fills a body matrix. The 8% figure for the four transputers can be accounted for by the fact that the wire filling efficiency (55%) is about 28% greater than the body filling efficiency (40%) for these problems and 28+8=36. The conclusion here is that for the JUNCTION code, sequentially speaking, wire filling takes about one third longer than body filling.

Some of the comparison data is displayed graphically in figures 7-1 through 7-3. The data is for an all-body matrix. The figures show comparisons between the four transputer array, the Convex (CPU time), and projected results for a sixteen transputer array. A four transputer array with 1 Megabyte of RAM per node can solve problems with up to 450 unknowns. With a sixteen transputer array problems with more than 900 unknowns could be solved.

Table 7-4. Time to factor & solve all-wire matrix, seconds.

Number of Unknowns	COMPUTER PLATFORM					
	Micro-Vax	1 Xputer	4 Xputer		CONVEX	
			Wrap Map	Block Map	CPU	Elapsed
47	1.6	0.7	0.2	0.2	0.1	0
97	12.3	5.3	1.5	1.5	0.4	1
147	41.2	18.1	4.8	4.8	1.2	5
197	97.4	42.9	11.1	11.1	2.7	10
247	189.9		21.5	21.5	5.0	26
297	327.8		37.0	37.0	8.6	35
347	520.2		58.6	58.6	13.4	39
397	776.0		87.4	87.4	19.8	57

The plots show that a sixteen transputer array would perform better than the Convex for filling the matrix and almost as good as the Convex for factoring and solving the matrix (Note: a sixteen transputer array, including the motherboard, would cost about $15K). However, no attempt was made to improve the vectorization of JUNCTION for a more efficient computation on the Convex. It is envisioned that considerable improvement could be made in the Convex times for factoring and solving of the matrix.

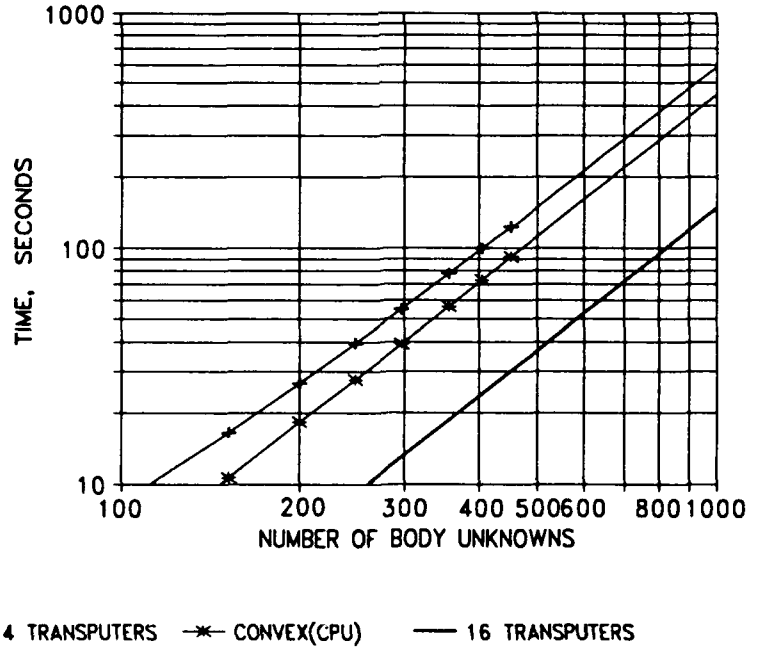

Figure 7-1. Matrix filling time comparisons, block mapping.

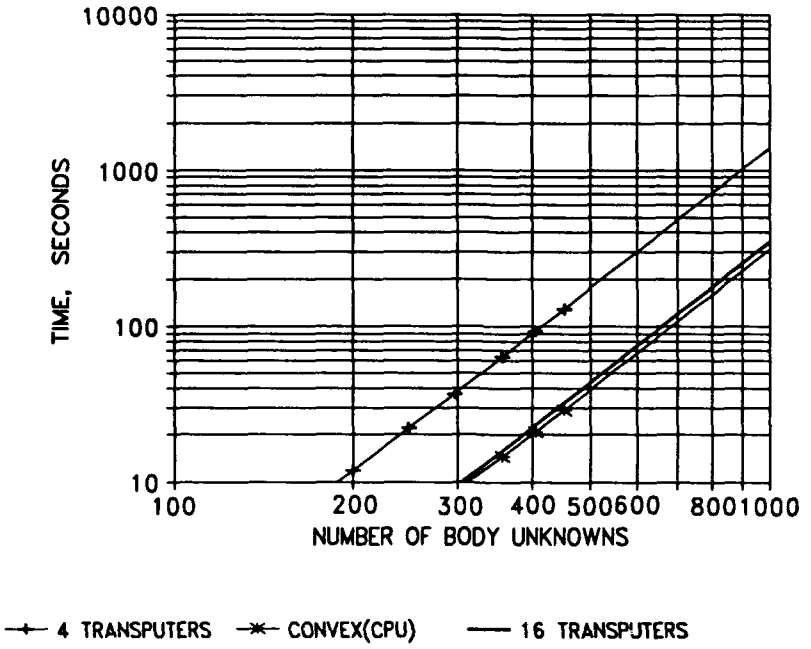

Figure 7-2. Matrix factoring and solving time comparisons.

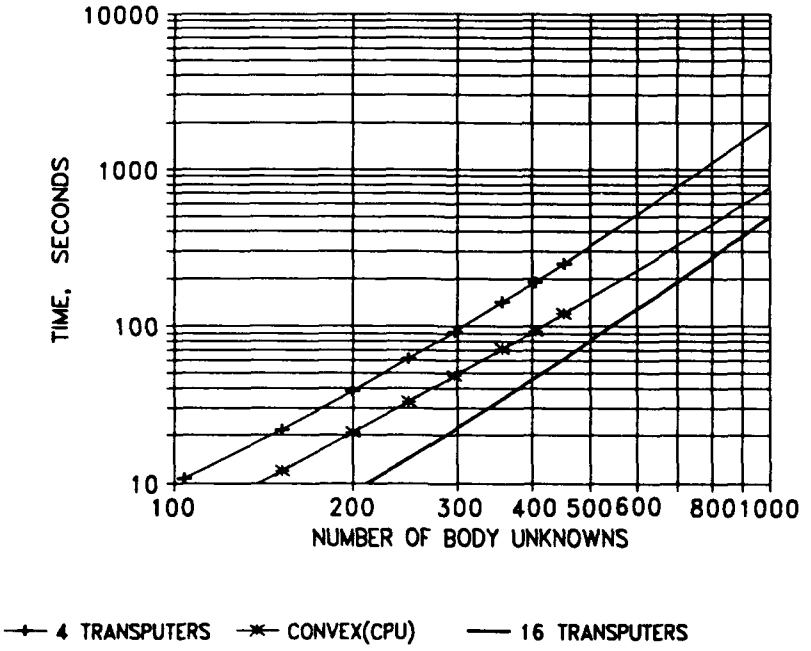

Figure 7-3. Total computation time comparisons, block mapping.

7.2 Observations

In the course of this effort a number of observations were made regarding transputers, ParaSoft EXPRESS, and parallel processing in general:

- ***A transputer array is an inexpensive, flexible parallel processing platform.*** An array of four transputer modules, each with 1 Megabyte of RAM, plus the PC motherboard cost less than $5K. The transputer array is very flexible since the number of processors can be easily expanded (just plug more modules in the sockets) and any Fortran or C code which runs on the PC can be modified to run on the transputer array.
- ***ParaSoft EXPRESS has been of great utility.*** Without EXPRESS it would have been very difficult to make the progress that was made in parallelizing the code. In addition, major modifications to the existing code would have been required, if not a complete rewriting of the code. EXPRESS will allow the porting of the code to another computer platform to be much more direct.
- ***Running an existing program on one transputer is very straightforward using EXPRESS.*** By adding just a few lines of code, then recompiling using the parallel compiler, and linking the object files to EXPRESS, an executable module which runs on a single transputer can be created for virtually any Fortran program which runs on the PC.
- ***The effort required to parallelize a code is algorithm dependent.*** Some algorithms can be parallelized just by adding a couple of lines of code. Other algorithms require extensive restructuring. Still other algorithms are not suited for implementation on a parallel computer and must be left as sequential code. It is not always obvious beforehand which algorithms will be efficient to parallelize and which won't.
- ***The optimal parallel code can be dependent on the number and type of processors as well as the size of the problem being solved.*** This was shown to be the case with the matrix solve algorithms. Two algorithms were tested: a cyclic implementation and a wavefront implementation. Although the cyclic implementation outperformed the wavefront implementation for the 4-transputer array, the literature suggests that the wavefront implementation will be the best performer for a massively parallel computing platform solving larger problems.

8.0 THE FUTURE

The state-of-the-art technology in the area of parallel processing changes monthly both for hardware platforms and software tools. The transputers used for this effort will soon be outdated, replaced by faster and more flexible processing units [Pountain, 1990]. New features are continuously being added to EXPRESS to make it more powerful and adaptable.

8.1 Future Hardware

The big news in the world of transputers is the development of the T9000. This next generation processor is being developed by the same company, INMOS, which did the original pioneering work on the development of the transputer [INMOS, 1988]. According to the manufacturer the key features of the T9000 are "a high performance pipelined superscalar processor and major support for multiprocessing applications. Peak performance will be more than 150 MIPS and 20 MFLOPS, representing a major advance in parallel computing and high speed communications...The design goals for T9000 were to enhance the transputer's position as the premier multiprocessing micro-

processor, and to establish a new standard in single processor performance, while maintaining compatibility with existing transputer products." Of course, there will be some delay between the release of the T9000 and the development of compatible motherboards and software.

8.2 Future Software

A great deal of effort is going into developing programming software for parallel computing environments. This software includes parallel compilers, debuggers, performance analysis tools, visualization tools, dynamic load balancing tools, and automatic parallelization tools. Most of the presently existing software in these areas are very crude.

ParaSoft is in the process of improving EXPRESS. New tools which are being added include VTOOL, ASPAR, and EXDIST. VTOOL will allow memory access visualization. ASPAR provides automatic parallelization of sequential C programs. EXDIST will provide dynamic load balancing. ParaSoft's ultimate goal is to run EXPRESS within a heterogeneous parallel processing environment - known as a "meta" computer. A "meta" computer is made up of a number of architecturally different computers which are networked together and perform as a single entity.

REFERENCES

Dongarra, J.J., C.B. Moler, J.R. Bunch, and G.W. Stewart. 1979. *LINPACK User's Guide*, SIAM, Philadelphia, PA.

Harrington, R.F. 1968. *Field Computation by Moment Methods*, The Macmillan Company, NY.

Heath, M.T., and C.H. Romine. 1988. "Parallel Solution of Triangular Systems on Distributed-Memory Multiprocessors," *SIAM Journal of Scientific and Statistical Computing*, Volume 9, Number 3, May.

Hwu, S.U., and D. R. Wilton. 1988. "Electromagnetic Scattering and Radiation by Arbitrary Configurations of Conducting Bodies and Wires." NOSC TD 1325 (August). Naval Ocean Systems Center, San Diego, CA.

INMOS. 1988. *The Transputer Databook*, Bath Press Ltd, Bath, England.

Li, S.T., J.C. Logan, and J.W. Rockway. 1988. "Ship EM Design Technology," *Naval Engineers Journal*, May.

ParaSoft Corporation. 1990. *EXPRESS Fortran Reference Guide, Version 3.0,* Pasadena, CA.

ParaSoft Corporation. 1990. *EXPRESS Fortran User's Guide, Version 3.0,* Pasadena, CA.

Pountain, D. 1990. "Virtual Channels: The Next Generation of Transputers," *BYTE Magazine*, April.

Tazelaar, J.M. 1988. "Parallel Processing," *BYTE Magazine*, November.

Wilton, D.R., and S.U. Hwu. 1988. "JUNCTION Code User's Manual." NOSC TD 1324 (August). Naval Ocean Systems Center, San Diego, CA.

Wilton, D.R., and S.U. Hwu. 1989. "JUNCTION: A Computer Code for the Computation of Radiation and Scattering by Arbitrary Conducting Wire/Surface Configurations," 5th Annual Review of Progress in Applied Computational Electromagnetics (March).

A RECURSIVE TECHNIQUE TO AVOID ARITHMETIC OVERFLOW AND UNDERFLOW WHEN COMPUTING SLOWLY CONVERGENT EIGENFUNCTION TYPE EXPANSIONS

Gary A. Somers and Benedikt A. Munk
The Ohio State University ElectroScience Laboratory
Department of Electrical Engineering
Columbus, Ohio 43212

Abstract

Eigenfunction expansions for fields scattered by large structures are generally very slowly convergent. The summation often consists of two factors where one factor approaches zero and the other factor grows in magnitude without bound as the summation index increases. Each term of the expansion is bounded; however, due to the extreme magnitude of the individual factors, computational overflow and underflow errors can limit the number of terms that can be computed in the summation thereby forcing the summation to be terminated before it has converged. In this paper an exact technique that circumvents these problems is presented. An auxiliary function is introduced which is proportional to the original factor with its asymptotic behavior factored out. When these auxiliary functions are introduced into the summation, we are left with the task of numerically summing products of well behaved factors. A recursion relationship is developed for computing this auxiliary function.

1 Introduction

When solving for the fields scattered by canonical geometries, the exact solution is often available in eigenfunction form. The eigenfunction form is a viable representation for the fields providing that some characteristic dimension of the structure is "small" with respect to the wavelength, otherwise, the eigenfunction expansion is very slowly convergent and additionally can exhibit the following computational difficulty. These pathological eigenfunction expansions are in the form of infinite summations of products and quotients. Each term of the summation is well-behaved, however, the magnitude of the individual factors and/or divisors become either too small or too large to handle on the computer resulting in overflow/overflow errors. Ideally, one should find an alternate representation of the series that is more quickly convergent using a technique such as Watson's transformation [*Tyras*, 1969]. For many geometries the topology of the characteristic plane may be too complicated to perform the necessary function theoretic manipulations. Therefore, one may be forced to sum the slowly convergent series.

The overflow/underflow problem can be alleviated by implementing an auxiliary function that is proportional to the original pathological function with the asymptotic behavior factored out. These auxiliary functions can be calculated "exactly" from new recursion relationships which are derived from the recursion relationship of the original function. In Section 2, the development of these auxiliary functions and the corresponding recursive techniques will be presented. Section 3 contains an example of the plane wave scattering by a circular cylinder using the techniques developed in this paper and Section 4 contains some concluding remarks. Throughout this paper an $e^{j\omega t}$ time dependence is assumed and suppressed.

2 Analytic Formulation

Symbolically, an eigenfunction expansion often has the form

$$\phi \;=\; \sum_n C_n \, S_n(x) \, L_n(x), \tag{1}$$

where C_n is a well-behaved constant, $S_n(x)$ is a factor that becomes increasingly small as n grows,

$$S_n(x) \;\stackrel{n\to\infty}{\longrightarrow}\; 0, \tag{2}$$

and $L_n(x)$ is a factor that grows without bound with increasing n,

$$L_n(x) \;\stackrel{n\to\infty}{\longrightarrow}\; \infty, \tag{3}$$

such that the product, $S_n(x)L_n(x)$, is bounded and the sum $\sum_n C_n S_n(x) L_n(x)$ is convergent.

2.1 Computation by Recursion

Recursion relationships are very convenient, and are a common way to calculate the $S_n(x)$ and $L_n(x)$ functions. Typically, the functions that arise in eigenfunction solutions to electromagnetic problems satisfy a three term recursion relationship which can be expressed as follows:

$$A(n,x)\, y_n(x) + B(n,x)\, y_{n+1}(x) + C(n,x)\, y_{n-1}(x) = 0. \tag{4}$$

For a fixed value of x, the recursion relation can be treated as a difference equation in n. A three term difference equation has 2 independent solutions [*Press, et al.*, 1988], i.e:

$$y_n(x) \;=\; \{P_n(x), Q_n(x)\}\,. \tag{5}$$

So the general solution to the recursion relation is:

$$y_n(x) \;=\; \alpha\, P_n(x) + \beta\, Q_n(x) \tag{6}$$

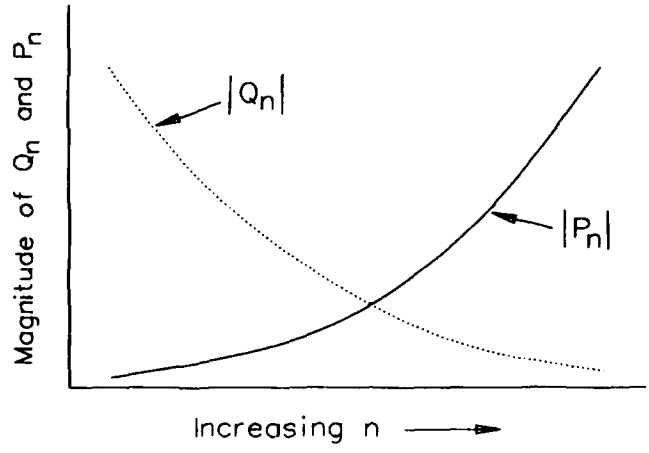

Figure 1: Relative magnitude trends of P_n and Q_n.

where α and β are constants that need to be determined by physical considerations.

Miller's algorithm [*Press, et al.*, 1988] is a commonly used technique to generate the sequence $\{P_n(x)\}$ or $\{Q_n(x)\}$. The algorithm begins by arbitrarily choosing two successive values to substitute into the recursion relationship which is used to generate the entire sequence. For example, let

$$y_0(x) = C_0(x) \quad \text{and} \quad y_1(x) = C_1(x), \tag{7}$$

which when substituted into Equation (6) yields:

$$C_0(x) = \alpha P_0(x) + \beta Q_0(x), \tag{8}$$
$$C_1(x) = \alpha P_1(x) + \beta Q_1(x). \tag{9}$$

Since $P_n(x)$ and $Q_n(x)$ are known to be independent, then by Equations (8)–(9) the values of α and β are determined uniquely, hence $y_n(x)$ is well-defined. Note that $y_n(x)$ contains components of both solutions, $\{P_n(x), Q_n(x)\}$, providing that the choice of $C_0(x)$ and $C_1(x)$ are not proportional to either $P_0(x)$ and $P_1(x)$, respectively or $Q_0(x)$ and $Q_1(x)$, respectively.

$$\begin{bmatrix} \alpha \\ \beta \end{bmatrix} = \begin{bmatrix} P_0 & Q_0 \\ P_1 & Q_1 \end{bmatrix}^{-1} \begin{bmatrix} C_0 \\ C_1 \end{bmatrix}; \qquad \begin{vmatrix} P_0 & Q_0 \\ P_1 & Q_1 \end{vmatrix} \neq 0. \tag{10}$$

At this point it is necessary to examine the stability of the desired solution. Stability refers to the relative rate of growth of the magnitude of the desired solution relative to the non-desired solution. Let's examine the common circumstance where $|P_n(x)|$ increases as n increases and $|Q_n(x)|$ decreases as n increases as shown in Figure 1. It is clear that since our solution, $y_n(x)$, contains components of both $P_n(x)$ and $Q_n(x)$, then if we consider larger

and larger values of n, $Q_n(x)$ will be less and less significant compared to $P_n(x)$, therefore:

$$y_n(x) \sim \alpha P_n(x); \qquad n \to \infty. \tag{11}$$

Under these circumstances, $P_n(x)$ is said to be stable recursing up (in n). Similarly we could have arbitrarily chosen values for $y_n(x)$ for two large successive values of n, and then recursed down thereby recovering the solution for $Q_n(x)$. In this case $Q_n(x)$ is said to be stable recursing down. Mathematically,

$$y_n(x) \sim \beta Q_n(x); \qquad n \to -\infty. \tag{12}$$

This process generates a sequence proportional to the desired $P_n(x)$ and $Q_n(x)$ sequences. $P_n(x)$ or $Q_n(x)$ can be recovered by multiplying the entire sequence $\{\alpha P_n(x)\}$ or $\{\beta Q_n(x)\}$ by $\frac{1}{\alpha}$ or $\frac{1}{\beta}$, respectively. α or β can be determined by calculating one value of $\{P_n(x)\}$ or $\{Q_n(x)\}$ and comparing it to the corresponding value of $\{\alpha P_n(x)\}$ or $\{\beta Q_n(x)\}$ which was calculated by recursion. An alternative is to use a normalization relationship of the form:

$$\sum_n \gamma_n P_n(x) = 1 \qquad \text{or} \qquad \sum_n \delta_n Q_n(x) = 1. \tag{13}$$

In the introduction of *Abramowitz and Stegun* [1972, p. XIII], there is a listing of many functions and their direction of recursive stability, and in the various chapters corresponding to the functions of interest, normalization relations of the form in Equation (13) can be found.

An alternative to Miller's algorithm can be applied if two successive values of the solution are known. If the desired solution contains only one component of the two independent solutions $\{P_n(x), Q_n(x)\}$, then it is necessary to recurse in the direction of recursive stability. Ideally, the direction of recursion should not matter, however, due to round off error in the computer, the undesired solution will be present and eventually grow to a significant value relative to the desired component of the solution.

As mentioned previously, the magnitude of the individual functions which we need to calculate can be either too large or too small for the computer to handle. This is why we introduce the auxiliary functions in Section 2.2.

2.2 The Auxiliary Functions

Since $S_n(x)$ and $L_n(x)$ are computed separately, before the sum converges individually they can become either too small or too large to calculate (due to computer limitations). To remove this upper bound limitation on the index of the summation, n, we first note the asymptotic behavior of $S_n(x)$ and $L_n(x)$.

$$S_n(x) \propto \sigma_n(x), \qquad n \to \infty, \tag{14}$$

and,

$$L_n(x) \propto \Lambda_n(x), \qquad n \to \infty. \tag{15}$$

Introduce the auxiliary functions $A_n^S(x)$ and $A_n^L(x)$ which are defined for an appropriate interval over n by the following expressions:

$$S_n(x) = A_n^S(x)\,\sigma_n(x), \tag{16}$$

and,

$$L_n(x) = A_n^L(x)\,\Lambda_n(x). \tag{17}$$

Since the auxiliary functions are equal to the original pathological functions with the asymptotic behavior factored out, the auxiliary functions remain well-behaved for all n and are therefore computationally preferable over the original $S_n(x)$ and $L_n(x)$ functions. These expressions (Equations (16) and (17)) for $S_n(x)$ and $L_n(x)$ can be substituted into the eigenfunction expansion, Equation (1), yielding:

$$\phi = \sum_n C_n\,A_n^S(x)\,\sigma_n(x)\,A_n^L(x)\,\Lambda_n(x), \tag{18}$$

or,

$$\phi = \sum_n C_n'(x)\,A_n^S(x)\,A_n^L(x), \tag{19}$$

where,

$$C_n'(x) = C_n\,\sigma_n(x)\,\Lambda_n(x). \tag{20}$$

The expression for $C_n'(x)$ can usually be significantly simplified which eliminates the necessity to compute the extremely small and extremely large values for $\sigma_n(x)$ and $\Lambda_n(x)$, respectively as $n \to \infty$.

The three factors in each term of Equation (19) are well-behaved for large values of n which makes this procedure convenient for computing a slowly convergent eigenfunction expansion.

It is common practice to extract a factor from functions that grow without bound. The main contribution of this paper is the computation procedure for the auxiliary functions which is presented in the next section.

2.2.1 Computation of the Auxiliary Functions by Recursion

The direction of recursive stability of an auxiliary function is the same as the function from which it was derived, therefore Miller's algorithm can also be applied to auxiliary functions. We begin by assuming that the recursion relationship for the original function (Equation (4)) is known. If we are trying to calculate $A_n^L(x)$, the auxiliary function for $L_n(x)$, then we simply substitute Equation (17) into the recursion relationship, Equation (4).

$$A_n(x)\,\Lambda_n(x)\,A_n^L(x) + B_n(x)\,\Lambda_{n+1}(x)\,A_{n+1}^L(x) + C_n(x)\,\Lambda_{n-1}(x)\,A_{n-1}^L(x) = 0 \tag{21}$$

In this form, the recursion relationship would experience the same overflow and underflow difficulties as the original function (due to the asymptotic factors $\Lambda_n(x)$, $\Lambda_{n+1}(x)$ and

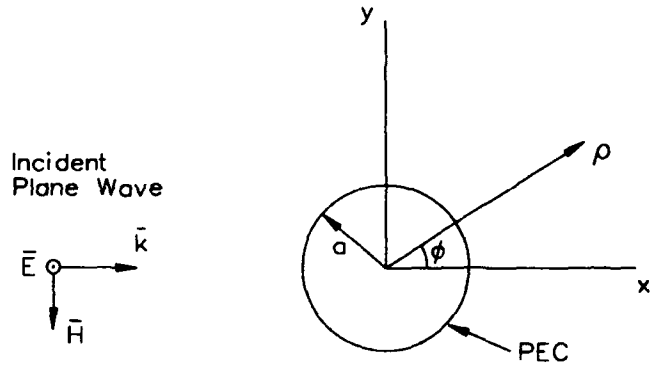

Figure 2: Plane wave incident upon PEC circular cylinder.

$\Lambda_{n-1}(x)$). It can, and must, be analytically simplified at this stage to avoid taking differences of very large numbers which is a computational faux pas. Section 3 illustrates this procedure by presenting an example which calculates the plane wave scattering by a circular cylinder.

3 Example: Scattering by a PEC Circular Cylinder

In this section we are presenting an example that applies the general technique outlined in this paper to the specific problem of determining the total (incident + scattered) z-directed electric field when a TM_z plane wave is incident upon a perfect electric conducting (PEC) circular cylinder which has its axis along the z-axis. The incident field is given by:

$$E_z^i = E_0\, e^{-jkx} = E_0\, e^{-jk\rho\cos\phi} = E_0 \sum_{n=-\infty}^{\infty} j^{-n} J_n(k\rho)\, e^{jn\phi}, \tag{22}$$

where E_0 is the complex amplitude and the coordinates x, ρ and ϕ are shown in Figure 2. The total z-directed field is given by [*Harrington*, 1961]:

$$E_z = E_0 \sum_{n=-\infty}^{\infty} j^{-n} \left[J_n(k\rho) - \frac{J_n(ka)}{H_n^{(2)}(ka)} H_n^{(2)}(k\rho) \right] e^{jn\phi} \tag{23}$$

It is possible to convert this series into a more quickly converging representation, however, this will not be done since the goal of this section is to illustrate the recursive technique outlined in this paper by a simple example. An additional numerical difficulty which will not be addressed in detail here, with the form of Equation (23) is that when computing the total fields near the cylinder, $\rho \approx a$, there can be a loss of significant digits. This may be overcome by computing the cross product directly by means of recursion relations

[*Abramowitz and Stegun*, 1972, p. 361]. Note that this problem does not occur when computing the scattered fields alone.

Using the relationship that Z_n, any integer order Bessel function $(J_n, Y_n, H_n^{(1)}, H_n^{(2)})$, satisfies:

$$Z_{-n} = (-1)^n Z_n, \tag{24}$$

we can express the total fields as:

$$E_z = E_0 \sum_{n=0}^{\infty} \epsilon_n j^{-n} \left[J_n(k\rho) - \frac{J_n(ka)}{H_n^{(2)}(ka)} H_n^{(2)}(k\rho) \right] \cos(n\phi), \tag{25}$$

where,

$$\epsilon_n = \begin{cases} 1 \; ; & n = 0, \\ 2 \; ; & n \neq 0. \end{cases} \tag{26}$$

Notice that the second term in the brackets exhibits the behavior that is discussed in this paper, namely that each individual factor grows without bound $(H_n^{(2)})$, or approaches zero (J_n), as n increases. The asymptotic behavior of the Bessel functions of the first and second kind are given by [*Abramowitz and Stegun*, 1972, p. 365]:

$$J_n(x) \sim \frac{1}{\sqrt{2\pi n}} \left(\frac{ex}{2n} \right)^n = \sigma_n(x), \qquad n \to \infty, \tag{27}$$

and,

$$Y_n(x) \sim -\sqrt{\frac{2}{\pi n}} \left(\frac{ex}{2n} \right)^{-n}, \qquad n \to \infty, \tag{28}$$

and since,

$$H_n^{(2)}(x) = J_n(x) - j\, Y_n(x). \tag{29}$$

Then,

$$H_n^{(2)}(x) \sim j\sqrt{\frac{2}{\pi n}} \left(\frac{ex}{2n} \right)^{-n} = \Lambda_n(x), \qquad n \to \infty. \tag{30}$$

So then the auxiliary functions are defined by:

$$J_n(x) = \frac{1}{\sqrt{2\pi n}} \left(\frac{ex}{2n} \right)^n A_n^J(x), \quad n = 1, 2, 3, \ldots, \infty, \tag{31}$$

and,

$$H_n^{(2)}(x) = j\sqrt{\frac{2}{\pi n}} \left(\frac{ex}{2n} \right)^{-n} A_n^{H^{(2)}}(x), \quad n = 1, 2, 3, \ldots, \infty. \tag{32}$$

All Bessel functions satisfy the same recursion relationship [*Abramowitz and Stegun*, 1972, p. 365]:

$$Z_{n-1}(x) + Z_{n+1}(x) = \frac{2n}{x} Z_n(x). \tag{33}$$

By comparing the asymptotic forms of $J_n(x)$ and $Y_n(x)$, $J_n(x)$ is downward stable and $Y_n(x)$ is upward stable [*Abramowitz and Stegun*, 1972, p. XIII]. Since the Hankel function consists of both $J_n(x)$ and $Y_n(x)$ and they differ in their direction of recursive stability, it is necessary to decompose the Hankel function to determine $J_n(x)$ and $Y_n(x)$ separately.

The definitions for the auxiliary functions (Equations (31) and (32)) are indeterminate for $n = 0$. For this reason, we will extract the $n = 0$ term of Equation (25) and begin the sum from $n = 1$.

$$\begin{aligned} E_z &= E_0 \left[J_0(k\rho) - \frac{J_0(ka)}{H_0^{(2)}(ka)} H_0^{(2)}(k\rho) \right] \\ &\quad + 2E_0 \sum_{n=1}^{\infty} \frac{j^{-n}}{\sqrt{2\pi n}} \left[\left(\frac{ek\rho}{2n} \right)^n A_n^J(k\rho) - \left(\frac{eka^2}{2n\rho} \right)^n \frac{A_n^J(ka)}{A_n^H(ka)} A_n^H(k\rho) \right] \cos(n\phi). \end{aligned} \tag{34}$$

Calculation of $A_n^J(x)$

The recursion relation which defines $A_n^J(x)$ is found by substituting Equation (31) into Equation (33). After algebraic simplification, the following form of the recursion relation is obtained:

$$A_n^J(x) = e \left(\frac{n}{n+1} \right)^{n+1/2} A_{n+1}^J(x) - \frac{(\frac{1}{2}ex)^2}{(n+2)^2} \left(\frac{n}{n+2} \right)^{n+1/2} A_{n+2}^J(x) \tag{35}$$

where e is the base of the natural logarithm. This is in a form suitable for downward recursion.

We will apply Miller's algorithm to determine a sequence denoted by $\tilde{A}_n^J(x)$ which is proportional to the desired $A_n^J(x)$ sequence. We choose N to be larger than the maximum number of terms expected to be summed by M. Also, let:

$$\tilde{A}_N^J(x) = 1, \tag{36}$$

and,

$$\tilde{A}_{N+1}^J(x) = 0. \tag{37}$$

Use the recursion relationship (Equation (35)) to determine $\{\tilde{A}_n^J(x)\}$ for $n = 1, 2, 3, \ldots N-1$. $\{\tilde{A}_n^J(x)\}$ is a sequence proportional to the desired sequence $\{A_n^J(x)\}$. There are many ways to normalize the sequence $\{\tilde{A}_n^J(x)\}$. Here we will use Equation (31) to determine $A_1^J(x)$ which will then be compared to $\tilde{A}_1^J(x)$ to determine the constant of proportionality, β.

$$\beta = \frac{ex}{2\sqrt{2\pi}} \frac{\tilde{A}_1^J(x)}{J_1(x)}, \tag{38}$$

So then,

$$\{A_n^J(x)\} = \frac{1}{\beta}\{\tilde{A}_n^J(x)\}; \qquad n = 1, 2, 3, \ldots N - M. \tag{39}$$

The following table was constructed, using these procedures, to emphasize the favorable behavior of the magnitude of the auxiliary functions compared to the magnitude of the Bessel functions. We are showing two arguments of the auxiliary function for a wide range of orders. This table illustrates the difficulty in computing the Bessel functions directly. The triple asterisk indicates that this term is larger than 10^{308}, the largest number our computer can handle.

n	$J_n(1)$	$A_n^J(1)$	$J_n(5)$	$A_n^J(5)$
1	4.4005×10^{-1}	0.81157	-3.2758×10^{-1}	−0.12083
2	1.1490×10^{-1}	0.88200	4.6565×10^{-2}	0.014297
5	2.4976×10^{-4}	0.94323	2.6114×10^{-1}	0.31559
20	3.8735×10^{-25}	0.98405	2.7703×10^{-11}	0.73798
50	2.9060×10^{-78}	0.99345	2.2942×10^{-45}	0.88306
100	8.4318×10^{-189}	0.99670	6.2678×10^{-119}	0.93919
200	***	0.99834	4.7600×10^{-296}	0.96898
500	***	0.99927	***	0.98737
1000	***	0.99965	***	0.99367

Calculation of $A_n^{H^{(2)}}(x)$

As mentioned previously, the Hankel function, $H_n^{(2)}(x)$, consists of Bessel functions of the first and second kind, $J_n(x)$ and $Y_n(x)$, respectively. $J_n(x)$ and $Y_n(x)$ differ in their direction of recursive stability, therefore, they must be computed separately. We note that as a consequence of Equations (29) and (32):

$$J_n(x) = -\sqrt{\frac{2}{\pi n}}\left(\frac{ex}{2n}\right)^{-n} \mathcal{I}m\{A_n^{H^{(2)}}(x)\} \tag{40}$$

and,

$$Y_n(x) = -\sqrt{\frac{2}{\pi n}}\left(\frac{ex}{2n}\right)^{-n} \mathcal{R}e\{A_n^{H^{(2)}}(x)\}. \tag{41}$$

From these relationships, we determine that $\mathcal{I}m\{A_n^{H^{(2)}}(x)\}$ is stable recursing down and that $\mathcal{R}e\{A_n^{H^{(2)}}(x)\}$ is stable recursing up. Substituting Equation (40) into Equation (33) yields the following recursion relation in a suitable form for downward recursion.

$$\begin{aligned}\mathcal{I}m\{A_n^{H^{(2)}}(x)\} = {} & \frac{1}{e}\left(\frac{2n}{x}\right)^2\left(\frac{n+1}{n}\right)^{n+\frac{3}{2}} \mathcal{I}m\{A_{n+1}^{H^{(2)}}(x)\} \\ & -\left(\frac{2n}{ex}\right)^2\left(\frac{n+2}{n}\right)^{n+\frac{3}{2}} \mathcal{I}m\{A_{n+2}^{H^{(2)}}(x)\}\end{aligned} \tag{42}$$

We can use this recursion relation along with Equation (40) with $n = 1$ (for normalization), to apply Miller's algorithm.

$$\mathcal{I}m\{A_1^{H^{(2)}}(x)\} = -\sqrt{\frac{\pi}{2}}\frac{ex}{2}\, J_1(x) \tag{43}$$

The calculation of $\mathcal{R}e\{A_n^{H^{(2)}}(x)\}$ requires two starting values and the recursion relationship since it is upward stable. The two starting values are obtained by substituting $n = 1$ and $n = 2$ into Equation (41).

$$\mathcal{R}e\{A_1^{H^{(2)}}(x)\} = -\sqrt{\frac{\pi}{2}}\frac{ex}{2}\, Y_1(x), \tag{44}$$

and,

$$\mathcal{R}e\{A_2^{H^{(2)}}(x)\} = -\sqrt{\pi}\left(\frac{ex}{4}\right)^2 Y_2(x). \tag{45}$$

The recursion relation is obtained by substituting Equation (41) into Equation (33) yielding the following recursion relationship for $\mathcal{R}e\{A_n^{H^{(2)}}(x)\}$ in a suitable form for upward recursion.

$$\begin{aligned}\mathcal{R}e\{A_n^{H^{(2)}}(x)\} \;=\; & e\left(\frac{n-1}{n}\right)^{n-1/2}\mathcal{R}e\{A_{n-1}^{H^{(2)}}(x)\} \\ & -\frac{\left(\frac{1}{2}ex\right)^2}{(n-2)^2}\left(\frac{n-2}{n}\right)^{n-1/2}\mathcal{R}e\{A_{n-2}^{H^{(2)}}(x)\}\end{aligned} \tag{46}$$

The following table is presented for a comparison of the Hankel function of the second kind with its auxiliary function. We are showing two arguments of the auxiliary function for a wide range of orders.

n	$H_n^{(2)}(1)$	$A_n^{H^{(2)}}(1)$	$H_n^{(2)}(5)$	$A_n^{H^{(2)}}(5)$
1	$(4.4005 + j7.8121) \times 10^{-1}$	$1.3307 - j0.74960$	$(-3.2758 - j1.4786) \times 10^{-1}$	$-1.2594 + j2.7900$
2	$(0.11490 + j1.6507) \times 10^{0}$	$1.3511 - j0.0940$	$(0.46565 - j3.6766) \times 10^{-1}$	$-7.5237 - j0.9529$
5	$(0.0000 + j2.6041) \times 10^{2}$	$1.0831 + j0.0000$	$(2.6114 + j4.5369) \times 10^{-1}$	$5.8970 - j3.3942$
20	$(0.0000 + j4.1140) \times 10^{22}$	$1.0175 + j0.0000$	$(0.0000 + j5.9340) \times 10^{8}$	$1.3996 + j0.0000$
50	$(0.0000 + j2.1911) \times 10^{77}$	$1.0068 + j0.0000$	$(0.0000 + j2.7888) \times 10^{42}$	$1.1381 + j0.0000$
100	$(0.0000 + j3.7753) \times 10^{185}$	$1.0034 + j0.0000$	$(0.0000 + j5.0849) \times 10^{115}$	$1.0661 + j0.0000$
200	* * *	$1.0017 + j0.0000$	$(0.0000 + j3.3446) \times 10^{292}$	$1.0323 + j0.0000$
500	* * *	$1.0007 + j0.0000$	* * *	$1.0128 + j0.0000$
1000	* * *	$1.0003 + j0.0000$	* * *	$1.0064 + j0.0000$

4 Conclusion

In this paper we introduce a technique which circumvents the need to compute very large or very small special functions that commonly appear in eigenfunction expansions. This was accomplished by introducing a set of well-behaved auxiliary functions which are equal to the original special function with its asymptotic behavior factored out. When the eigenfunction expansion is expressed in terms of these auxiliary functions, the summation can be simplified resulting in well-behaved factors in the sum. The auxiliary functions can be computed via modified recursion formulas.

This procedure is formally exact since we are not making any approximations – only substitutions. Typically, when calculating summations of the type addressed here without the use of the auxiliary functions, at some point in the summation (which needs to be determined), an asymptotic form is substituted into the expression. The procedure described herein avoids the need to switch functional representations thereby eliminating the need to determine the value of the index to implement the asymptotic representation.

In this paper we have restricted our development of the auxiliary functions to the extraction of the asymptotic form of the function. The procedure is not limited to this asymptotic extraction. Any functional form that is convenient for the formulation of the problem at hand can be extracted in a similar manner.

References

Abramowitz, M. and Stegun, I. E., *Handbook of Mathematical Functions with Formulas, Graphs, and Mathematical Tables*, National Bureau of Standards Applied Mathematics Series 55, Washington, D.C., 1972.

Harrington, R. F., *Time-Harmonic Electromagnetic Fields*, p. 232, McGraw-Hill Book Company, New York, 1961.

Press, W. H., Flannery, B. P. Teukolsky, S. A. and Vetterling, W. T., *Numerical Recipes*, p. 141, Cambridge University Press, Cambridge, 1988.

Tyras, G., *Radiation and Propagation of Electromagnetic Waves*, p. 286, Academic Press, New York, 1969.

'H-ORIENTED' AND 'B-ORIENTED' METHODS IN A PROBLEM OF NONLINEAR MAGNETOSTATICS: SOME METHODOLOGICAL REMARKS

A. Bossavit
Électricité de France, 1 Av. du Général de Gaulle,
92141 Clamart

ABSTRACT

Problems which depend on a small parameter in their formulation can often be studied by a perturbation approach. Whether the perturbation is "regular" or "singular" is important in many respects. In magnetostatics, due to some inherent duality, both kinds of perturbation may happen, depending on the chosen formulation ("b-oriented" vs. "h-oriented" methods). Singularly perturbed problems are numerically more difficult than regularly perturbed ones. We suggest that this might explain why, as some recent numerical observations seem to suggest, b-oriented methods should give better accuracy in a specific class of nonlinear magnetostatic problems at high permeability.

INTRODUCTION

This paper is a case study, which butts on a methodological question of such generality that it seems almost preposterous to address it in written form: how should the particularities of a physical problem (here, the presence of "small parameters") guide the modeler in the selection of a numerical method? This is a basic subject, one about which everybody has definite opinions (and even, sometimes, strong feelings), but also an elusive one, difficult to treat in a comprehensive way. (This is why there are relatively so few books or paper collections devoted to mathematical modelling, like e.g., [1, 2, 3, 6, 7, 9, 11, 13, 15, 22]. Why most of them seem so remote from the kind of mathematical modelling *we* do is a puzzling question.)

One might say that, after all, this is quite normal. Why should "tricks of the trade" be honored with formal dissertations? But a moment of reflection will show that some of the most powerful of such tricks deserve to be thus treated, that they are, and that it is eventually beneficial for all those concerned. Take Fourier analysis, for instance. On one level, it is an efficient *dimensionality-reduction* device, which helps replace the numerical solution of a fully three-dimensional problem with a series of simpler ones, in one or two dimensions. On another level, it is the practical and usable by-product of a majestic mathematical theory: harmonic analysis [12, 17]. Is this a coincidence? Probably not. The development of the theory was stirred by the efficiency of what was at the time a modelling trick, the use of trigonometric series in the study of heat transfer, and it has payed back largely, as far as mathematical modelling is concerned. This is the classical example of a practical modelling tool—a trade trick—backed by a strong mathematical theory, and of the dialectics of their historical development. Other examples will come to

mind (the "least squares" trick in relation with control and identification theory, some aspects of Geometrical Diffraction Theory, some statistical tests . . .).

The small parameter issue (an instance of which will be presented in a moment) might deserve such a status. Here there is, no doubt, a trick: use dimensional analysis to expose "small parameters", identify the corresponding terms in the equations, drop them. There is also a grandiose theory, or rather, theories: asymptotic analysis, perturbation theory. But the theory appears incomplete, it lacks unity, and the trick itself is far from being fail-safe: when your equation is $-\varepsilon u'' + u = f$, or $-u'' + \varepsilon u = f$, should you drop the ε-term, or not? (Think of ε as related, for instance, with the skin-depth.) The answer to this particular question is known, but lots of similar ones are still to be addressed. Here is a rich field of study, full of prospects for both intellectually stimulating mathematical theories and usable practical recipes.

Yet, case studies may prove more effective than comprehensive studies of large scope, at this stage. One such study comes from the experience of a small electromagnetism community (the "TEAM workshop", [22, 23]) whose emphasis is on low-frequency and static situations. The test-case, described below in general terms, is a non-linear magnetostatics problem on which the same observation has been made by several independent investigators: numerical methods based on the use of the vector potential tend to perform better than those using a scalar potential. This calls for an explanation, which is the theme of the present paper. In short, there are two "small parameters" in this problem, the ratio of the airgap to some characteristic length, and the ratio of permeabilities in the air and in the iron. Their interplay results in the possibility of formulating the problem as a perturbation with respect to some similar, much simpler problem. This is a standard idea. What is new here is that, due to some symmetry inherent in Maxwell equations, there are *two* ways to do this, based respectively on the use of the scalar and of the vector potential, and that the nature of the perturbation is not the same for both: it's "regular" perturbation in the former case, "singular" perturbation in the latter. An attempt is made to link these facts with the numerical observations.

Similar situations where two small parameters are "competing", each one driving the problem toward different limits, seem to be common to other areas of electromagnetics, for example, skin effect, current flow around a crack, and even (for higher frequencies) surface impedance.

'H-ORIENTED' AND 'B-ORIENTED' METHODS IN MAGNETOSTATICS

We shall consider the following general situation (Fig. 1): a coil C (sustaining a given, permanent, current-density j^g), and a ferromagnetic piece M. The whole space is E, and $A = E - C - M$ is the air-region. A non-linear behavior law $b = \Gamma(h)$ is given (no

hysteresis). For the present discussion, we assume a Γ such that vectors b(x) and h(x) are collinear at all points x in M, and that b(x) vanishes if h(x) does. One is requested to compute the fields b and h. The relevant equations are

(1) $\quad \text{curl } h = j^g \text{ in E, } b = \Gamma(h), \text{ div } b = 0 \text{ in E.}$

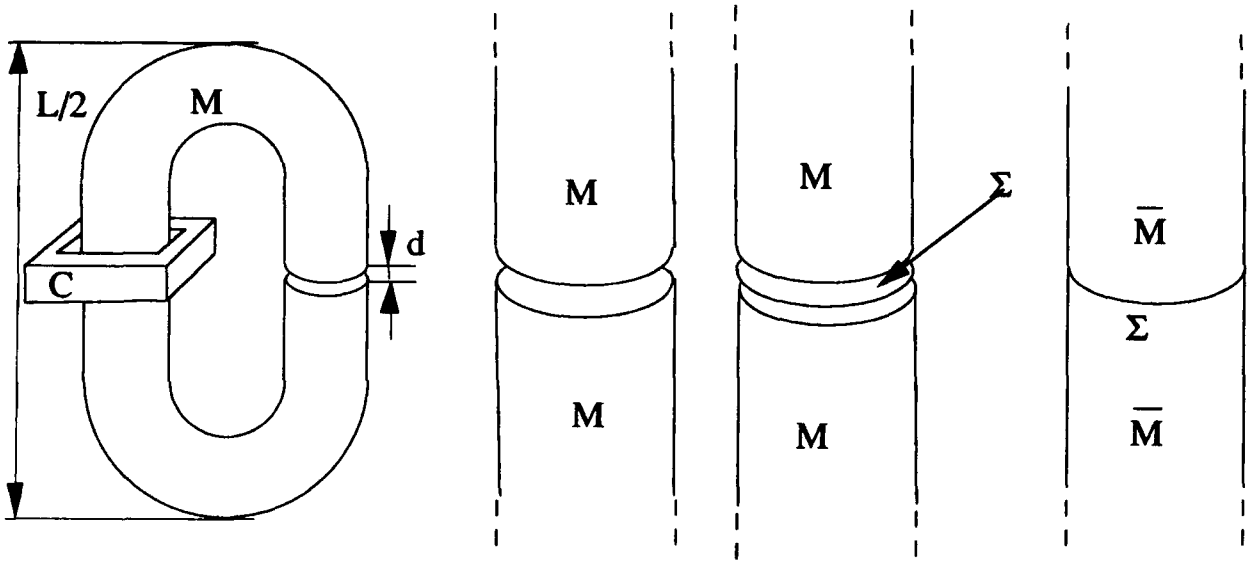

Figure 1. A typical problem (left). Definition of surface Σ and domain $\overline{M}$, to be used in the sequel (right).

We are only interested here in comparing the accuracy achievable with various methods, not in things like the computing time, the number of steps in iterative procedures, etc. So we may consider a *linear* problem with the same solution as (1), namely

(2) $\quad \text{curl } h = j^g \text{ in E, } b = \mu\, h, \text{ div } b = 0 \text{ in E,}$

where μ is the function $x \rightarrow |b(x)|/|h(x)|$, as computed from the actual solution $\{b, h\}$. Whatever can be said about the merits of various methods as regards (2) will thus be relevant to (1).

The ratio $\mu(x)/\mu_0$ is a feature of the solution (and as such, it depends on the imposed current j^g). It is usually high (about 2000, typically), but tends to decrease when the driving current j^g is increased (*saturation* phenomenon). Let us call ε the average of $\mu_0/\mu(x)$ over M. We define, for all x in M, $\mu_1(x) = \varepsilon\, \mu(x)$. Note that μ_1 is close to μ_0, except perhaps in saturated zones. This ε is one of the small parameters alluded to in the Introduction. It will play an important role in what follows. The other small parameter is

the ratio d/L of the gap-width d to the average length L of the magnetic circuit M. We shall assume that d/L, though small, is still large with respect to ε: thus, the reluctance of the whole device is mainly due to the air gap. This is the assumption used in the TEAM workshop study, and is the rule in problems of this kind. (But the assumption is a crucial one: if the reluctance was mainly due to the iron core, this would modify our conclusions.)

Although the discussion will be limited to linear problems, we are not losing anything significant in generality, because one can always tackle (1) by iterating on μ, Newton-Raphson style, a linear system being solved at each step. In fact, almost all methods in actual use in nonlinear magnetostatics seem to rely on this approach. They fall into two main families: 'b-oriented' methods, which yield b (for instance by computing the magnetic vector potential), and 'h-oriented' methods, which aim at h (for instance by computing the magnetic scalar potential). For the sake of definiteness, let us formalize this:

Definition 1. *A vector field* h *[resp.* b*] is said "curl-conformal" [resp. "div-conformal"] if its tangential [resp. normal] part is continuous across all surfaces in its domain of definition.*

Definition 2. *A method will qualify as "h-oriented" [resp. as "b-oriented"] if it computes* h *[resp.* b*] in such a way that its tangential [resp. normal] continuity is exactly enforced, i.e., if it yields a curl-conformal* h *[resp. a div-conformal* b*].*

Let us develop an example of b-oriented method. A tetrahedral mesh is first designed, large enough to cover M, C, and enough of the air-region to justify neglecting what happens outside the meshed volume. Let $\mathcal{N}$ be the set of nodes. Let λ_n be the "hat-function" associated with node n (i.e., the unique continuous, piecewise affine, function equal to 1 at node n and to 0 at all other nodes). Call IP^1 the set of all vector fields of the form

$$(3) \qquad a = \Sigma_{n \in \mathcal{N}} \mathbf{a}_n \lambda_n,$$

where the degrees of freedom (DoF) $\mathbf{a}_n$ are vectors, one per node. Now look for a in IP^1 such that

$$(4) \qquad \int_E \mu^{-1} \operatorname{curl} a \,.\, \operatorname{curl} a' = \int_E j^g \,.\, a' \quad \forall\ a' \in IP^1$$

(the so-called "weak form" of the equation $\operatorname{curl}(\mu^{-1} \operatorname{curl} a) = j^g$). This is a linear system in terms of the 3 x N components of the $\mathbf{a}_n$s (N, the number of nodes in the mesh). There exists a solution (because $\operatorname{div} j^g = 0$), perhaps not unique, but anyway, all solutions will have the same curl. (Numerical difficulties that one may encounter in solving (4) are not our concern.) This is a b-oriented method, because it gives $b = \operatorname{curl} a$, thus enforcing the

essential requirement about the continuity of the normal component of b across all surfaces, including the faces of the mesh. The field $h = \mu^{-1}$ curl a fails to have the symmetric property of continuity of its tangential part through surfaces. This is so because the relation curl $h = j^g$ is only *weakly* enforced by (4).

On the other hand, the well-known "single magnetic potential" method is h-oriented. Its principle is to look for the field h in the form $h = \text{grad } \varphi + h^g$, where h^g is a field that satisfies rot $h^g = j^g$ and div $h^g = 0$. (Such a field can be constructed from j^g by Biot-Savart integration.) The unknown in this problem is thus the potential φ. According to the general finite element approach, one thus has to find a function φ of the form

$$(5) \qquad \varphi = \Sigma_{n \in \mathcal{N}} \varphi_n \lambda_n$$

such that

$$(6) \qquad \int_E \mu \, (\text{grad } \varphi + h^g) \, . \, \text{grad } \varphi' = 0$$

for all test-functions φ' themselves of the form (5). (This is a way to enforce the condition $\text{div}(\mu h) = 0$, in weak form.) Here the φ_ns are *scalar* degrees of freedom. This time h has the required tangential continuity, but $b = \mu h$ fails to have normal continuity, because div $b = 0$ is only weakly enforced: the method is "h-oriented".

Remark. Note that φ is single-valued here. There are variants in which a similar, but possibly *multivalued* magnetic potential is used [19], or more than one potential [18]. Clearly, such methods also are h-oriented.

Not all methods fall in one of the previous categories. A method can have both orientations. But in that case the behaviour law $b = \mu h$ will fail to be exactly satisfied, in general. (This point is developed in [5].)

Now the scene is set. We shall argue as follows: "b-oriented" methods should in general work better, because the smallness of the ratio μ_0/μ results in a *regularly* perturbed problem with such formulations, whereas "h-oriented" methods suffer from *singular* behavior with respect to this same parameter. Therefore, they are more sensitive to numerical error.

SINGULAR VS. REGULAR PERTURBATIONS

Let us first recall the difference between regular and singular perturbation, with the help of a simple example. Suppose we have to solve the two-points boundary-value problem

(7) $\quad -u'' + \varepsilon\, k(x)\, u = f,\ \ u'(0) = 0,\ \ u(1) = 0,$

for a numerically small value of ε, and a given positive function k. Note that this is equivalent to minimizing the functional $F_\varepsilon(v) = \int_{[0,\,1]} (|v'|^2 + \varepsilon\, k\, |v|^2 - 2\, f\, v)$ among all those in the set $V = \{v \in C^0[0, 1] : \int_{[0,\,1]} |v'|^2 < \infty,\ v(1) = 0\}$, which can easily be done by numerical methods. But instead, in order to take advantage of ε's smallness, one would rather make use of the "limit-problem", corresponding to $\varepsilon = 0$, whose solution u_0 is obtained directly, by quadratures, without having to solve a linear system. The idea is to expand u as $u_0 + \varepsilon\, u_1 + \ldots$, and to throw this into (7): again, u_1 can be obtained by straightforward integration, the same way u_0 was. And so on. Problem (7) is a perturbation of a simpler one (namely, to find u such that $-u'' = f,\ u'(0) = 0,\ u(1) = 0$), and therefore can be solved by a cascade of similar problems. Note that u_0 still achieves the minimum of some functional (namely, $F_0(v)$) over the same set V. This is what makes the perturbation "regular": the limit solution is solution to the limit problem, as obtained by setting $\varepsilon = 0$ in either (7) or its equivalent variational formulation, "minimize $F_\varepsilon(v)$ over V". Note also that u_ε *and* its first derivative both converge (in the sense of quadratic means) to u_0 and u'_0 respectively.

In contrast, "singular perturbation" occurs with

(8) $\quad -\varepsilon\, u'' + k(x)\, u = f,\ \ u'(0) = 0,\ \ u(1) = 0.$

If one wants to solve this numerically, the smallness of ε imposes a small discretization step, which is cumbersome, so making use of the limit problem seems again a good idea. But now two things go wrong. First, the would-be "limit-problem", i.e., (7) with $\varepsilon = 0$, or its variational version, "minimize $\int_{[0,\,1]} (|k\, |v|^2 - 2\, f\, v)$ over V", has no solution. Next, when one relaxes its requirements by dropping the boundary conditions, the solution u_0 of the relaxed problem, "minimize over $L^2([0, 1])$", which is $u_0 = f$, is not the limit of u_ε in the above sense: only u_ε converges towards u_0 in L^2, whereas u'_ε does not converge to u'_0 (Fig. 2).

Singular perturbation is thus characterized by the fact that, when passing to the limit, the solution "escapes" from the set where it naturally lives, and while it still does converge to something, it is in a weaker sense, and to an object which belongs to a larger universe. It does not mean that the (non-acceptable) "limit solution" u_0 is useless as a stepping stone to obtaining the true solution, u_ε, of (8). Indeed, u_0 is a term in some asymptotic expansion of u_ε, that can be derived via a moderately involved process called "matching asymptotic expansions". (Some references to these things are [10, 14, 16, 20, 21].) Quite often, a lot of numerical work can be avoided by such an asymptotic approach to the solution. This is so because, from the numerical point of view, singularly perturbed problems are tougher than regularly perturbed ones. In the case of (8) vs. (7), a glance at Fig. 2 shows why: the

step-size has to be very small, at least in the "boundary layers" near the ends of the interval.

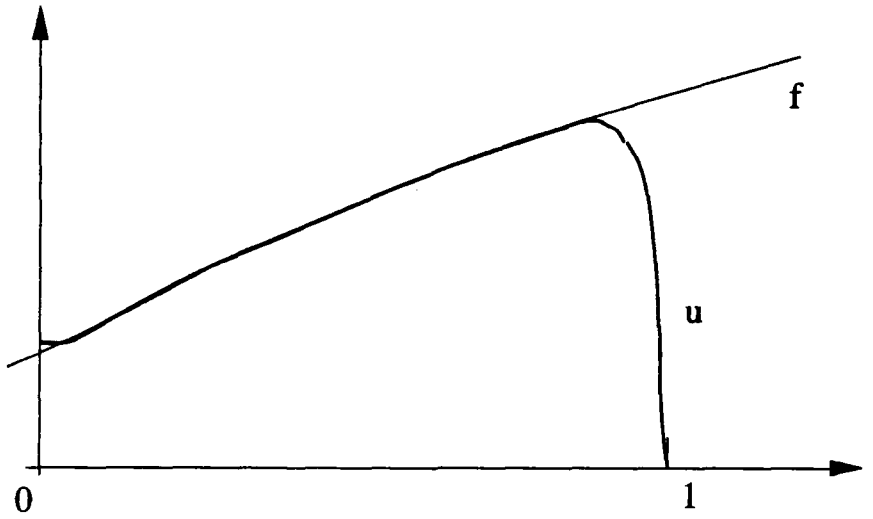

Figure 2. Solution of (7) for ε small (k = 1).

PROBLEM (2) AS A PERTUBED PROBLEM

For reference, let us write weak formulations analogous to (4) and (6), as they stand before any commitment to particular finite elements has been made. Call A (resp. Φ) the set of all square-integrable vector fields (resp. functions), with a square integrable curl (resp. gradient), over the whole space. The weak formulations are, for the (b-oriented) "a-method": *find* $a_\varepsilon \in A$ *such that*

$$\int_E \mu^{-1} \operatorname{curl} a_\varepsilon \,.\, \operatorname{curl} a' = \int_E j^g \,.\, a' \quad \forall\, a' \in A$$

(which can be rewritten as

(9) $$\int_{E-M} \mu_0^{-1} \operatorname{curl} a_\varepsilon \,.\, \operatorname{curl} a' + \varepsilon \int_M \mu_1^{-1} \operatorname{curl} a_\varepsilon \,.\, \operatorname{curl} a' = \int_E j^g \,.\, a' \quad \forall\, a' \in A),$$

and for the (h-oriented) φ-method: *find* $\varphi_\varepsilon \in \Phi$ *such that*

$$\int_E \mu\, (\operatorname{grad} \varphi_\varepsilon + h^g) \,.\, \operatorname{grad} \varphi' = 0 \quad \forall\, \varphi' \in \Phi$$

(which can be rewritten as

(10) $$\int_{E-M} \mu_0\, (\operatorname{grad} \varphi_\varepsilon + h^g) \,.\, \operatorname{grad} \varphi' + \varepsilon^{-1} \int_M \mu_1\, (\operatorname{grad} \varphi_\varepsilon + h^g) \,.\, \operatorname{grad} \varphi'$$

$$= 0 \quad \forall\, \varphi' \in \Phi).$$

Remark. one should compare (9) with the following:

$$\int \partial_x u_\varepsilon \, \partial_x u' + \varepsilon \int k \, u \, u' = \int f \, u' \quad \forall \; u' \in U,$$

which is equation (7) in weak formulation. The analogy we rely on is due to the presence of the small parameter ε in front of the second integral in both cases.

Let us now see in which way our problem (2), when formulated as (9) or as (10), can be considered a "perturbation" of some simpler one. A difficulty is that there are *two* small parameters in the picture: the above ratio ε ($\sim \mu_0/\mu$), and the ratio d/L of the gap-width to the circuit-length. The analysis in terms of two such "competing" small parameters is quite interesting; it leads—depending on which parameter dominates—to very different limit models (called "significant degenerations" in [10]), which do have meaningful interpretations within the present context. (See an application to skin-effect, and to the concept of "surface impedance" [8], in [4].) There is no space here to justify our main assumption that ε, not d/L, is the dominant small parameter in the present case: this would call for some lengthy dimensional analysis (whose principles, anyway, are familiar to all readers). We cannot either dwell on the Taylor expansions in terms of ε, and similar techniques, by which models (11) and (12) below are derived: although these are familiar and elementary mathematical tools, their application to the present case requires a heavy apparatus of functional analysis, that seems out of place. So we shall proceed more dogmatically: first, some notation, next a terse statement of the results, then some a posteriori justification.

Let us call $\overline{M}$ the union of M (cf. Fig. 1) and the gap, and Σ a surface congruent to the pole surfaces, located in the middle of the gap. Enlarge space Φ by accepting into it functions which are allowed to be *discontinuous* across Σ. Call $\overline{\Phi}$ the bigger space so obtained.

Now, the limit problems. The one in terms of the vector potential a splits into two successive problems: *find* $a_0 \in A$ *such that both conditions*

$$(11) \qquad \begin{cases} \int_{E-\overline{M}} \mu_0^{-1} \, \mathrm{curl}\, a_0 \,.\, \mathrm{curl}\, a' = \int_E j^g \,.\, a' \quad \forall \; a' \in A, \\ \\ \mathrm{curl}(\mu_1^{-1} \, \mathrm{curl}\, a_0) = 0 \quad \text{in } \overline{M}, \end{cases}$$

hold. The one in φ is *find* $\varphi_0 \in \overline{\Phi}$ *such that both conditions*

$$(12) \qquad \begin{cases} \int_{E-\overline{M}} \mu_0 \, (\mathrm{grad}\, \varphi_0 + h^g) \,.\, \mathrm{grad}\, \varphi' = 0 \quad \forall \; \varphi' \in \overline{\Phi}. \\ \\ \mathrm{grad}\, \varphi_0 + h^g = 0 \text{ in } \overline{M} - \Sigma, \end{cases}$$

hold. Then $b = \text{curl } a_0$ and $h = \text{grad } \varphi_0 + h^g$ are the limit solutions.

Why, on physical grounds? Imagine the air gap is shrunk to Σ, while the ratio $\varepsilon = \mu_0/\mu_1$ tends to zero. Then h tends to zero in the core, hence the second line of (12), and (since its circulation is held constant) tends to infinity in the air gap, hence the eventual discontinuity of the magnetic potential. As for b, one has $\text{div } b = 0$ and $\text{curl}(\mu_0^{-1} b) = j^g$ out of the core, and its flux lines impinge orthogonally to the surface of the core in the case of an infinite permeability: indeed, the first line of (11) implies all that. The second line of (11) describes what happens inside the core, and (since the tangential values of a are now known, from solving (11), first line) constitutes a well-posed problem. (All this, though it may not be obvious, relies on the above observation that d/L is large with respect to ε.)

Remark. Neither (11) or (12) are practical ways to solve the problem, if only because of the non-linearity: μ_1, of course, is not known in advance, so no useful information on the field in the core could be obtained that way. (The stray-field thus obtained, however, might be reasonably accurate.) We do not advocate the actual *use* of limit models in the specific case of Pb. 13. We just expect to get insight—about how difficult it will be to solve the *true* problem—from an examination of the *limit* one.◊

Now it should be clear that *the limit process from* (9) *to* (11) *is regular, while the one from* (10) *to* (12) *is singular:* for in the latter, there is this tendency of φ_ε to "escape from" space Φ (towards the larger one $\overline{\Phi}$), while nothing similar happens to a_ε, which stays in A.

The difference can be seen more concretely from what happens in the air at the boundary of Σ: a singularity of φ (actually, a jump-discontinuity), whereas a is regular (Fig. 3). Figure 3 is two-dimensional for convenience, but what is described here is a feature of the three-dimensional situation: the magnetic potential changes very rapidly across the airgap (Fig. 3, right). So, if one tries to model the situation by treating the airgap as a surface, across which φ can be discontinuous—which is precisely model (12)—the computed φ will look as on the left part of the figure, with an obvious singularity. Our point is that, although this limit model is not the one which is actually solved for, the latter is sufficiently closed to it for the singular character of the limit case to be felt, in various ways, when actually solving for φ.

The nature of the finite elements has not been a factor in this discussion. So we may conclude that regularity (resp. singularity) pertains to the whole family of a-methods (resp. φ-methods). Singularly perturbed problems are notoriously more difficult to solve numerically than regularly perturbed ones. Hence the tentative conclusion: b-oriented

methods *as a whole* should be considered with a favorable bias, for this particular problem. Of course, this should not be construed as a seal of approval for any *particular* b-oriented methods.

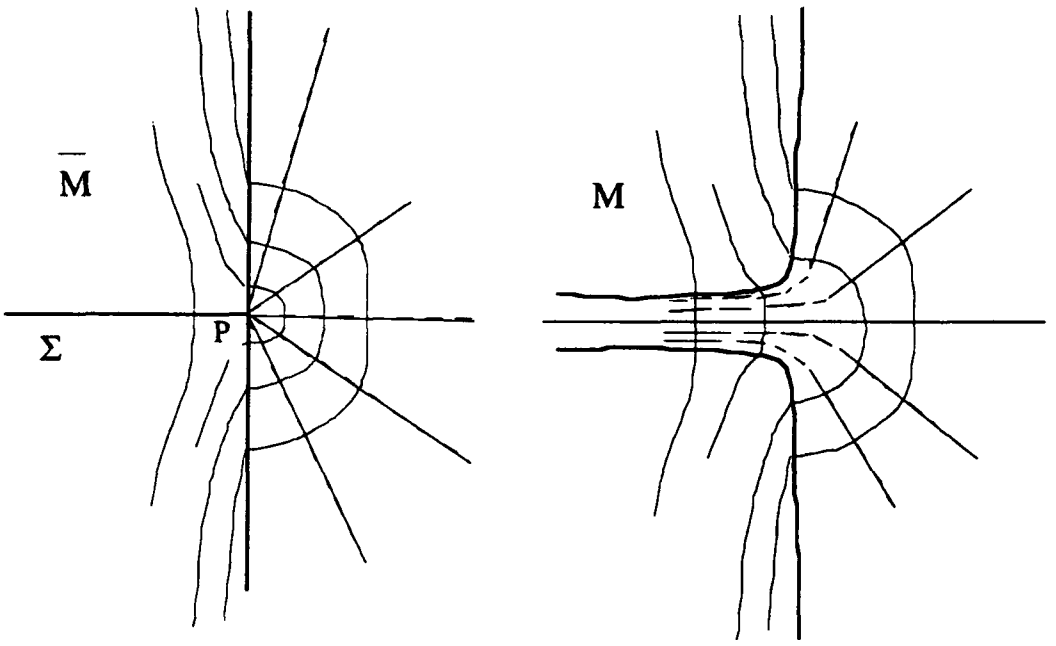

Figure 3. Flux lines in the vertical symmetry plane, near the edge of the air gap, showing the singularity of the field: left, as predicted by the limit models, right, as it really is. The situation is nearly two-dimensional. In that case, a is a scalar, whose isolines are precisely the flux-lines shown. Dotted lines are isovalues of φ, the magnetic potential. Clearly, a is continuous at point P, but φ is not, in the limit model.

CONCLUSION

Let us summarize the main line of our argumententation. The problem which is actually solved (the one with a small but non-zero ε) is closed to a singular limit when h-oriented methods are used, and to a regular limit when b-oriented methods are used. So in the critical region (near the edges of the poles), h-oriented methods are likely to behave in a nastier way than b-oriented ones. For instance, they may require a finer mesh if the same precision is to be achieved. But meshes, as a rule, are not what would be desirable, they are what computing resources allow. So we may expect, on the average, better precision from b-oriented methods in reported numerical experiments. This seems indeed to be the present trend, as regards this particular problem.

We have seen how an analysis of the nature of the perturbation (regular or singular) in a small parameter problem can be used to predict the relative success of a particular

family of numerical methods with respect to another. This was, at best, heuristics. Can the reasoning eventually be refined into one that would yield precise, provable, statements? Perhaps, but I tend to think efforts in this direction would be misdirected. In the present state of the art, it seems better to view the above explanation as a route towards a *conjecture*, to be confirmed or rejected on the basis of numerical experiments: that, for these problems of non-linear magnetostatics with high relative permeability, "b-oriented methods work better".

ACKNOWLEDGMENTS

I thank Harold Sabbagh for his encouragements to publish this study, in spite of its still immature form, and referees for their careful reading.

REFERENCES

[1] R. Aris: **Mathematical modelling techniques**, Pitman (London), 1978.

[2] E.A. Bender: **An introduction to mathematical modeling**, J. Wiley (New York), 1978.

[3] J.S. Berry et al. (eds.): **Teaching and applying mathematical modelling**, Ellis Horwood (Chichester), 1984.

[4] A. Bossavit: "Stiff problems and boundary layers in electricity: A mathematical analysis of skin-effect", in **BAIL IV** (S.K. Godunov, J.J.H. Miller, V.A. Novikov, eds.), Boole Press (Dublin), 1986, pp. 233-40.

[5] A. Bossavit: "Simplicial finite elements for scattering problems in electromagnetism", **Comp. Meth. Appl. Mech. Engng., 76**, 1989, pp. 299-316.

[6] F.H. Branin, Jr., K. Huseyin (eds.): **Problem Analysis in Science and Engineering**, Ac. Press (New York), 1977.

[7] D.N. Burghes, I. Huntley, J. McDonald: **Applying Mathematics: A Course in Mathematical Modelling**, Ellis Horwood (Chichester), 1982.

[8] E.M. Deeley: "Surface impedance near edges and corners in three-dimensional media", **IEEE Trans., MAG-26**, 2 (1990), pp. 712-14.

[9] M.D. Denn: **Process Modeling**, Longman Sc. & T. (New York), 1986.

[10] W. Eckhaus: **Asymptotic Analysis of Singular Perturbations**, North-Holland (Amsterdam), 1979.

[11] A. Friedman: **Mathematics in Industrial Problems**, Springer-Verlag (New York), 1988 (Vol. 1), 1989 (Vol. 2).

[12] R.A. Herb: "Harish-Chandra and his work", **Bull. AMS, 25**, 1 (1991), pp. 1-17.

[13] D.J.G. James, J.J. McDonald (Eds.): **Case Studies in Mathematical Modelling**, Stanley Thornes (Publishers) Ltd. (Cheltenham, U.K.), 1981.

[14] W.D. Lakin, D.A. Sanchez: **Topics in Ordinary Differential Equations**, Prindle, Weber & Schmidt (Boston), 1970 (Dover edition, New York, 1982).

[15] C.C. Lin, L.A. Segel: **Mathematics Applied to Deterministic Problems in the Natural Sciences**, SIAM (Philadelphia), 1989.

[16] J.L. Lions: **Perturbations Singulières dans les Problèmes aux Limites et en Contrôle Optimal**, Springer-Verlag (Berlin), 1973.

[17] G.W. Mackey: "Harmonic Analysis as the Exploitation of Symmetry—A Historical Survey", **Bull. A.M.S., 3**, 1, Pt. 1 (1980), pp. 543-698.

[18] S. Pissanetzky: "Solution of Three-Dimensional, Anisotropic, Nonlinear Problems of Magnetostatics Using Two Scalar Potentials, Finite and Infinite Multipolar Elements and Automatic Mesh Generation", **IEEE Trans., MAG-18**, 2 (1982), pp. 346-50.

[19] J. Simkin, C.W. Trowbridge: "Three-dimensional nonlinear electromagnetic field computations, using scalar potentials", **Proc. IEE, 127** (1980), pp. 368-74.

[20] J.G. Simmonds, J.E. Mann: **A First Look at Pertubation Theory**, Robert E. Krieger (Malabar, Fla), 1986.

[21] D.R. Smith: **Singular-perturbation Theory**, Cambridge University Press (Cambridge), 1985.

[22] L.R. Turner et al.: "Problems and Workshops for Eddy Current Code Comparison", **IEEE Trans., MAG-24**, 1 (1988), pp. 431-34.

[23] L. Turner, H. Sabbagh et al (Eds.): **Proceedings of the ACES/TEAM Workshop** (Toronto, Canada, 25-26 Oct. 1990), the Fusion Power Program at Argonne Nat. Lab., Argonne, Ill., 60439-4814.

[24] F.Y.M. Wan: **Mathematical Models and their Analysis**, Harper and Row (New York), 1989.

1992 INSTITUTIONAL MEMBERS

ANDREW CORPORATION
10500 W. 153rd St.
Orland Park, IL 60462

ARC, INC.
8201 Corporate Dr.
Landover, MD 20785

ARRL
225 Main St.
Newington, CT 06111

ASELSAN
PO Box 101
Yenimahalle, Ankara, TURKEY

BBC RESEARCH
Kingswood Warren
Tadworth, Surrey, UK K2TO 6NP

BNR EUROPE LTD.
London Rd.
Harlow, Essex, UK CM17 9NA

BOEING CO.
PO Box 3707
Seattle, WA 98124-2207

BOFORS ELECTRONICS
J-17588
Jarfalla, SWEDEN S-17588

BOLT BERANEK & NEWMAN INC.
10 Moulton St.
Cambridge, MA 02138

BOMBARDIER INC. - CANADAIR
Cargo Rd. A-4
Mirabel, Quebec, CANADA J7N 1C7

BRITISH AEROSPACE
FPC 267 PO Box 5
Filton, Bristol, UK BS12 7QW

COMPAQ COMPUTER CORPORATION
PO Bpx 692000
Houston, TX 77269-2000

CSELT - RADIO , ANTENNA DIVISION
Via Guglielmo Reiss Romoli, 274
Turin, ITALY 10148

CULHAM LAB
UK Atomic Energy Authority
Abingdon, Oxfordshr, UK OX14 3DB

D L R OBERPFAFFENHOFEN
Zentralbibliothek
Wessling, GERMANY

D S T O SALISBURY LIBRARY
Box 1500
Salisbury, SA, AUSTRALIA 5108

DAWSON SUBSCRIPTION SERVICE
PO Box 191
Mt. Morris, IL 61054-0191

DEFENCE RESEARCH ESTABLISHMENT
3701 Carling Ave/Shirley Bay
Ottawa, CANADA K1A 024

DYNETICS INC.
PO Drawer B
Huntsville, AL 35814

ECOLE SUPERIEURE D'ELECTRICITE'LSS
Plateay Du Moulon
Gif-Sur-Yvette Cedex, FRANCE

ELECTRONICS RESEARCH INC.
108 Market St.
Newburg, IN 47630

ENGINEERING DEVELOPMENT ESTAB.
Private Bag 12
Ascot Vale, Victoria, AUSTRALIA

ERIM INFORMATION CENTER
PO Box 134001 EE
Ann Arbor, MI 48113

FGAN/FHP
Neuenaher Strabe 20
Wachtberg,-Werthoven, GERMANY D-5307

FOKKER AIRCRAFT B.V.
Postbus 7600
Schiphol, NETHERLANDS 1117ZJ

GL/LID
Hanscom Department Local
Hanscom AFB, MA 01731

GRUMMAN AEROSPACE
Dept. 0589 & 0582
Bethpage, NY 11714

HARRIS CORPORATION
170 Dickinson St. NE
Palm Bay, FL 32907

HATFIELD & DAWSON
4226 Sixth Ave. NW
Seattle, WA 98107

HELSINKI UNIVERSITY OF TECHNOLOGY
Otakaari 1
Espoo, FINLAND 02150

HUNTING ENGINEERING LTD.
Reddings Wood
Ampthill, Bedford, UK MK45 2HD

IABG
Einsteinstr. 20
Ottobrunn, Bavaria, GERMANY D-8012

IMAGINEERING LTD.
95 Barber Greene Rd. #112
Don Mills, Ontario, CANADA M3C 3E9

ITT AEROSPACE/OPT DIVISION
7310 Innovation Blvd. Box 731
Ft. Wayne, IN 46801

JAMPRO ANTENNAS, INC.
6939 Power Inn Rd. Box 28425
Sacramento, CA 95828

KATHREIN-WERKE KG
Postfach 260
Rosenheim 2, GERMANY D-8200

KERSHNER, WRIGHT & HAGAMAN
5730 General Washington Dr.
Alexandria, VA 22312

KTH MIKROVAGSTEKNIK
Sandkullen
Akersberga, SWEDEN S-18492

LINDA HALL LIBRARY
5109 Cherry St.
Kansas City, MO 64110

LITTON ELECTRON DEVICES
960 Industrial Rd.
San Carlos, CA 94404

MATRA DEFENSE
37 Av. Louis Breguet
Velizy, FRANCE 78146

MCDONNELL DOUGLASTECH INC.
16761 Via Del Campo Ct.
San Diego, CA 92127-1713

MIT LINCOLN LABORATORY LIBRARY
244 Wood St.
Lexington, MA 02173-0073

MONASH UNIVERSITY
PO Box 197/.Caulfield East
Melbourne, Victoria, AUSTRALIA 3145

MOTOROLA INCORPORATED
1301 E. Algonquin Rd.
Schamburg, IL 60196

MPB TECHNOLOGIES
151 Hymus Blvd.
Point-Claire, Quebec, CANADA H9R 1E9

MRJ INCORPORATED
10455 White Granite Dr. Ste 200
Oakton, VA 22124

NAVAL AIR TEST CENTER
Bldg. 1703
Patuxent River, MD 20670

NAVAL RESEARCH LABORATORY
4555 Overlook Ave. SW
Washington, D.C. 20375-5000

NORWEGIAN TELECOM RESEARCH
PO Box 83
Kjeller, NORWAY N-2007

NOVATEL COMMUNICATIONS
1020 64th Ave. NE
Calgary, Alberta, CANADA T2E 7V8

1992 INSTITUTIONAL MEMBERS

NTL
Crawley Ct.
Winchester, Hants, UK S021 2QA

OCEAN APPLIED RESEARCH CORP
10447 Roselle St.
San Diego, CA 92121

OFFICE OF RESEARCH
PO Box 15183
Arlington, VA 22215-0183

POTCHEFSTROOM UNIVERSITY
PU for CHE
Potchefstroom, S. AFRICA 2520

PTT TELECOM B.V.
Postbus 3053
Amersfoort, NETHERLANDS 3800

RACAL-REDAC GROUP LTD.
Newtown
Tewkesbury, Glos, UK L20 8HE

RACAL-DECCA CANADA LTD.
71 Selby Rd.
Brampton, Ontario, CANADA L6W 1K5

ROCKWELL INTERNATIONAL
1745 Jeff Davis Hwy
Arlington, VA 22202

ROLM SYSTEMS INC.
4900 Old Ironsides Dr.
Santa Clara, CA 95052-8075

ROYAL AIRCRAFT ESTABLISHMENT
Main Library Q4 Building
Farnborough, Hants, UK QU14 6TD

SAAB-SCANIA AB
Dept Tustas
Linkoping, SWEDEN S-58188

SAIC
300 Nickerson Rd.
Marlborough, MA 01752

SEAVEY ENGINEERING ASSOC, INC.
135 King St. PO Box 44
Cohasset, MA 02025

SFA, INCORPORATED
1401 McCormick Dr.
Landover, MD 20785

SPEARS ASSOCIATES INC.
249 Vanderbilt Ave.
Norwood, MA 02062

STG NATIONAL LUCHE-EM
Anthony Fokkerweg 2
Ansterdam NETHERLANDS 1059

SWISS FEDERAL INSTITUTE OF TECH.
ETH Zentrum, ETZ G94
Zurich, SWITZERLAND CH-8092

SYRACUSE RESEARCH CORP.
Merrill Lane
Syracuse, NY 13210-4080

TASC
55 Walkers Brook Dr.
Reading, MA 01867

TECH NICAL RESEARCH LABORATORY
Telecomm Lab/Otakaari 7B
Espoo, FINLAND SF-01250

TELECOM AUSTRALIA
770 Blackburn Rd.
Clayton, Victoria, AUSTRALIA 3168

UNIVERSITAT DER BUNDESWEHR
Werner Heisenberg Weg 39
Neubiberg, GERMANY W 8014

VISTA RESEARCH, INC.
100 View St. #202 Box 998
Mountain View, CA 94042

XETRON CORPORATION
40 W. Crescentville Rd.
Cincinnati, OH 45246-1286

ACES COPYRIGHT FORM

This form is intended for original, previously unpublished manuscripts submitted to ACES periodicals and conference publications. The signed form, appropriately completed, MUST ACCOMPANY any paper in order to be published by ACES. PLEASE READ REVERSE SIDE OF THIS FORM FOR FURTHER DETAILS.

TITLE OF PAPER:

AUTHORS(S)

PUBLICATION TITLE/DATE:

RETURN FORM TO:
Dr. Richard W. Adler
Naval Postgraduate School
Code EC/AB
Monterey, CA 93943

PART A - COPYRIGHT TRANSFER FORM

(NOTE: Company or other forms may not be substituted for this form. U.S. Government employees whose work is not subject to copyright may so certify by signing Part B below. Authors whose work is subject to Crown Copyright may sign Part C overleaf).

The undersigned, desiring to publish the above paper in a publication of ACES, hereby transfer their copyrights in the above paper to The Applied Computational Electromagnetics Society (ACES). The undersigned hereby represents and warrants that the paper is original and that he/she is the author of the paper or otherwise has the power and authority to make and execute this assignment.

Returned Rights: In return for these rights, ACES hereby grants to the above authors, and the employers for whom the work was performed, royalty-free permission to:

1. Retain all proprietary rights other than copyright, such as patent rights.
2. Reuse all or portions of the above paper in other works.
3. Reproduce, or have reproduced, the above paper for the author's personal use or for internal company use provided that (a) the source and ACES copyright are indicated, (b) the copies are not used in a way that implies ACES endorsement of a product or service of an employer, and (c) the copies per se are not offered for sale.
4. Make limited distribution of all or portions of the above paper prior to publication.
5. In the case of work performed under U.S. Government contract, ACES grants the U.S. Government royalty-free permission to reproduce all or portions of the above paper, and to authorize others to do so, for U.S. Government purposes only.

ACES Obligations: In exercising its rights under copyright, ACES will make all reasonable efforts to act in the interests of the authors and employers as well as in its own interest. In particular, ACES REQUIRES that:

1. The consent of the first-named author be sought as a condition in granting re-publication permission to others.
2. The consent of the undersigned employer be obtained as a condition in granting permission to others to reuse all or portions of the paper for promotion or marketing purposes.

In the event the above paper is not accepted and published by ACES or is withdrawn by the author(s) before acceptance by ACES, this agreement becomes null and void.

AUTHORIZED SIGNATURE — TITLE (IIF NOT AUTHOR)

EMPLOYER FOR WHOM WORK WAS PERFORMED — DATE FORM SIGNED

PART B - U.S. GOVERNMENT EMPLOYEE CERTIFICATION

(NOTE: If your work was performed under Government contract but you are not a Government employee, sign transfer form above and see item 5 under Returned Rights).

This certifies that all authors of the above paper are employees of the U.S. Government and performed this work as part of their employment and that the paper is therefore not subject to U.S. copyright protection.

AUTHORIZED SIGNATURE — TITLE (IF NOT AUTHOR)

NAME OF GOVERNMENT ORGANIZATION — DATE FORM SIGNED

PART C - CROWN COPYRIGHT

(Note: ACES recognizes and will honor Crown Copyright as it does U.S. Copyright. It is understood that, in asserting Crown Copyright, ACES in no way diminishes its rights as publisher. Sign only if *ALL* authors are subject to Crown Copyright.

This certifies that all authors of the above Paper are subject to Crown Copyright. (Appropriate documentation and instructions regarding form of Crown Copyright notice may be attached).

AUTHORIZED SIGNATURE — TITLE OF SIGNEE

NAME OF GOVERNMENT BRANCH — DATE FORM SIGNED

Information to Authors

ACES POLICY

ACES distributes its technical publications throughout the world, and it may be necessary to translate and abstract its publications, and articles contained therein, for inclusion in various compendiums and similar publications, etc. When an article is submitted for publication by ACES, acceptance of the article implies that ACES has the rights to do all of the things it normally does with such an article.

In connection with its publishing activities, it is the policy of ACES to own the copyrights in its technical publications, and to the contributions contained therein, in order to protect the interests of ACES, its authors and their employers, and at the same time to facilitate the appropriate re-use of this material by others.

The new United States copyright law requires that the transfer of copyrights in each contribution from the author to ACES be confirmed in writing. It is therefore necessary that you execute either Part A-Copyright Transfer Form or Part B-U.S. Government Employee Certification or Part C-Crown Copyright on this sheet and return it to the Managing Editor (or person who supplied this sheet) as promptly as possible.

CLEARANCE OF PAPERS

ACES must of necessity assume that materials presented at its meetings or submitted to its publications is properly available for general dissemination to the audiences these activities are organized to serve. It is the responsibility of the authors, not ACES, to determine whether disclosure of their material requires the prior consent of other parties and if so, to obtain it. Furthermore, ACES must assume that, if an author uses within his/her article previously published and/or copyrighted material that permission has been obtained for such use and that any required credit lines, copyright notices, etc. are duly noted.

AUTHOR/COMPANY RIGHTS

If you are employed and you prepared your paper as a part of your job, the rights to your paper initially rest with your employer. In that case, when you sign the copyright form, we assume you are authorized to do so by your employer and that your employer has consented to all of the terms and conditions of this form. If not, it should be signed by someone so authorized.

> NOTE RE RETURNED RIGHTS: Just as ACES now requires a signed copyright transfer form in order to do "business as usual", it is the intent of this form to return rights to the author and employer so that they too may do "business as usual". If further clarification is required, please contact: The Managing Editor, R.W. Adler, Naval Postgraduate School, Code EC/AB, Monterey, CA, 93943, USA (408)646-2352.

Please note that, although authors are permitted to re-use all or portions of their ACES copyrighted material in other works, this does not include granting third party requests for reprinting, republishing, or other types of re-use.

JOINT AUTHORSHIP

For jointly authored papers, only one signature is required, but we assume all authors have been advised and have consented to the terms of this form.

U.S. GOVERNMENT EMPLOYEES

Authors who are U.S. Government employees are not required to sign the Copyright Transfer Form (Part A), but any co-authors outside the Government are.

Part B of the form is to be used instead of Part A only if all authors are U.S. Government employees and prepared the paper as part of their job.

> NOTE RE GOVERNMENT CONTRACT WORK: Authors whose work was performed under a U.S Government contract but who are not Government employees are required to sign Part A-Copyright Transfer Form. However, item 5 of the form returns reproduction rights to the U.S. Government when required, even though ACES copyright policy is in effect with respect to the reuse of material by the general public.

JULY 1992

INFORMATION FOR AUTHORS

PUBLICATION CRITERIA

Each paper is required to manifest some relation to applied computational electromagnetics. Papers may address general issues in applied computational electromagnetics, or they may focus on specific applications, techniques, codes, or computational issues. While the following list is not exhaustive, each paper will generally relate to at least one of these areas:

1. Code validation. This is done using internal checks or experimental, analytical or other computational data. Measured data of potential utility to code validation efforts will also be considered for publication.

2. Code performance analysis. This usually involves identification of numerical accuracy or other limitations, solution convergence, numerical and physical modeling error, and parameter tradeoffs. However, it is also permissible to address issues such as ease-of-use, set-up time, run time, special outputs, or other special features.

3. Computational studies of basic physics. This involves using a code, algorithm, or computational technique to simulate reality in such a way that better or new physical insight or understanding is achieved.

4. New computational techniques, or new applications for existing computational techniques or codes.

5. "Tricks of the trade" in selecting and applying codes and techniques.

6. New codes, algorithms, code enhancement, and code fixes. This category is self-explanatory but includes significant changes to existing codes, such as applicability extensions, algorithm optimization, problem correction, limitation removal, or other performance improvement. NOTE: CODE (OR ALGORITHM) CAPABILITY DESCRIPTIONS ARE NOT ACCEPTABLE, UNLESS THEY CONTAIN SUFFICIENT TECHNICAL MATERIAL TO JUSTIFY CONSIDERATION.

7. Code input/output issues. This normally involves innovations in input (such as input geometry standardization, automatic mesh generation, or computer-aided design) or in output (whether it be tabular, graphical, statistical, Fourier-transformed, or otherwise signal-processed). Material dealing with input/output data base management, output interpretation, or other input/output issues will also be considered for publication.

8. Computer hardware issues. This is the category for analysis of hardware capabilities and limitations in meeting various types of electromagnetics computational requirements. Vector and parallel computational techniques and implementation are of particular interest.

Applications of interest include, but are not limited to, antennas (and their electromagnetic environments), networks, static fields, radar cross section, shielding, radiation hazards, biological effects, electromagnetic pulse (EMP), electromagnetic interference (EMI), electromagnetic compatibility, power transmission, charge transport, dielectric and magnetic materials, microwave components, MMIC technology, remote sensing and geophysics, communications systems, fiber optics, plasmas, particle accelerators, generators and motors, electromagnetic wave propagation, non-destructive evaluation, eddy currents, and inverse scattering.

Techniques of interest include frequency-domain and time-domain techniques, integral equation and differential equation techniques, diffraction theories, physical optics, moment methods, finite differences and finite element techniques, modal expansions, perturbation methods, and hybrid methods. This list is not exhaustive.

A unique feature of the Journal is the publication of unsuccessful efforts in applied computational electromagnetics. Publication of such material provides a means to discuss problem areas in electromagnetic modeling. Material representing an unsuccessful application or negative results in computational electromagnetics will be considered for publication only if a reasonable expectation of success (and a reasonable effort) are reflected. Moreover, such material must represent a problem area of potential interest to the ACES membership.

EDITORIAL REVIEW

In order to ensure an appropriate level of quality control, papers are refereed. They are reviewed both for technical correctness and for adherence to the listed guidelines regarding information content. Authors should submit the initial manuscript in draft form so that any suggested changes can be made before the photo-ready copy is prepared.

STYLE

The ACES Journal is flexible, within reason, in regard to style. However, certain requirements are in effect:

1. The paper title should NOT be placed on a separate page. The title, author(s), abstract, and (space permitting) beginning of the paper itself should all be on the first page. The title, author(s), and author affiliations should be centered (center-justified) on the first page.

2. An abstract is REQUIRED. The abstract should state the computer codes, computational techniques, and applications discussed in the paper (as applicable) and should otherwise be usable by technical abstracting and indexing services.

3. Either British English or American English spellings may be used, provided that each word is spelled consistently throughout the paper.

4. Any commonly-accepted format for referencing is permitted, provided that internal consistency of format is maintained. As a guideline for authors who have no other preference, we recommend that references be given by author(s) name and year in the body of the paper (with alphabetical listing of all references at the end of the paper). Titles of journals, monographs, and similar publications should be in boldface or italic font or should be underlined. Titles of papers or articles should be in quotation marks.

5. Internal consistency shall also be maintained for other elements of style, such as equation numbering. As a guideline for authors who have no other preference, we suggest that equation numbers be placed in parentheses at the right column margin.

6. The intent and meaning of all text must be clear. For authors who are NOT masters of the English language, the ACES Editorial Staff will provide assistance with grammar (subject to clarity of intent and meaning).

7. Unused space should be minimized. For this reason, sections and subsections should not normally begin on a new page.

MATERIAL SUBMITTAL FORMAT AND PROCEDURE

Only camera-ready copies are accepted for publication, although authors may submit other copies for publication review. The term "camera-ready" means that the material is neat, legible, and reproducible. There is NO requirement for India ink or for special paper; any plain white paper may be used. However, faded lines on figures and white streaks along fold lines should be avoided. Original figures — even paste-ups — are preferred over "nth-generation" photocopies. These original figures will be returned if you so request.

While ACES reserves the right to re-type any submitted material, this is not generally done.

All submissions should be sent in triplicate to the Editor-in-Chief. Each submission should be accompanied by a cover letter. The cover letter should include the name, address, and telephone of at least one of the authors.

PUBLICATION CHARGES

At the present time, there are no page charges for camera-ready articles. Authors are entitled to 20 free reprints of their articles and must request these from the Managing Editor. Additional reprints are available to authors, and reprints available to non-authors, for a nominal fee.

COPYRIGHTS AND RELEASES

Each author must sign a copyright form and obtain a release from his organization vesting the copyright with ACES. Both forms will be provided by ACES and allow both the author and his organization to use the copyrighted material freely for their own private purposes.

Permission is granted to quote short passages and reproduce figures and tables from an ACES Journal issue provided the source is cited. Copies of ACES Journal articles may be made in accordance with usage permitted by Sections 107 or 108 of the U.S. Copyright Law. This consent does not extend to other kinds of copying, such as for general distribution, for advertising or promotional purposes, for creating new collective works, or for resale. The reproduction of multiple copies and the use of articles or extracts for commercial purposes require the consent of the author and specific permission from ACES. Institutional members are allowed to copy any ACES Journal issue for their internal distribution only.